

**Repair of Steel Beam/Girder Ends with Ultra
High-Strength Concrete – Phase II**

Prepared by: Arash E. Zaghi, Ph.D., P.E., Kay Wille, Ph.D.,
Kevin Zmetra, Ph.D., Kevin McMullen, Dominic Kruszewski,
and Alexandra Hain

Report Number: CT-2295-1-17-2
Interim Report
January 31, 2017

Research Project: SPR-2295

University of Connecticut
School of Engineering
Department of Civil and Environmental Engineering

Submitted to:
Connecticut Department of Transportation
Bureau of Policy and Planning
Roadway Information Systems Unit
Research Section

Michael J. Connors
Assistant Director of Policy and Planning

TECHNICAL REPORT DOCUMENTATION PAGE

1. Report No. CT-2295-1-17-2	2. Government Accession No.	3. Recipients Catalog No.	
4. Title and Subtitle Repair of Steel Beam/Girder Ends with Ultra High-Strength Concrete – Phase II		5. Report Date January 2016	
		6. Performing Organization Code SPR-2295	
7. Author(s) Arash Esmaili Zaghi, Kay Wille, Kevin Zmetra, Kevin McMullen, Dominic Kruszewski, and Alexandra Hain		8. Performing Organization Report No. CT-2295-1-17-2	
9. Performing Organization Name and Address University of Connecticut Department of Civil & Environmental Engineering 261 Glenbrook Road, Unit 3037 Storrs, CT 06269-7546		10. Work Unit No. (TRIS)	
		11. Contract or Grant No. CT Study No. 2295	
		13. Type of Report and Period Covered Interim Report June 2015 – December 2016	
12. Sponsoring Agency Name and Address Connecticut Department of Transportation 2800 Berlin Turnpike Newington, CT 06131-7546		14. Sponsoring Agency Code SPR-2295	
15. Supplementary Notes A study conducted in cooperation with the U.S. Department of Transportation and Federal Highway Administration			
16. Abstract A novel repair method has been developed at the University of Connecticut for corroded steel bridge girder ends. The repair method consists of encasing the corroded steel area with UHPC. The UHPC panel is bonded to the steel girder using headed shear studs welded to the uncorroded portions of the web and flange. The repair provides a secondary load path to restore the bearing and shear strength of the girder which was reduced due to corroded section loss. This research project investigates the application and performance of this repair for field implementation. Full-scale experimental tests will be conducted on plate girders with reduced steel sections to simulate corrosion damage. The plate girder specimens will be repaired using various repair geometries. Small-scale push-off tests will be conducted on shear studs welded to the web of a girder when embedded in UHPC. These tests are conducted to analyze the behavior of the shear studs in UHPC and to develop a formulation for the stud capacities. In addition to experimental strength tests, durability test will be conducted on the full-scale plate girders and push-off specimens to determine various field requirements and constraints for the repair. The results of both the large-scale and small-scale test will be used to develop and calibrate finite element models which will be used to test and evaluate the performance of the repair for a variety of different existing conditions and repair geometries for full-scale bridges in need of girder end repairs. A design guide will be developed to allow engineers to develop and implement this repair method for different designs. Collaboration is ongoing to assist CTDOT in a field implementation of the repair for a bridge with extensive corrosion of steel girder ends.			
17. Key Words Ultra-High Performance Concrete (UHPC), Steel Girder Repair, Beam end corrosion, Bridge Maintenance Repair method, Concrete encasing		18. Distribution Statement No restrictions. This document is available to the public through the National Technical Information Service, Springfield, VA. 22161	
19. Security Classif. (Of this report) Unclassified	20. Security Classif.(Of this page) Unclassified	21. No. of Pages 124	22. Price N/A

DISCLAIMER STATEMENT

This report does not constitute a standard, specification, or regulation. The contents of this report reflect the views of the authors who are responsible for the facts and the accuracy of the data presented herein. The contents do not necessarily reflect the views of the Connecticut Department of Transportation or the Federal Highway Administration.

ACKNOWLEDGEMENT

The research presented in this report was funded by the Connecticut Department of Transportation (CTDOT) and the Federal Highway Administration Contract number: SPR-2295. Special thanks are due to Bradley Overturf, Richard Hanley, Timothy Fields, Rabih Barakat, Anne-Marie McDonnell, and Mary Baker for their strong support and advice through the course of this project. The significant contribution of Michael Culmo of CME Associates is highly appreciated.

The authors would like to thank James Mahoney, Carolyn Ward, and Lori Judd of the Connecticut Transportation Institute for managing the project and funds. The support of Peter Glaude and Mark Bouley of the UCONN School of Engineering Machine Shop is also greatly appreciated in preparing experimental specimens. The tremendous support of Phil Romegialli and United Steel, Inc. in fabricating experimental samples and manufacturing the test frame is greatly appreciated. The authors would like to thank Mike Feder and Infra-Metals for donating steel material used for this research project and Andrew Ross and Lafarge for donating the UHPC. The student support of Samuel Turek, Ryan Enos, Richard Breitenbach, and Daniel Lubinitsky is appreciated.

METRIC CONVERSION FACTORS

APPROXIMATE CONVERSIONS TO SI UNITS				
SYMBOL	WHEN YOU KNOW	MULTIPLY BY	TO FIND	SYMBOL
LENGTH				
in	inches	25.4	millimeters	mm
ft	feet	0.305	meters	m
yd	yards	0.914	meters	m
mi	miles	1.61	kilometers	km
AREA				
in²	square inches	645.2	square millimeters	mm ²
ft²	square feet	0.093	square meters	m ²
yd²	square yard	0.836	square meters	m ²
ac	acres	0.405	hectares	ha
mi²	square miles	2.59	square kilometers	km ²
VOLUME				
fl oz	fluid ounces	29.57	milliliters	mL
gal	gallons	3.785	liters	L
ft³	cubic feet	0.028	cubic meters	m ³
yd³	cubic yards	0.765	cubic meters	m ³
NOTE: volumes greater than 1000 L shall be shown in m ³				
MASS				
oz	ounces	28.35	grams	g
lb	pounds	0.454	kilograms	kg
T	short tons (2000 lb)	0.907	megagrams (or "metric ton")	Mg (or "t")
TEMPERATURE (exact degrees)				
°F	Fahrenheit	5 (F-32)/9 or (F-32)/1.8	Celsius	°C
ILLUMINATION				
fc	foot-candles	10.76	lux	lx
fl	foot-Lamberts	3.426	candela/m ²	cd/m ²
FORCE and PRESSURE or STRESS				
lbf	poundforce	4.45	newtons	N
lbf/in²	poundforce per square inch	6.89	kilopascals	kPa

TABLE OF CONTENT

TITLE PAGE	i
TECHNICAL REPORT DOCUMENTATION PAGE	ii
DISCLAIMER STATEMENT.....	iii
ACKNOWLEDGEMENT	iv
METRIC CONVERSION FACTORS.....	v
TABLE OF CONTENT	vi
LIST OF FIGURES	viii
LIST OF TABLES	x
1 Introduction.....	1
1.1 Background and Problem Statement	1
1.2 Current Repair Solutions	3
1.3 History of Encased composite girders.....	5
1.4 Advantages of UHPC Material	6
1.5 Methodology.....	7
2 UHPC-Shear Stud Push-off Tests	9
2.1 Introduction	9
2.2 Literature Assessment of Stud Capacity	9
2.3 Push-off Experiments.....	11
2.3.1 Specimen Fabrication	11
2.3.2 Experimental Program.....	15
2.3.3 Results and Discussion	18
2.4 Durability testing – Electrochemical Corrosion.....	22
3 Full-Scale Plate Girder Testing	26
3.1 Selection of Specimen	26
3.2 Preliminary Finite Element Modeling.....	26
3.3 Design of Plate Girder Specimens	27
3.4 Design of Test Setup and Load Frame	31
3.5 Instrumentation	34
4 Bearing Corrosion Analysis.....	37
4.1 3D Scanner for Corrosion Detection	37
4.2 Importing 3D Scan Data To Finite Element Models	38
4.3 Experimental Testing of Corroded steel girder sections.....	41
5 Design of Field Repair	43
5.1 Bridge No. 3094 in New Haven, CT	43
5.2 Design Methods to determine Repair Capacity	45
5.3 Design of Girder End UHPC Repair	46

REFERENCES	50
APPENDIX A Experimental Push-Off Data	53
A1 Graph Terminology	53
A2 S1-8-2-NS-1/2 – Benchmark Specimen	53
A3 S2-4-2.5-NS-5/8 – 5/8” Studs.....	55
A4 S3-8-2-VHS-1/2 – VERTICAL and horizontal STAGGER	57
A5 S4-8-1.5-NS-1/2 – 3d _b Stud Spacing	59
A6 S5-8-2-VS-1/2 – Vertical Stagger.....	61
A7 S6-8-2-NS-1/2 – Regular Strength Concrete.....	63
A8 S7-8-2-NS-1/2 – Reduced Cover (1/4”).....	65
A9 S8-8-2-NS-1/2 – f’c = 28-ksi.....	67
Appendix B Shop Drawings of Push-off Specimens	69
Appendix C Experimental Plate Girder Specimen Shop Drawings	78
Appendix D Drawings of the Experimental Test Setup	88
Appendix E Experimental Load Frame Shop Drawings	90
Appendix F UHPC Repair Sample Calculations	96
Appendix G UHPC Repair Sample Drawings	102

LIST OF FIGURES

Figure 1.1: Typical corrosion damage of girder ends beneath the expansion joint.....	2
Figure 1.2: Corrosion damage and conventional repair method	3
Figure 1.3: Conventional Repair Method for corroded girder ends including jacking of the superstructure during construction	4
Figure 1.4: Phase 1 – a) Undamaged Girder, b) Damaged Girder, & c) Repaired Girder	5
Figure 1.5: Material Testing of UHPC – a) good flowability, b) high compressive strength, & c) added tensile strength from steel fibers	7
Figure 1.6: 3D rendering of the proposed UHPC repair method -1) Girder End Corrosion, 2) Welded Shear Studs, & 3) UHPC repair panel	8
Figure 2.1: Force distribution of stud shank and weld collar under pure shear (Hegger et al. 2001)	11
Figure 2.2: (a) bend test on studs; (b) welding using stud gun	12
Figure 2.3: Mixing of (a) dry premix, (b) addition of water and superplasticizer, (c) addition of chemicals, & (d) addition of steel fibers.....	14
Figure 2.4: (a) spread test of UHPC; (b) Compressive strength development of Ductal JS121214	
Figure 2.5: (a) Beam prior to casting; (b) beam installed into forms; (c) completed push-off sample.....	15
Figure 2.6: Typical experimental setup for push-off test	15
Figure 2.7: Typical instrumentation assembly for push-off test	17
Figure 2.8: Typical failure of push-off specimen	18
Figure 2.9: Failure of regular strength concrete sample via tensile panel splitting	20
Figure 2.10: Force vs. slip summary for all specimens	20
Figure 2.11: Panel slip vs. concrete f_c for all UHPC push-off specimens.....	21
Figure 2.12: Typical strain transfer behavior between the web and shear stud.....	22
Figure 2.13: Experimental assembly of electrochemical corrosion test.....	23
Figure 2.14: Corrosion at: (a) 0-hrs; (b) 42-Hrs; (c) 186-hrs; (d) 325-hrs	24
Figure 2.15: Steel Thickness vs. Time during Electrochemical corrosion	25
Figure 3.1: Full scale FE models of an interior girder from CT Bridge #818.....	27
Figure 3.2: Cross Section of the Plate Girder Specimen	28
Figure 3.3: 3D rendering plate girder specimen for experimental testing with splice connection	29
Figure 3.4: Plate girder specimen design for experimental testing	29
Figure 3.5: Fabrication of plate girder specimens by United Steel.....	30
Figure 3.6: Complete Plate Girder Specimens at United Steel in East Hartford, CT	30
Figure 3.7: Simulation of corrosion damage by sandblasting steel beams.....	31
Figure 3.8: Rendering of Phase 1 Test Setup	32
Figure 3.9: Phase 1 completed test setup	32
Figure 3.10: Enerpac CLRG-25012 (500-kip) and 50012 (1,000-kip) Hydraulic Cylinder.....	33
Figure 3.11: MTS ASSY-244.41S Hydraulic Actuator for dynamic loading to simulate live load traffic.....	33
Figure 3.12: Rendering of Full-Scale Experimental Test Setup	33
Figure 3.13: Progress of Experimental Test Setup	33
Figure 3.14: New plate girder spreader beams for the experimental test setup	34

Figure 3.15: Load frame plate girder assembly with slip resistant paint.....	34
Figure 3.16: Setup of DIC cameras for experimental testing of corroded girders.....	36
Figure 4.1: Artec Eva 3D Scanner.....	38
Figure 4.2: 3D Scanning using the Artec Eva.....	38
Figure 4.3: 3D point cloud of corroded girder.....	38
Figure 4.4: Finite Element 3D scanned mesh.....	39
Figure 4.5: Overall deformed shape of the corroded steel girder.....	39
Figure 4.6: Stress contour of the corrosion damaged section of the steel girder.....	39
Figure 4.7: FE geometry with the scanned corroded area and the idealized geometry for the intact rolled-steel shape.....	40
Figure 4.8: Deformed shape for corroded rolled-steel girder.....	40
Figure 4.9: Experimental test setup for corroded beam ends.....	42
Figure 5.1: Bridge No. 03094 in New Haven, CT servicing I-91 over Amtrak Railroad.....	43
Figure 5.2: Severe corrosion damage of girder ends.....	44
Figure 5.3: Design of potential shear stud layout for a corroded girder end.....	47
Figure 5.4: Proposed UHPC repair panel for corroded steel girder.....	48
Figure 5.5: Finite Element model of Bridge No. 3094.....	49

LIST OF TABLES

Table 2.1: Composition of Ductal JS1212	13
Table 2.2: Summary of Tests	19
Table 3.1: Selected plate girders (units: kip,in).....	26
Table 4.1: Steps for finite element analysis of corroded beams using 3D scanned geometry	41

1 Introduction

This study documents a novel repair method for corroded steel bridge girder ends using ultra high performance concrete (UHPC) encasement. The UHPC repair panel is bonded to the girder through headed shear studs welded to the undamaged steel portions of the web and flange. This repair may be used to recover bearing and shear capacity which was lost due to section loss induced by corrosion. The UHPC repair has several advantages over the competing methods, which are documented in this report. UHPC was chosen as the repair material because of its proven strength and durability, which is far superior to conventional concrete. This project is the second phase of a research program to develop and implement this novel repair method. The first phase was completed and is documented in CTDOT Report CT-2282-F-15-2; project number SPR-2282 (Esmaili Zaghi et al. 2015; Zmetra 2015; Zmetra et al. 2015). The information presented in this report is for the work completed prior to January 1st, 2017. This includes, but is not limited to preliminary finite element modeling, design and construction of the experimental load frame for testing, design and construction of full-scale plate girder test specimens, push-off tests using UHPC-embedded shear studs, and preliminary design for a pilot implementation of the repair.

1.1 BACKGROUND AND PROBLEM STATEMENT

In 2013, the American Society of Civil Engineers (ASCE) released a Report Card grading the state of America's Infrastructure (ASCE 2014). The infrastructure earned a poor overall grade of a D+. The bridges in the United States were awarded a grade of a C+. The average age of these bridges was 42 years when this report was released. One out of nine bridges maintained in the United States has a structurally deficient rating. FHWA estimated that it would cost approximately \$76 billion to repair or replace all of the structurally deficient bridges across the United States. This overwhelmingly high estimate is due in part to the current cost of repair methods. New, innovative, and cost effective repair solutions are necessary to improve the structural integrity and service life of existing bridges.

In 2015, the total number of structurally deficient bridges maintained in the United States was 59,000 (FHWA 2014). Many of these bridges have exceeded their 50-year design life. Corrosion damage is the cause of approximately 15% of the structurally deficient bridges maintained in the United States. Koch et al. (2002) estimates that the United States spends \$273 billion on corrosion maintenance annually; \$8.3 billion of which goes to repair and replacement of highway bridges. Approximately 50% of the

structurally deficient bridges utilize a steel superstructure. Steel superstructures are typically used because of their high strength to weight ratio. However, structural steel corrodes when exposed to oxygen and moisture. The extent of corrosion is dependent on time, temperature, humidity, exposure, and the presence of chemicals (Albrecht and Hall Jr 2003). The chief accelerator of corrosion damage in transportation infrastructure systems is deicer chemicals used to control ice and snow on roadways in cold-climate regions (Shi et al. 2009).

Extensive corrosion of bridge girders is most commonly found directly beneath deck expansion joints, which are usually located above girder supports at abutments and piers as shown in Figure 1.1 (Kayser and Nowak 1989; Usukura et al. 2013; Van de Lindt and Pei 2006). Purdue University completed an extensive investigation on the performance of expansion joints. Common problems cited with expansion joint systems were water leakage and deterioration at bridge bearings (Chang and Lee 2001). Figure 1.2 shows a girder end with corrosion damage beneath the expansion joint and a girder that has been repair because of corrosion damage.



Figure 1.1: Typical corrosion damage of girder ends beneath the expansion joint



Figure 1.2: Corrosion damage and conventional repair method

Corrosion of steel girder ends can result in significant section loss of the web and flanges, which reduces the bearing and shear capacity of the member. Several research projects have been conducted on the performance of steel girders with corrosion damage. Liu et al. (Liu et al. 2011) studied the effect of corrosion height and thickness on shear capacity of steel I-girders near bridge supports. The results showed the height of corrosion had a more significant impact on the capacity of the girder compared to the length of corrosion. Ahn et al. (2013) performed large scale experiments and extensive analytical studies on the performance of plate girders with simulated corrosion damage. The study determined the shear capacity of the plate girders drastically decreased when the corrosion pattern intersected the tension field in the girder's end panel. Yamaguchi and Akagi (2013) completed more analytical studies of the effect of corrosion damage on the load carrying capacity of I-girders. They found the reduction in load-carrying capacity was more detrimental if the corroded region had a free boundary. Khurram et al. (2014b; 2014a) investigated the performance of plate girders with corrosion damaged webs and bearing stiffeners. Experimental tests and finite element analyses (FEA) using Abaqus were completed to determine the loss in bearing capacity. The results indicated that a 50% reduction of the bottom section of the web decreased the bearing capacity by 39%.

1.2 CURRENT REPAIR SOLUTIONS

Current repair methods for corrosion damage of steel girder ends are expensive and difficult to implement. The Federal Highway Administration and several Departments of Transportation (DOTs) have developed standard procedures to repair corroded steel girder ends: 1) jacking the structure to relieve the load from the bearing, 2) cutting out the corroded section of steel, 3) welding a new steel section into place, and 4) lowering the span and remove the jacking equipment (Figure 1.3) (FLDOT 2011; Rossow 2003 ; Wipf et al. 2003; WisDOT 2015). The conventional repair method requires extensive

manual labor. Jacking of the superstructure is required in order to provide a stress-free condition for implementation of the repair. Jacking often constitutes a large percentage of the project cost. For a bearing replacement project on the Putnam Bridge in Connecticut, 50% of the project cost was due to jacking (Close 2011). Figure 1.3(c) shows the extent of the rigorous jacking systems needed to raise and lower superstructures during repair. Jacking towers are indicated with an arrow. Surface preparation is also required before removing the corroded steel and welding new steel. Preparation requires lead abatement if the existing paint is lead-based.



Figure 1.3: Conventional Repair Method for corroded girder ends including jacking of the superstructure during construction

Few research projects have been completed on new repair methods for corrosion of steel girder ends. Ahn (2013) and Miyashita (2015) completed extensive experimental and analytical studies on the application and performance of carbon fiber-reinforced polymer (CFRP) sheets. CFRP sheets are lightweight, durable, and high strength. CFRP sheets can be applied over localized corrosion at steel girder ends to recover bearing and shear capacities. The load carrying capacity of the CFRP repaired corroded girder surpassed that of an undamaged girder (Miyashita et al. 2015). Ogami (2015) developed a repair method for plate girder ends where studs and rebar were attached to the girder and the corroded area was enveloped in resin. Axial compression tests were

conducted on the girder ends to measure bearing capacity. Applying the resin repair to corroded girder ends was able to improve the bearing capacity of the specimen.

New, cost effective rehabilitation designs are necessary to make corrosion repair projects more viable for bridge owners. New techniques must be structurally effective, durable, and easy to implement. Repairs should minimize interruptions to traffic, increase work zone safety, and reduce construction costs. During Phase 1 of this research project, researchers at the University of Connecticut (UCONN) completed a proof-of-concept research project to develop a novel repair method for steel girder ends with significant section loss due to corrosion. The rehabilitation technique used UHPC to encase corroded steel bridge girder ends. UHPC provides improved tensile strength, high early strength, good workability, and superior durability, which made it an ideal repair material over conventional concrete. Half-scale experiments were conducted on an undamaged, a damaged, and a repaired rolled steel girder shown in Figure 1.4. The test results were used to: 1) determine the decrease in bearing capacity due to section loss, 2) demonstrate the ability of the UHPC repair to restore lost girder capacity, and 3) investigate the constructability of the repair method. The experimental results concluded that the UHPC repair was easily implemented and succeeded in restoring the bearing capacity lost due to corrosion damage.



Figure 1.4: Phase 1 – a) Undamaged Girder, b) Damaged Girder, & c) Repaired Girder

1.3 HISTORY OF ENCASED COMPOSITE GIRDERS

Previous research was performed on a similar composite girder system where concrete was placed on the web of steel girders in between the top and bottom flange. The concept of concrete-encased steel beams was originally proposed by Elnashai et al. (1991) as a novel beam-column design for buildings. A small cage of rebar was welded to the interior section of the girder and was filled with concrete. Nakamura extended this idea to bridge plate girders and concentrated on the beam's performance in shear and bending (Nakamura et al. 2002; Nakamura and Narita 2003). Rebar was welded between the flanges and stiffeners. Stiffeners were installed at the center bearing to resist shear and hogging moments. A full web height concrete panel was cast

between the flanges and stiffeners to improve bending and shear strength of the girder. Hyashi et al (2003) noted this composite beam method could be used to rehabilitate steel girders which have experienced deformations from buckling. He et al. (2012a; 2012b) extended this method to encase a steel girder with an offset, corrugated web with concrete on only one side in order to improve the shear strength of the girder.

1.4 ADVANTAGES OF UHPC MATERIAL

UHPC material was chosen as the desired repair material over conventional concrete because of unique material benefits that it provided to the repair design. The UHPC mix used in this project has been accepted and tested by FHWA for several research projects (Graybeal 2014; Russell and Graybeal 2013; Yaun and Graybeal 2014). Russell and Graybeal (2013) document many of the advantages of UHPC compared to conventional concrete specific to the current application. The UHPC ready mix used in this research project (Ductal® JS-1212) significantly reduces onsite complications and inconsistencies with the constructability and performance of the repair. The flowability of UHPC may allow the repair to be poured or pumped to encase complex geometries with no concerns of clogging when used with tightly spaced shear studs. Figure 1.5(a) shows the results of a slump test with UHPC and the good flowability of the material. The high early strength of UHPC would allow for reduced lane closures and construction delays, as this particular mix is specified to achieve a compressive strength of 12-ksi (82.7-MPa) after 12 hours of curing at 120°F. UHPC has proven durability when exposed to moisture, freeze-thaw conditions, and abrasion. It has a very low permeability and water absorption capacity, which is approximately 10 and 60 times less than high-performance concrete and normal strength concrete, respectively (Abbas et al. 2016). Figure 1.5(b) shows a concrete cylinder used to determine compressive strength after 3 days of curing. The impervious nature of UHPC would prevent the repair panel or the base steel material of the girder from corroding further in the future. The crack resistance of UHPC due to its high tensile strength and ductility eliminate the need for the addition of reinforcing bars. Figure 1.5(c) shows how the steel fibers bridge micro cracks in the concrete to improve the compressive and tensile strength of fiber reinforced UHPC. Studies performed on the fatigue resistance of UHPC and UHPC shear connectors demonstrated the improved resistance compared to conventional concrete (Classen et al. 2016; Feldmann et al. 2011; Grünberg et al. 2008; Shaheen and Shrive 2008). The superior characteristics of UHPC may justify the added costs of the material.



Figure 1.5: Material Testing of UHPC – a) good flowability, b) high compressive strength, & c) added tensile strength from steel fibers

The small volume of UHPC needed for the repair only introduces a small additional dead load to the girder, which is carried directly into the bearing without affecting shear and flexural demands on the girders. Compared to the conventional repair, the UHPC repair may be applied to the in situ condition of the bridge without the need for jacking of the superstructure. The repair may be used to provide a secondary load path to service live load demands while the remaining steel section continues to carry in situ stresses. In addition, UHPC's low permeability and corrosion resistance would prevent the need for further repairs.

1.5 METHODOLOGY

The second phase of this project was devised to evaluate the performance of the repair for a variety of different scenarios and optimize the final design. Optimization of the design is important to facilitate the implementation of the repair for different geometries and configurations of bridges. This will prevent the need for tedious, individualized designs for specific bridges and geometries; instead, it will provide a set of repair guidelines that may be adapted to each individual project. The results of this project will allow the repair to be effectively implemented on actual with a significant reduction in repair costs. This study will accomplish the following:

- Demonstrate that jacking is not required in order to implement this repair method
- Provide a time frame, if any, where the bridge must be closed to traffic
- Optimize the design and develop standard drawings and calculations
- Test the long-term durability of the repair
- Assist the Connecticut Department of Transportation (CTDOT) with the design of the repair for field implementation.

Evaluation of the repair will be conducted through a series of experimental tests along with a set of high fidelity finite element (FE) simulations. The full-scale

experimental test will include several push-off tests to assess the interaction between shear studs cast into the UHPC repair panel. For the push-off tests, the shear studs will be welded to the thin web of the girder as opposed to the thick flange, which is most common. Experimental tests will be conducted on full-scale plate girders to investigate the performance of different repair geometries. The results for the experimental tests will be used to calibrate FE models which may then be used to test different configurations and various parameters. The results from both the experimental and analytical studies may be used to create a design guide to allow engineers to implement the design. The team will work with CTDOT to implement the repair in the field for an in-service bridge. This will include scope, design, construction, and monitoring the repair. Figure 1.6 shows a rendering of the proposed repair method sequence.

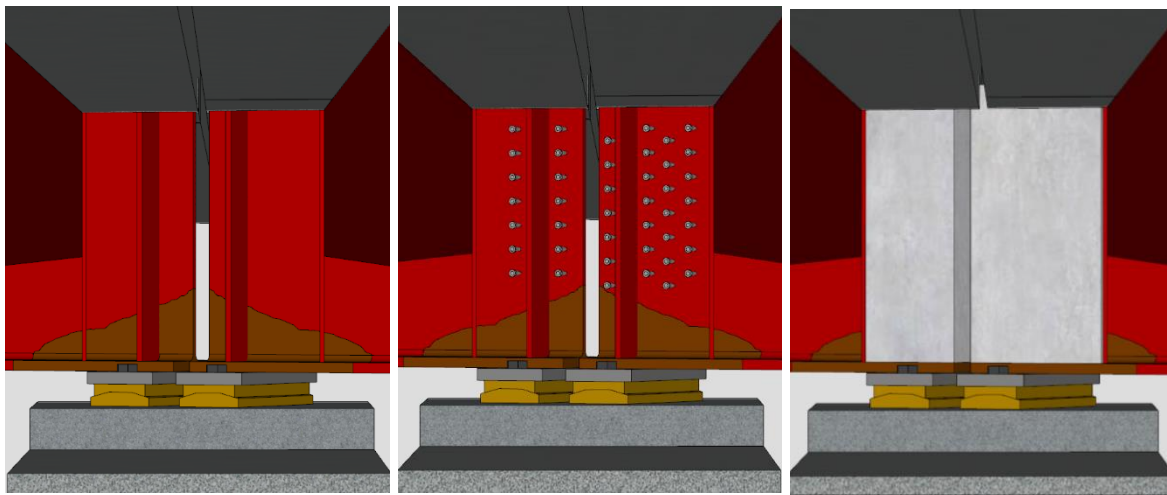


Figure 1.6: 3D rendering of the proposed UHPC repair method -1) Girder End Corrosion, 2) Welded Shear Studs, & 3) UHPC repair panel

2 UHPC-Shear Stud Push-off Tests

2.1 INTRODUCTION

In the proposed repair method, the main transfer mechanism that contributes to increased bearing capacity hinges on the interaction between the web of the old material, the welded studs, and the panel of UHPC. To generate reliable stud capacities, the mechanical behavior and failure mechanism must be thoroughly understood. The most common method to determine stud shear capacity is the “push-off” test. This test involves pushing the embedded studs against the concrete in pure shear until failure. The Euro Code (Eurocode-4 2004) provides a standard for the test, but it involves headed studs welded to the flanges, which are often thicker than the web. Furthermore, the push-off test specified in EC-4 pertains to headed studs embedded in regular strength concrete.

The testing method for these experiments will be a modified version of the standard outlined in the EC-4 with the studs being welded to the web of a rolled girder section (instead of the flanges) and embedded in UHPC (instead of regular concrete). So far, the following parameters were investigated through this experimental study:

1. The behavior of studs welded on old, weathered steel
2. The performance of the studs welded to a thin 3/8 inch web
3. The effect of various stud layouts, spacing, diameters, and numbers of studs
4. The durability of the repair by inducing electrochemical corrosion.

2.2 LITERATURE ASSESSMENT OF STUD CAPACITY

Current literature shows that several research groups have investigated the behavior of headed shear studs embedded in concrete, especially for the purposes of a typical composite connection between the bridge deck and girders. A vast majority of groups have reported the interaction between studs and regular strength concrete, citing the primary modes of failure as conical crushing of surrounding concrete, shear failure of the stud shank, or a combination of both. Li and Kristen (1996) first reported that the concrete compressive strength f'_c plays a major role in enhancing the strength of the shear connector, and that an increase from 30 to 81 MPa generates an increase in maximum shear capacity by about 34%. Lam and El-Lobody (2005) reported that, when conducting push-out tests with normal strength concrete, a compressive strength of 20 MPa resulted in complete conical failure of the surrounding concrete, with only partial yielding of the stud. When comparing these results to push-out tests conducted by Kim

et al. (2015) using UHPC instead of normal strength concrete, the failure mode was primarily governed by stud shank failure (with little to no concrete cracking).

Current design codes such as AASHTO-LRFD section 6.10.10.4.3 (AASHTO 2012) provide equations to define the static strength of a stud shear connector as the following:

$$Q_r = \phi_{sc} Q_n = \phi_{sc} 0.5 A_{sc} \sqrt{f'_c E_c} \leq \phi_{sc} F_u A_{sc} \quad (1)$$

Similarly, Eurocode-4 provides an estimation of shear capacity as the following:

$$P_{Rd} = \frac{0.29 \alpha d^2 \sqrt{f'_c E_c}}{\gamma_v} \leq \frac{0.8 F_u A_{sc}}{\gamma_v} \quad (2)$$

Hegger et al. (2001) reported that the presence of a weld collar in headed studs embedded in UHPC provides an increase in direct shear capacity because of its bearing contribution onto the concrete, which does not crack. A formula for predicting the shear capacity of headed studs embedded in high strength concrete was consequently devised as the following:

$$P_u = A_{sc} f_{su} + \eta f_{cu} d_{wc} l_{wc} \quad (3)$$

Where A_{sc} is the area of the stud shank, f_{su} is the ultimate tensile capacity of the stud, f_{cu} is the compressive strength of the concrete, d_{wc} is the diameter of the weld collar, l_{wc} is the height of the weld collar, and η is an empirical factor typically taken as 2.5 for UHPC (Kim et al. 2015). A schematic of the mechanical behavior of the stud and weld collar under a pure shear load is provided in Figure 2.1.

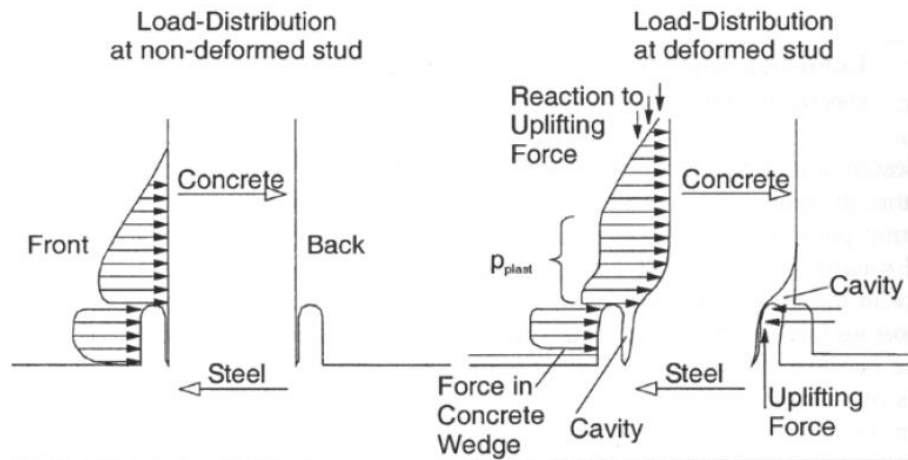


Figure 2.1: Force distribution of stud shank and weld collar under pure shear (Hegger et al. 2001)

The influence of UHPC is significant when considering the failure mode of push-out specimens as the use of typical concrete results in a ductile, plastic behavior of the headed studs but ultimately failure via compressive crushing of surrounding concrete. However, since UHPC has a much larger compressive strength, the failure mechanism is influenced by the quality of the weld and the shear capacity of the headed stud. The superior compressive strength of the UHPC also generates higher shear capacities due to direct bearing of the weld collar, which has a slightly larger diameter than the shear stud (Figure 2.1). The high compressive strength and inclusion of steel fibers to bridge tensile cracking allows little to no cracking of concrete – at this point, the concrete confines the stud, resulting in a pure shear failure of the stud shank at the interface of the two materials.

When applying information from current literature and design codes to determine the potential of the proposed repair, many questions are still posed. Current literature does not use older steel with reduced mechanical properties, which may affect the performance of the composite system. Additionally, no literature was found on the performance of shear studs when welded onto webs (or flanges thinner than 0.5 inches). Therefore, a comprehensive experimental program was designed to gain confidence in the mechanical behavior of the studs.

2.3 PUSH-OFF EXPERIMENTS

2.3.1 Specimen Fabrication

Several push-off tests were conducted to evaluate the performance of shear studs embedded in UHPC. In order to produce results relevant to the envisioned repair, rolled steel girders were salvaged from the old Pearl Harbor Memorial Bridge in New

Haven, CT, which was erected in 1958. According to the American Institute of Steel Construction, specifications at that time called for grade A7 structural steel, which has a corresponding yield strength of 32 ksi (Brockenbrough 2002). The girder sections obtained were W18x55 with a 3/8 inch thick web and a nominal depth between 18 and 21 inches. The steel from these girders served as the base material onto which the studs would be welded for all push-off experiments.

To fabricate the specimens, the girders were cut into 12 inch sections so that several parameters could be studied from the same material. All specimens were designed according to AASHTO's design equations and fabricated by United Steel. In accordance with the American Welding Society, the shear studs were shot on a scrap piece of steel and bent to 30 degrees from their original axis to ensure the quality of the weld (Figure 2.2(a)). After the voltage was adjusted to produce the desired weld, the studs were shot onto the beam sample using a stud gun (Figure 2.2(b)). This is the typical method used in the field.



Figure 2.2: (a) bend test on studs; (b) welding using stud gun

The concrete mix design selected for these experiments was JS1212 (Ductal), provided by LaFarge Holcim. The formulation is composed of a premix powder (containing a mixture of cement, silica fume, ground quartz, and sand), high tensile strength steel fibers, admixtures, and water. The steel fibers are 0.008 inch in diameter and 0.5 inch long, specified for a minimum tensile strength of 290 ksi. The admixtures include Optima 100 (a modified polycarboxylate high-range water-reducing agent), Turbocast 650A (a non-chloride accelerator), and Premia 150 (a modified phosphonate plasticizer). This mix is specified to achieve a compressive strength, f'_c , of 12 ksi in 12 hours with 120°F curing. The composition by weight is shown in Table 2.1.

Table 2.1: Composition of Ductal JS1212

Component	% by weight
Premix	86.6
Water	5.1
Premia 150	0.7
Optima 100	0.5
TurboCast	0.9
Steel Fibers (2%)	6.2

The mix design was cast and tested several times prior to casting the specimen in order to gain familiarity with the consistency and mechanical behavior of the material. All mixing and casting was conducted in the UConn Advanced Cementitious Materials and Composites Laboratory. The mixing procedure consisted of stirring the dry premix for approximately 5 minutes to eliminate any clumps (Figure 2.3(a)). Next, water and superplasticizer were slowly added and allowed to disperse (Figure 2.3(b)). Half of the water was substituted with ice in order to gain additional workability time. Next, all chemicals (Premia 150, Optima 100, and TurboCast) were slowly added (Figure 2.3(c)). Mixing continued until the concrete turned over and a uniform consistency was achieved. Finally, the steel fibers were slowly added and thoroughly mixed to ensure optimal dispersion (Figure 2.3(d)). This procedure was strictly adhered to for every specimen cast to establish consistency.





Figure 2.3: Mixing of (a) dry premix; (b) addition of water and superplasticizer,; (c) addition of chemicals; and, (d) addition of steel fibers

Quality control of UHPC flowability was established by checking the spread of the concrete immediately after mixing. A spread of 10.125 – 10.375 inches was achieved consistently (Figure 4a). Additionally, eighteen (18) cylinders were cast from the same batch to evaluate the concrete compressive strength at 12 hours, 24 hours, and 3, 7, 14, and 28 days. The experimental strength development over time is shown in Figure 4b.

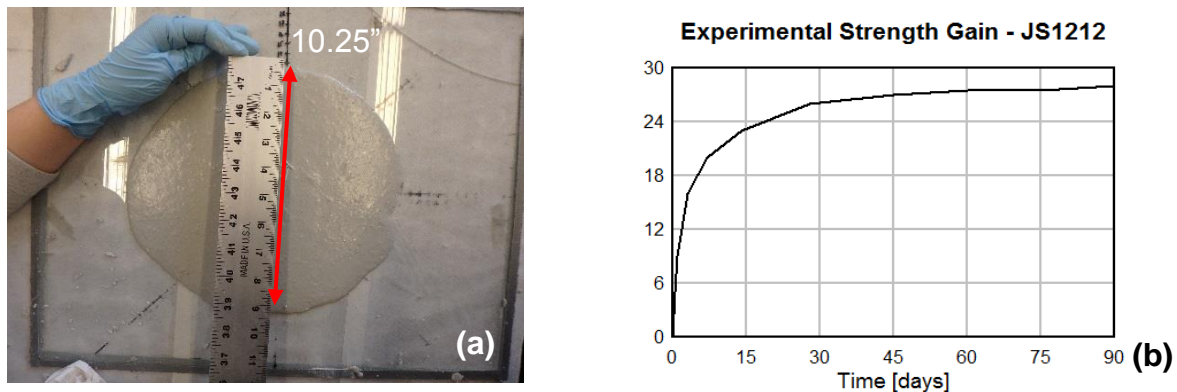


Figure 2.4: (a) spread test of UHPC; (b) Compressive strength development of Ductal JS1212

The forms used to cast each specimen were fabricated by United Steel to ensure consistency in the concrete panel shape. They consisted of two steel panels resting on a base plate with a perfectly flat surface. The panels covered both sides of the web with a clear cover of 0.75 inch from the edge of studs. The steel beam was propped 2.5 inch above the base plate to allow room for vertical displacement of the beam during testing. Additionally, a 0.5 -inch gap was left between the concrete panels using collapsible foam to prevent the web from bearing on the concrete panel. This ensured that the full load applied was transferred solely from the embedded studs into the UHPC panel. Prior to casting, the forms were lubricated with a heavy-duty debonding agent to ensure

an easy release. Figure 2.5 shows the push-off specimen before casting, in the formwork, and after casting.

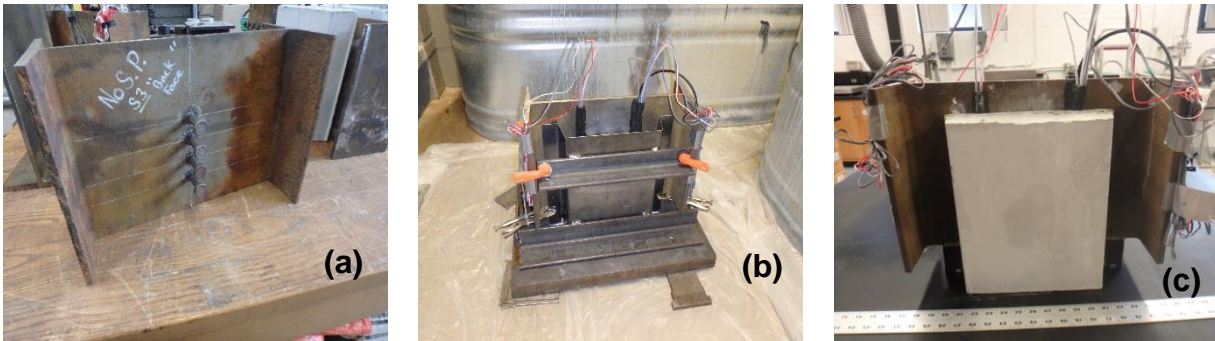


Figure 2.5: (a) Beam prior to casting; (b) beam installed into forms; (c) completed push-off sample

2.3.2 Experimental Program

All specimens were tested in the UConn Structural Testing Laboratory using the SATEC 400 kip load frame with a MTS FlexTest-40 controller. Each specimen was mounted such that the concrete panels were bearing on a 10 inch spherical bearing, placed on the bottom platen of the machine. Prior to installation, the spherical bearing was cleaned and lubricated to minimize any friction. The loading was applied on the flanges and a small portion of the web to ensure a pure shear loading was applied on the studs. The web was not directly loaded to prevent local buckling between the concrete panel and the top platen. The experimental setup is shown in Figure 2.6.

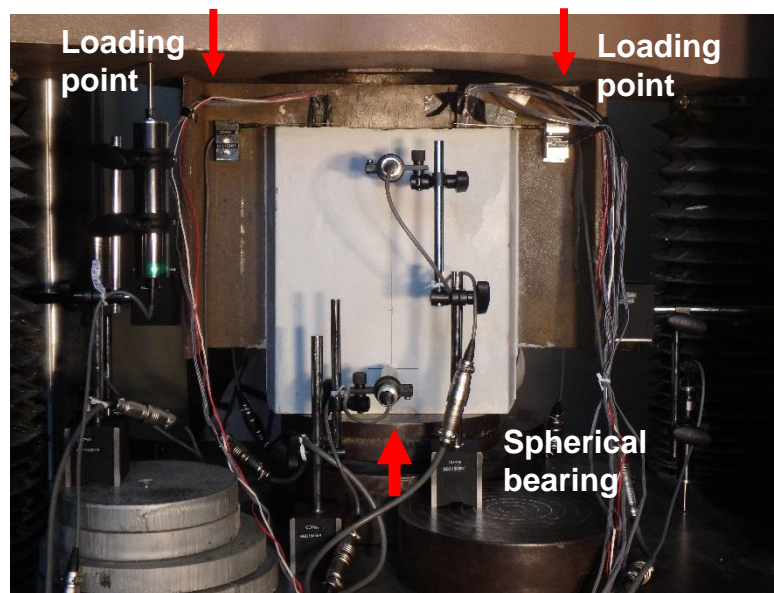


Figure 2.6: Typical experimental setup for push-off test

Comprehensive instrumentation was installed on each specimen to extract all relevant data (Figure 2.7). The studs located on the front side were all instrumented with uniaxial strain gauges to capture axial deformation during loading. Biaxial strain gauges were installed just above the top and bottom stud to observe the demand on the web when the load is transferred to the adjacent studs. The panel was instrumented with displacement gauges which measured out of plane displacement, which occurs when the studs start to deform axially. Additionally, slip gauges were installed onto the web using high strength magnets to monitor the relative vertical displacement between the steel and the concrete. This movement showed the ductility of the system.

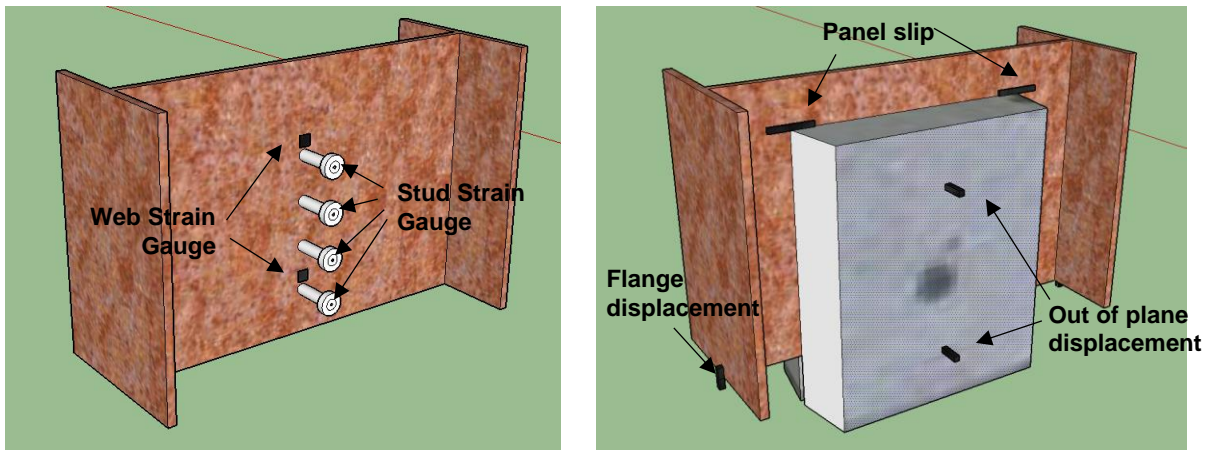


Figure 2.7: Typical instrumentation assembly for push-off test

Each specimen was designed to evaluate a parameter of interest, including stud diameter, stud layout, stud spacing, and varying concrete strengths. Appendix B contains detailed drawings and dimensions for each specimen. Thus far, the following samples have been tested:

- S1^a-8^b-2^c-NS^d-1/2^e (Benchmark Specimen) – The benchmark test contained a total of eight $\phi 1/2$ " studs (four on each side) welded in a straight line relative to the loading with 2 inch (4db) spacing, per AASHTO specifications.
- S2-4-2.5-NS-5/8 (5/8" Studs) – Contained four $\phi 5/8$ " studs (two on each side) welded in a straight line relative to the loading with 2.5 inch (4db) spacing.
- S3-8-2-VHS-1/2 (Vertical and Horizontal Stagger) – Similar to the benchmark specimen, but the studs were staggered horizontally and vertically to examine any demand effects on the web.
- S4-8-1.5-NS-1/2 (3db Stud Spacing) – The same as the benchmark, but the studs were spaced at 1.5 inch (3db).
- S5-8-2-VS-1/2 (Vertical Stagger) – Designed similar to the benchmark, but the studs were shot slightly higher on one side of the web than the other to examine the effect of vertical stagger.
- S6-8-2-NS-1/2 (Regular Strength Concrete) – Identical to the benchmark, but the studs were embedded in regular strength concrete instead of UHPC.
- S7-8-2-NS-1/2 (Reduced Cover) – Similar layout to the benchmark specimen, but the clear cover of the studs was pushed to 1/4 inch (0.5db).
- S8-8-2-NS-1/2 (Ultimate Strength UHPC) – Same layout as the benchmark, but the UHPC was allowed to cure for six months to examine the behavior at ultimate concrete strength.

^aSpecimen number; ^bNumber of studs; ^cSpacing of studs (in); ^dNo Stagger (NS), Vertical Stagger (VS), Horizontal Stagger (HS); ^eStud Diameter (in)

Since AASHTO design equations were used to predict the capacity of each specimen, the machine was set to force control for the first few load cycles. Each specimen was loaded in 20 kip increments. After each loading, the specimen was unloaded back down to a baseline of 1 kip, and then loaded again. After 80 kip was attained, displacement control was used to safely push the studs to failure.

2.3.3 Results and Discussion

The shear connection developed by the studs embedded in the UHPC generated a significant load bearing capacity even with the old steel as the base material. Excluding the regular strength concrete specimen, the capacity of the samples with $\phi 1/2$ " studs ranged between 118-134 kip. The specimen with $\phi 5/8$ " studs generated a load bearing capacity of 96 kip. The stud layout did not have any significant effect on the load bearing capacity as every specimen exceeded the theoretical capacity outlined in AASHTO. All of the specimens (except the regular strength concrete sample) failed via shear failure of the stud shank directly adjacent to the weld collar (Figure 2.8). There was little to no cracking observed in the concrete panel. However, a thin portion of the UHPC sheared off underneath each stud, indicating high shear forces concentrated in the region due to the weld collar.



Figure 2.8: Typical failure of push-off specimen

Table 2.2 shows a detailed summary of all tests, including experimental capacity, stiffness of the system, yield points, and maximum slip for all specimens. It was observed that the specimen with a concrete compressive strength of 28 ksi yielded the highest capacity of 134 kip. This may be considered the expected behavior of headed shear studs embedded in UHPC at its ultimate strength. Specimens containing any type of stagger (vertical, or vertical and horizontal) generated a similar load bearing capacity

of 118 kip with a corresponding slip of 0.185 - 0.202 inch (4.7 - 5.1 mm). However, the specimen with vertically staggered studs demonstrated a much larger elastic stiffness of 3,148 kip/in. Both samples were tested at relatively low compressive strengths of 16-17 ksi, hence a lower capacity was expected per Hegger's formulation. Consistent capacities were still achieved even when pushing current design limits, such as tighter spacing of the studs or applying a reduced cover of 1/4 inch. Both samples generated capacities between 130 and 132 kip of load bearing capacity.

Table 2.2: Summary of Tests

Description	Specimen ID	# of studs	f'c (ksi)	Experimental Capacity (kip)	Elastic Stiffness of System (kip/in)	Yield Force (kip)	Max Slip (in)	Slip at Yield (in)
Benchmark	A1-8-2-NS-1/2	8	19	126	3202	84	0.183	0.013
5/8" Studs V+H Stagger	S2-4-2.5-NS-5/8	4	16	96	3391	65	0.173	0.009
3db Spacing	S3-8-2-VHS-1/2	8	16.5	118	2437	85	0.185	0.011
V Stagger	S4-8-1.5-NS-1/2	8	21	130	2431	82	0.199	0.011
RSC	S5-8-2-VS-1/2	8	17	118	3148	84	0.202	0.008
Red. Cover	S6-8-2-NS-1/2	8	8	86	2230	68	0.029	0.013
28 ksi f'c	S7-8-2-NS-1/2	8	21	132	2344	89	0.176	0.009
	S8-8-2-NS-1/2	8	28	134	3246	86	0.128	0.007

The regular strength concrete sample showed that conventional concrete materials was not suitable for the envisioned repair method, as the panels split under tension when larger loads were applied (Figure 2.9). This demonstrates the need for reinforcement in the panel, which may be difficult to install. However, the specimens containing UHPC exhibited almost no cracking, due to the high-strength steels fibers that are dispersed throughout the matrix. These fibers activate to take on any tensile action in the panel that may arise when the studs bear on the concrete.

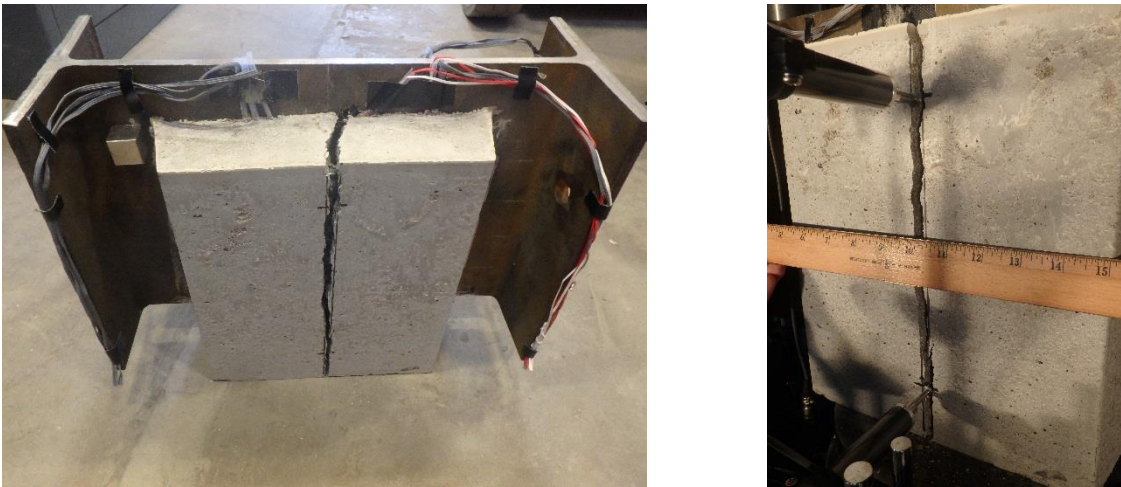


Figure 2.9: Failure of regular strength concrete sample via tensile panel splitting

Figure 2.10 shows the force vs. slip curves for all specimens tested. When compared to the specimens with UHPC embedded studs, the regular strength concrete sample with 8 ksi panels clearly generated a much lower ultimate capacity and achieved no plastic load bearing capacity. However, the specimens with UHPC sustained their ultimate load over a large slip range, characterized by the long plastic plateaus (Figure 2.10). This indicated that the shear connection demonstrates ductile behavior and is controlled by the stud material strength. The shear studs experienced much larger strains than the web itself. The lack of cracking observed in the UHPC panel above and below the studs indicated that the concrete's superior compressive strength was able to accommodate the stresses that developed between the studs.

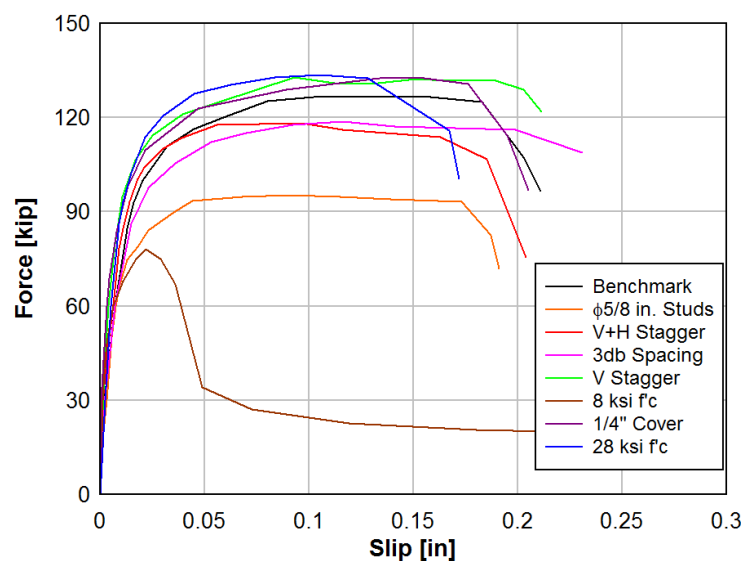


Figure 2.10: Force vs. slip summary for all specimens

Most of the specimens failed at a consistent slip between 0.17 - 0.2 inch (4.3 - 5.1 mm). However, the ultimate strength specimen demonstrated a much lower slip at

failure of approximately 0.128 inch (3.25 mm). This was most likely due to the confining effect of the UHPC as indicated by the increased elastic stiffness. At higher compressive strengths, confining action of the UHPC around the stud shank prevented the stud from deforming in a ductile manner. Less axial strain was generated throughout the length of the stud and a higher shear force was developed in the shank near the weld collar. Figure 2.11 shows the relationship between experimental panel slip and compressive strength of the UHPC panels, indicating a reduction in panel slip as concrete strength increases.

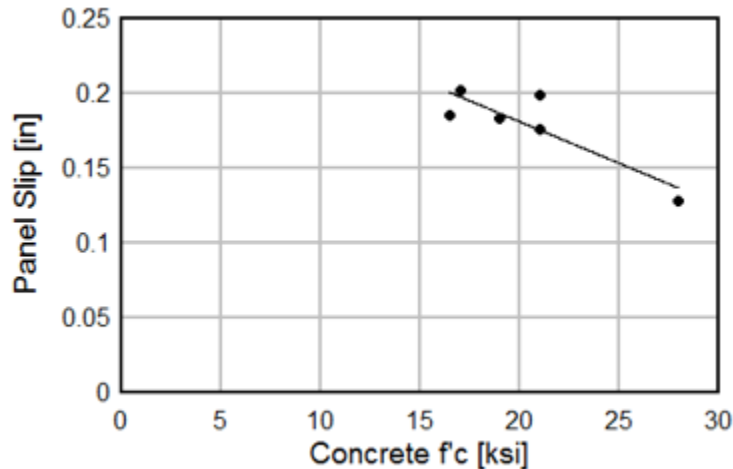


Figure 2.11: Panel slip vs. concrete f'_c for all UHPC push-off specimens

Figure 2.12 shows the transfer of strain between the stud and adjacent web on which it was welded. When initial loads were applied to the system, the web and studs act together to resist the demands in the elastic range. However, when larger displacements were induced, the web began to undergo larger plastic deformations (possibly because it is composed of a weaker grade steel), while the studs just began to activate. Upon further displacement, the web transferred the load into the studs, which eventually experienced yielding. At this point, the studs became the weak link in the system and continued to undergo plastic shear deformation until failure.

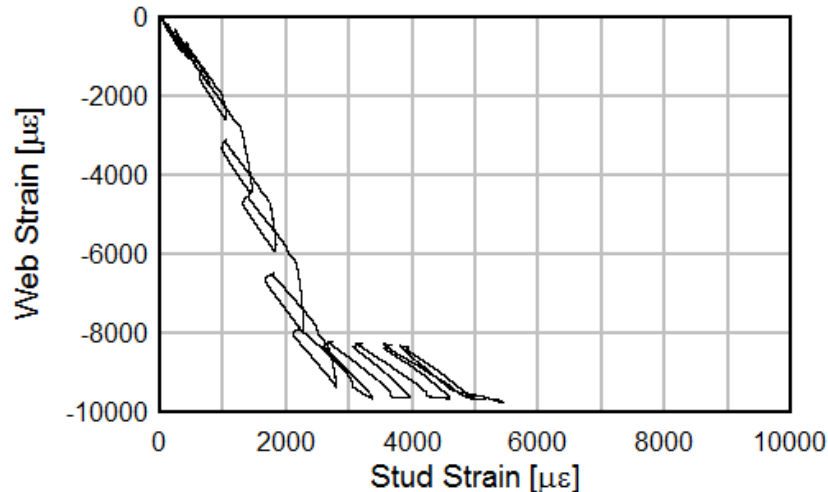


Figure 2.12: Typical strain transfer behavior between the web and shear stud

Overall, the experiments conducted thus far have generated valuable information pertaining to design of future repairs. The per-stud capacity for ϕ 1/2 inch studs was found to be 14.75 – 16.75 kip with a corresponding slip of 0.12 – 0.20 inches. Studs with 5/8 inch diameter generated a per-stud capacity of 24 kip. These values surpass the capacities given by research formulations and AASHTO and EC-4 design codes, as the inclusion of UHPC generates a shear capacity due to direct bearing of the weld collar. In general, the web initially takes on strain at small loadings, and then transfers the load to the studs once initial yielding occurs. The system is then controlled by the studs, which typically fail due to ductile shear failure at the stud shank.

2.4 DURABILITY TESTING – ELECTROCHEMICAL CORROSION

One of the parameters of interest for future experiments involves testing a push-off sample with induced corrosion in the web. This will shed light on how far the web can be pushed when significant corrosion is present in regions where studs are welded and actively taking loads. Therefore, measures were taken to explore potential accelerated corrosion techniques, some of which include salt-fog testing, sand-blasting to reduce cross sectional area, and electrochemical corrosion. Although salt-fog testing was strongly considered, the research team decided that electrochemical corrosion was most suitable since it is easy to control the section loss and it provides a more realistic degraded surface in a shorter time span. Although electrochemical corrosion was chosen for push-off testing, other methods may be considered in the future for the large scale experiments.

Electrochemical corrosion involves deterioration of a charged metal when it comes into contact with an electrolyte solution. Two half reactions occur during this

process; a cathodic and anodic reaction. The cathode, or the material to be corroded, is submerged in an electrolyte solution (which is typically acidic) during which its atoms dissolve into a moisture film, exposing the bare surface of the material. Next, a current must be applied to the target metal to transfer ions into the solution. Corrosion occurs when the anode, or a cation of a more-noble metal (such as stainless steel or copper), receives the electrons generated on the sample's surface (ASM-International 2000; Revie and Uglig 2008). This method offers a convenient way to achieve a desired section loss in a particular time frame by adjusting the magnitude of current impressed on the sample, as derived by Faraday's law. Equation 4 shows the equation used to calculate mass loss, where A_m is the atomic mass of the sample material (grams), I is the corrosion current (amperes), t is the required time for corrosion (sec), Z is the valence (taken as 2 for rust product of iron), and F is Faraday's constant (96,487 coulombs).

$$\Delta w = \frac{A_m I t}{ZF} \quad (4)$$

In order to gain confidence with the deterioration process, a formal experiment was conducted on a sample piece of steel that was also used as the base material for the push-off experiments. The experimental setup is shown in Figure 2.13. The bottom flange and lower portion of the web were submerged in a 5% NaCl (sodium chloride) solution, which served as the electrolyte. A piece of stainless steel, which served as the cathode, was also submerged in the solution. A positive current of 2 amperes was impressed onto the sample piece of steel, and the negative wire was attached to the piece of stainless steel to complete the circuit and allow electrons to flow. The mass loss and change in web and flange thickness were monitored as a function of time.

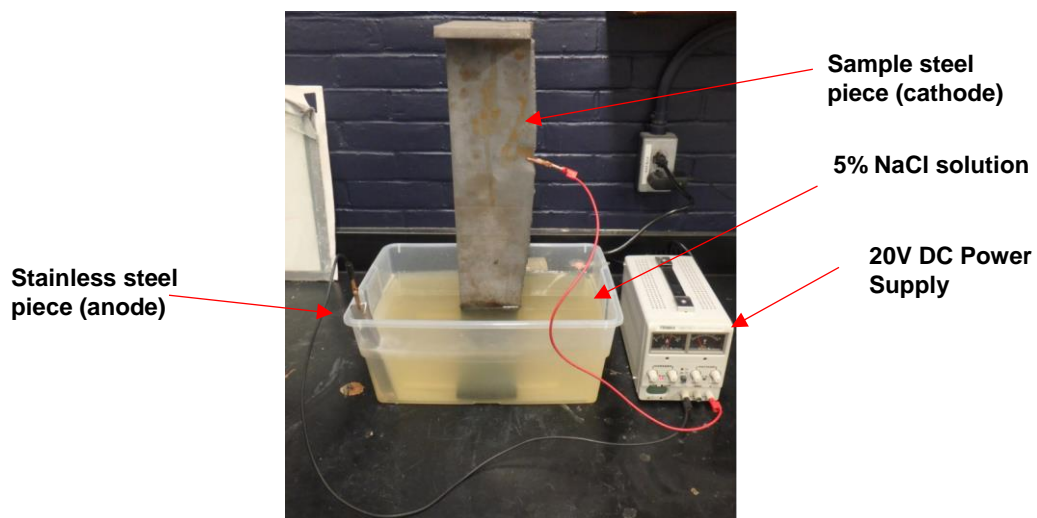


Figure 2.13: Experimental assembly of electrochemical corrosion test

Figure 2.14 shows the progression of section loss of a rolled-steel girder section due to electrochemical corrosion. Figure 2.15 shows the extent of corrosion and degree of section loss as a function of time. Over time, the solution became darker and black sludge accumulated at the surface, and eventually dropped to the bottom of the container. This sludge is the oxidized byproduct of the steel, which accumulates at the surface when in contact with oxygen. Throughout the duration of testing, the web experienced approximately 30% section loss in about 14 days, while the flanges thicknesses reduced by about 12%. The difference in section loss between the web and the flange stems from varying initial thicknesses. The entire specimen, however, experienced a constant mass loss of about 2.07 grams per hour, which is consistent with Faraday's theoretical mass loss of 2.04 grams per hour.

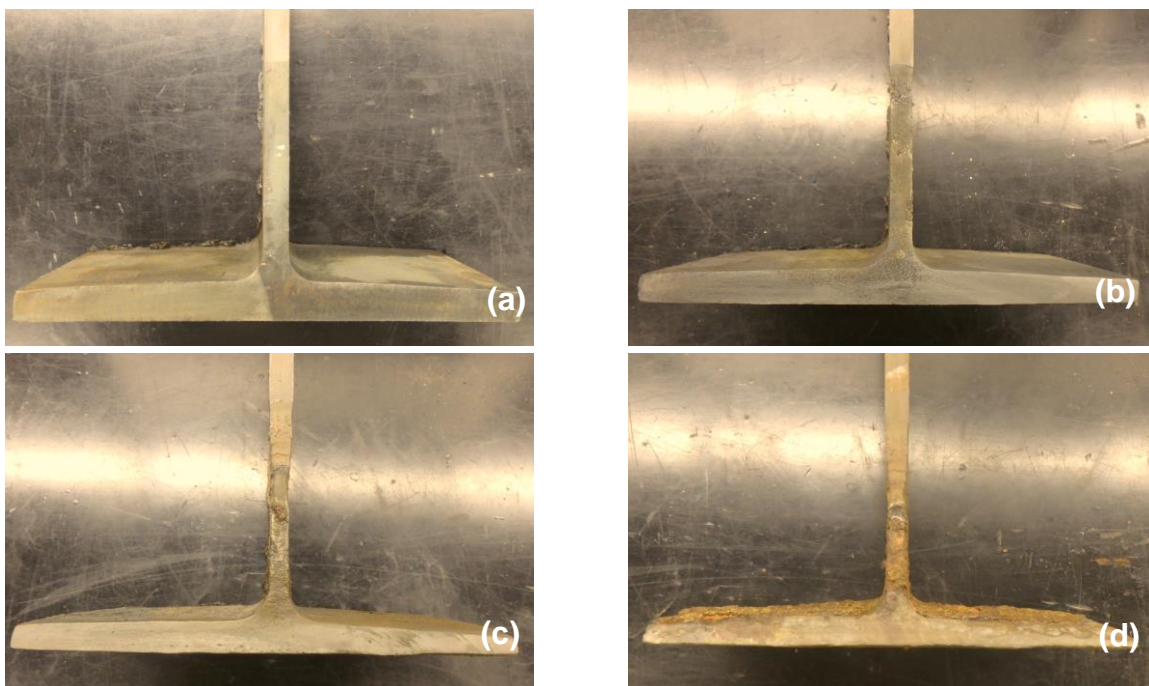


Figure 2.14: Corrosion at: (a) 0-hrs; (b) 42-Hrs; (c) 186-hrs; (d) 325-hrs

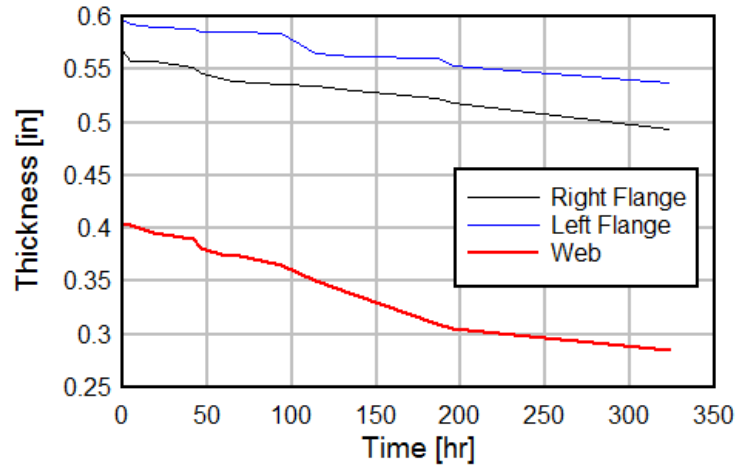


Figure 2.15: Steel Thickness vs. Time during Electrochemical corrosion

Electrochemical corrosion has been found as an effective way to test the durability of the UHPC repair method compare to steel girder sections. A push-off test will be conducted on a specimen exposed to electrochemical corrosion to investigate the effect of corrosion on the performance of the repair and the interaction between the girder web, the shear studs, and the UHPC repair panel.

3 Full-Scale Plate Girder Testing

A series of experiments will be conducted on full-scale plate girders. These tests will aim to determine the full-scale abilities of the repair method on plate girders with various repair geometries and configurations. The experimental setup for this test will be designed to accommodate the capacity of the plate girder specimens, the repair capacity, and the structures lab load frame. The load frame will be modified to increase its capacity.

3.1 SELECTION OF SPECIMEN

Complete data from the Connecticut bridge inventory was reviewed and summarized in Table 3.1. These entries accurately represent the larger selection of bridges, where the UHPC repair may be applicable. The bridges vary in year built, span length, number of spans, and ADT. A statistical approach was used to select 35 bridges to accurately represent the overall population. ProjectWise (CTDOT's project inventory) was used to collect drawings from each of the selected bridges. From the drawings, geometric information and common details were reviewed and summarized to be used in the creation of standard repair details. Generalized geometries were created for each structure type by combining the information from all of the selected designs. Typical plate girder designs were extracted for bridges built between the 1950s and 1960s which are currently reaching their design life.

Table 3.1: Selected plate girders (units: kip,in)

CT Bridge Number	Year Built	Web Thick	Beam Depth	D/t	Stiffener Spacing	d_0/D	K_{min}	V_{cr}	C_{el}	V_p	C	V_n
58a	1958	0.375	54	144.0	36	0.67	16.25	414	0.892	470	0.845	396.9
104d	1959	0.375	58	154.7	42	0.72	14.54	345	0.692	505	0.692	349.0
250	1958	0.4375	42	96.0	35.76	0.85	11.90	619	1.469	426	1.000	426.3
818	1963	0.375	52	138.7	36	0.69	15.43	408	0.914	452	0.855	386.7
956b	1960	0.375	60	160.0	42	0.70	15.20	349	0.676	522	0.676	352.9
3096	1965	0.375	62	165.3	54	0.87	11.59	257	0.483	539	0.483	260.3
Test	2016	0.375	52	138.67	40	0.77	13.45	356	0.796	452	0.796	360.2

3.2 PRELIMINARY FINITE ELEMENT MODELING

Relevant literature was reviewed on FE simulation of UHPC material and bridge girders. Literature on UHPC material properties was collected in order to affirm the most

accurate material property was used in Phase 1. Research suggests that the UHPC material from Phase 1 is the most comprehensive, but two additional materials will be further studied moving forward. Literature on modeling of plate and rolled girders was collected to provide detail on the elements, contact surfaces, and meshes used as well as potential limitations of the software.

Different options for the geometry of the full-scale plate girder specimen were studied based on the existing plate girder bridges from CT discussed in the previous section. Models were created to analyze performance of each of the designs. Preliminary controls were performed to verify the adequacy of the capacity of the anchor holes on the strong floor of the Structure Lab. The design of the experimental setup will be detailed in a following section.

Multiple modeling methods from Phase I were refined to decrease analysis time and increase reliability and accuracy. Major changes include how the shear studs, bearings, and load ram are modeled. These changes were implemented in the Phase I models and compared against the experimental data for validation. Modeling methods are currently finalized, but will be adjusted on an as needed basis. Models were created for the full-scale experimental test setup to verify failure modes and to ensure the limits of the system remained within the capacity of the load frame and structures lab.

An additional model was also created for CT Bridge #818 as it was the main bridge studied for the test specimen design. Models have also been created for this bridge with and without skew. Different designs and methodologies have been studied to ensure the models are accurate and efficient. Figure 3.1 shows a snap shot of the geometric model of full scale girders modeled after CT Bridge #818.

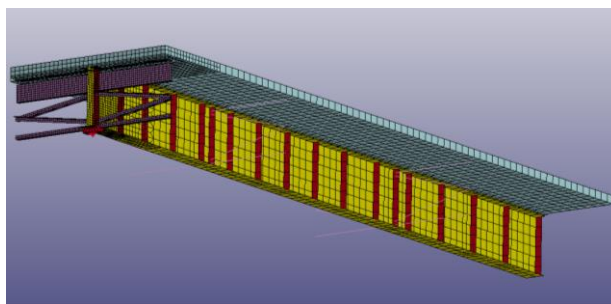


Figure 3.1: Full scale FE models of an interior girder from CT Bridge #818

3.3 DESIGN OF PLATE GIRDER SPECIMENS

For the second phase of this study, the UHPC repair will be experimentally tested on a typical plate girder design. Using the plate girders outlined in the previous section, dimensions were chosen for the plate girder design. The test specimens are 52 inch

deep (D) plate girders with a $3/8$ inch web (t_w). The width of the flanges (b_f) is 18 inch. The bottom flange has a thickness (t_{bf}) of 1 inch and the top flange has a thickness (t_{tf}) of 1.5 inch. The top flange had a larger thickness than the bottom flange in order to provide additional resistance from lateral torsional buckling (LTB), similar to a composite deck. The flanges were connected to the web with a $5/16$ inch weld. The plate girder specimens have two different size stiffeners. The web stiffeners were 6 inch wide and $3/8$ inch thick. The bearing stiffeners were 6 inch wide and $1/2$ inch thick. The cross section of the plate girder specimens is shown in Figure 3.2. Complete shop drawings of the plate girder specimens may be found in Appendix C.

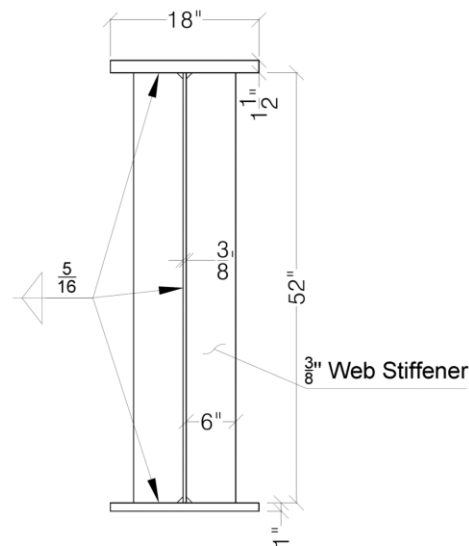


Figure 3.2: Cross Section of the Plate Girder Specimen

Calculations were completed to determine the shear strength of the specimen design. AASHTO (2012) Article 6.10.9.3 shear resistance equations for steel I-sections under flexure were used for the plate girder specimens. Table 3.1 shows the buckling ratio (K), elastic shear buckling capacity (V_{cr}), plastic shear resistance (V_p), elastic-plastic shear strength ratio (C_{el}), ratio of plastic shear strength (C), and nominal shear strength (V_n). The shear strength of the plate girder specimens was necessary for determining the anticipated maximum strength of the entire experimental system. The results of these calculations were compared to the results of the analytical FE models detailed in the following section.

In order to improve the efficiency of the experimental testing system, a splice connection designed to allow testing of multiple panels. This enabled the end test panel with corrosion damage to be interchangeable for each subsequent experiment, so that the entire plate girder will not need to be discarded after each test. The splice connection was placed directly after the web stiffener before the loading location. The splice was designed to carry the total plastic shear and moment capacity of the plate

girder. The splice connection was checked for shear and bearing of the bolts and yielding, rupture, and block shear of the web and flanges using the AISC Steel Construction Manual (AISC 2011). Preliminary finite element models were completed with and without the splice connection to ensure it did not have a detrimental effect on the performance of the plate girder. The results showed the load transfer through the end panel was not greatly affected by the splice connection. Figure 3.3 and Figure 3.4 show the design of the full-scale plate girder specimens with the splice connection. The final shop drawings for the plate girder specimens may be found in Appendix C.

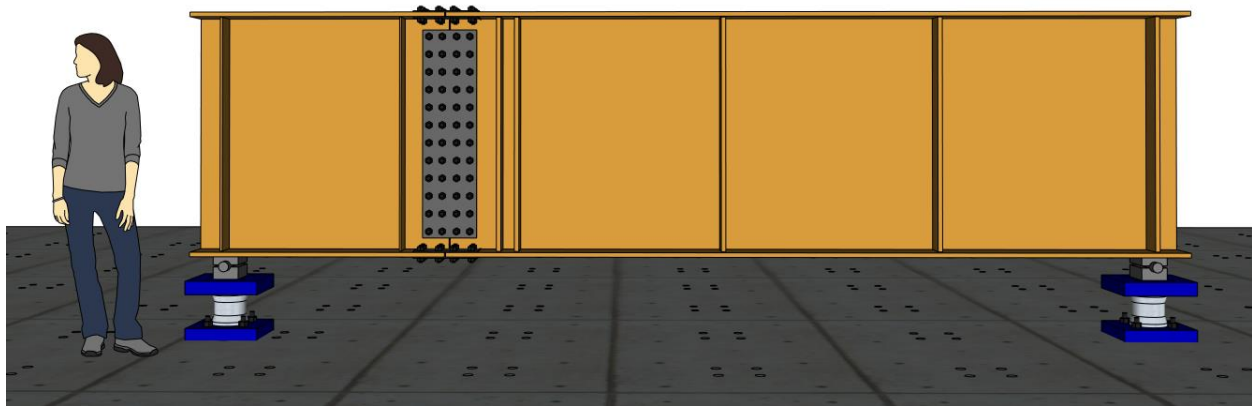


Figure 3.3: 3D rendering plate girder specimen for experimental testing with splice connection

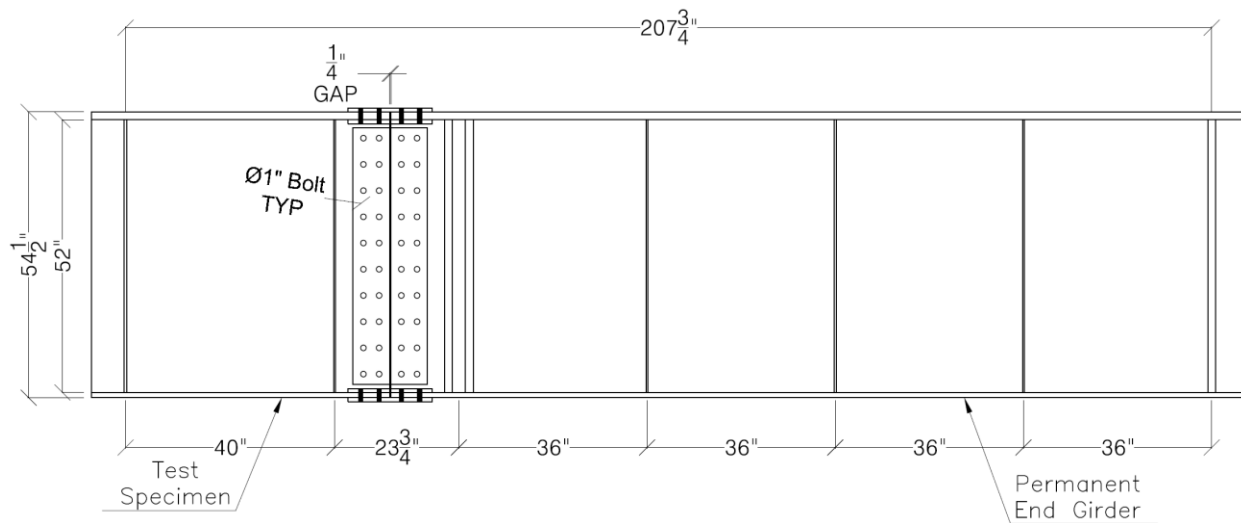


Figure 3.4: Plate girder specimen design for experimental testing

The plate girders were made from new, A36 steel plates purchased from Infra-Metals Co. in Wallingford, CT. The plate girders were fabricated by United Steel, Inc. from East Hartford, CT, who has extensive experience with fabrication of plate girders. Each specimen was fabricated with high quality craftsmanship. The specimens have

been delivered and are currently being prepared for testing. Figure 3.5 and Figure 3.6 show the plate girder specimens being fabricated and completed.

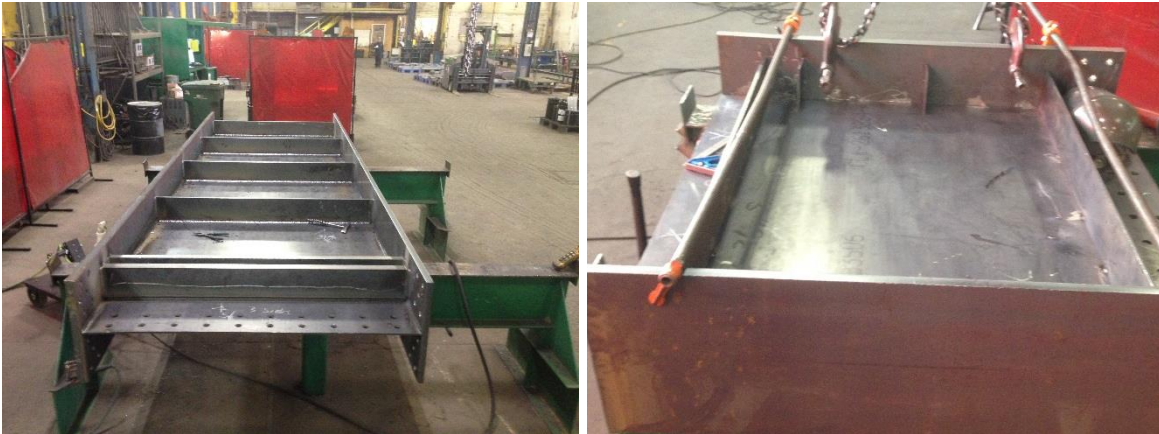


Figure 3.5: Fabrication of plate girder specimens by United Steel



Figure 3.6: Complete Plate Girder Specimens at United Steel in East Hartford, CT

Modification of the test specimens will commence beginning with the simulation of corrosion damage of the girder end. In phase one of this study, the corrosion damage was simulated by removing a uniform section of steel material through CNC milling. However, this was a limitation for the study because inspection reports show that corrosion damage is non-uniform and varies in depth and size. Therefore, for this study, corrosion section loss will be simulated by sandblasting the material at locations where corrosion typically occurs in order to create a more relevant experimental test. Sandblasting has been found as a capable method to remove steel material. It may be easily performed and is simple to monitor and control. Figure 3.7 shows a test steel beam end with section loss from sandblasting. Other methods such as electrochemical corrosion (which is being used for the push-off tests) may be unpredictable to achieve a desired section loss at precise locations for large-scale samples. Section 4 provides additional information on experimental and analytical corrosion test.



Figure 3.7: Simulation of corrosion damage by sandblasting steel beams

3.4 DESIGN OF TEST SETUP AND LOAD FRAME

The experimental testing for this research project will require more force demand than previous large-scale experimentation that has taken place at the University of Connecticut. Therefore, the large-scale test load frame in the UCONN Structures Laboratory has been modified and strengthened to achieve the desired capacity for this project. In phase one of this project, half-scale rolled girders were tested until failure. The existing load frame consisted of four 20-foot tall HP14x89 columns and a single W36x160 spreader beam; two sets of two columns were connected by welding HSS8x8x $\frac{1}{2}$ tubes in K-braces with the spreader beam connecting the two units as shown in Figure 3.8. Each column was tied into the UCONN Structures Lab with four $1\frac{1}{8}$ inch anchor rods secured to the 4-foot thick strong floor. This load frame setup was designed for a 500 kip Enerpac double-acting hydraulic load ram attached to the spreader beam which spanned 8 foot between two columns. The complete test setup for phase one is shown in Figure 3.9.

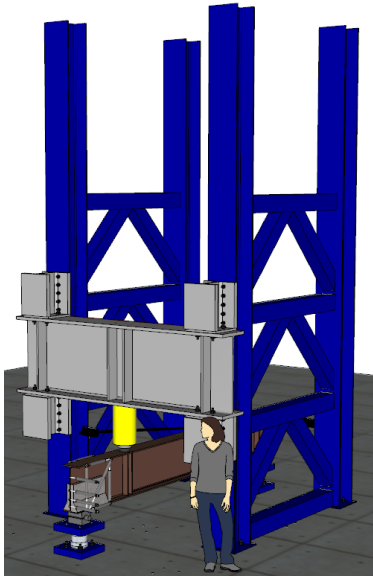


Figure 3.8: Rendering of Phase 1 Test Setup



Figure 3.9: Phase 1 completed test setup

The second phase of this research project required a much larger force range for testing. An Enerpac CLRG-50012 1,000 kip hydraulic load ram will be used for experimental testing of the plate girder specimens. Figure 3.10 shows the 1,000 kip and 500 kip Enerpac load rams. The controlling element from the existing setup was the tensile strength of the anchor rods. Since the existing spreader beam spanned between two columns, they placed a much higher demand on the anchor rods. For the new test setup three additional spreader beams will be added to the system to equally engage all four columns and clusters of anchor rods. Two spreader beams will span between the columns of the two units and a third beam will connect the two spreader beams. Depending on the desired capacity of the system, the load ram may be placed at several locations along the middle spreader beam. The static load capacity of the load frame will be 1,000 kip with a maximum bearing reaction force of 750-800 kips depending on the length of the test specimen. The load frame will also be modified to allow an MTS ASSY-244.41S Actuator to be mounted directly over the bearing of the plate girder to provide a dynamic load to simulate traffic. This actuator may apply a maximum force of 110 kip. A photo of the MTS Hydraulic Actuator is shown in Figure 3.11. Figure 3.12 shows a rendering of the new load frame design. Figure 3.13 shows the erected load frame in the UCONN Structures lab. AutoCAD drawings of the complete experimental test setup are shown in Appendix D.



Figure 3.10: Enerpac CLRG-25012 (500-kip) and 50012 (1,000-kip) Hydraulic Cylinder



Figure 3.11: MTS ASSY-244.41S Hydraulic Actuator for dynamic loading to simulate live load traffic

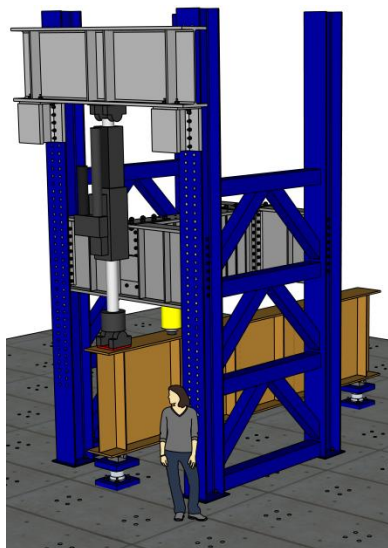


Figure 3.12: Rendering of Full-Scale Experimental Test Setup



Figure 3.13: Progress of Experimental Test Setup

Due to dimensional constraints the spreader beams were designed as plate girders. In order to improve the overall stiffness of the test setup, the spreader beams needed to

be deep while still fitting between the flanges of the columns. The spreader beams between the columns are 7'10" long and have a depth of 36 inch, a web thickness of 1 inch, a flange width of 11 inch, and a flange thickness of 1.5 inch. The cross spreader beam connecting the two spreader beams is 7'10" long and has a depth of 36 inch, a web thickness of 1.25 inch, a flange width of 16 inch, and a flange thickness of 1.5 inch. During phase I, reduced stiffness of the overall test setup affected the results of the tests because of slip in the load frame connections. Therefore, for this test, a Sherwin Williams Protective and Marine Coating was used on the load frame to provide a Class B slip coefficient with an acceptable coefficient of friction for slip critical condition. Calculations were completed to ensure that the entire testing system could withstand the demands of the experimental tests. The capacity of the floor bolts, beam connections, and spreader beams were designed and checked to provide adequate stiffness and strength during testing. The new spreader beams are shown in Figure 3.14. Shop drawings for the new load frame members are shown in Appendix E. The load frame assembly with the slip resistant paint applied is shown in Figure 3.15.



Figure 3.14: New plate girder spreader beams for the experimental test setup



Figure 3.15: Load frame plate girder assembly with slip resistant paint

3.5 INSTRUMENTATION

During the full-scale experimental tests, extensive instrumentation will be used to monitor the performance of each plate girder specimen. Force, displacement, strain, and temperature data will be collected for each individual test. The data will be collected to a single file using a high power and quality data acquisition system. The experimental

tests for the full-scale plate girders will require the collection of over 75 channels of data. To accommodate the increase in data collection, an HBM MGCplus will be used. This module is a high-channel count data acquisition system (DAQ) which will allow for the integration of a large number of sensors to collect a variety of different data parameters. This HBM DAQ is also compatible with other HBM devices such as the HBM MX1615B which will provide flexibility and versatility for collecting experimental data. Combining multiple HBM acquisition systems will improve the synchronization and compatibility of data collection during testing and during data analysis. The HBM software CatmanEasy will be used to collect the data.

Force will be measured throughout the experimental test using 6 degree of freedom load cells that have been designed and manufactured at the University of Connecticut during the first phase. These load cells will provide axial, shear, and moment reactions from each of the two bearings at each end of the plate girder specimens. Pressure transducers will be used to measure the pressure of the forward and return lines of the Enerpac Hydraulic load ram.

Displacement measurements will be collected using rod potentiometers, string potentiometers, and strain based displacement transducers. Novotechnik LGW series potentiometers will be widely used to record vertical displacement of the plate girder specimens, horizontal displacement of the plate girder web, rotation of the bearing, and other points of interest. String potentiometers will be used to measure and capture shear deformation of the plate girder specimen end panel. Tokyo Sokki Kenkyujo strain based displacement transducers will be used to capture the interaction between the UHPC repair panel and the plate girder web. This includes separation, out of plane displacement, and displacement of the repair panel.

The strain gauges which will be used are sold by Texas Measurements. These gauges will be used to measure vertical and shear strain in the web of the steel girder, flexural strain in the bottom flange, bearing strain in the stiffeners, bearing strain in the UHPC repair panel, and several other locations. Uniaxial, biaxial, and triaxial gauges will be used to measure these strain values. Internal bolt gauges will be used to measure the strain in shear studs connecting the UHPC repair panel to the web.

Strain measurements will also be taken using 3D Digital Image Correlation (DIC) of one side of the plate girder end panel. DIC is a photographic system with the ability of precisely tracking the position of a very large number of points (pixels) on a specimen during load testing. By tracking the movement of these points, DIC systems are capable of capturing full strain field distributions over the surface of the plate girder specimens and the UHPC repair panels. This system will significantly benefit the study by providing valuable information on the performance of the large-scale plate girder specimens

before and after the repair is applied. It will provide invaluable understanding regarding the transfer of load from the plate girder to the repair. 3D DIC systems are capable of capturing out of plane displacements and protrusions including buckling. The DIC system consists of two charge-coupled device (CCD) progressive scanner cameras along with full-spectrum LED lighting, ultra-low distortion lenses, and a mounting system. The surface of the specimen being tested should be painted with a speckle pattern in order to improve the software's ability to track points along the surface. Figure 3.16 shows the test setup of the 3D DIC system for a corroded beam test which will be explained in the next section.

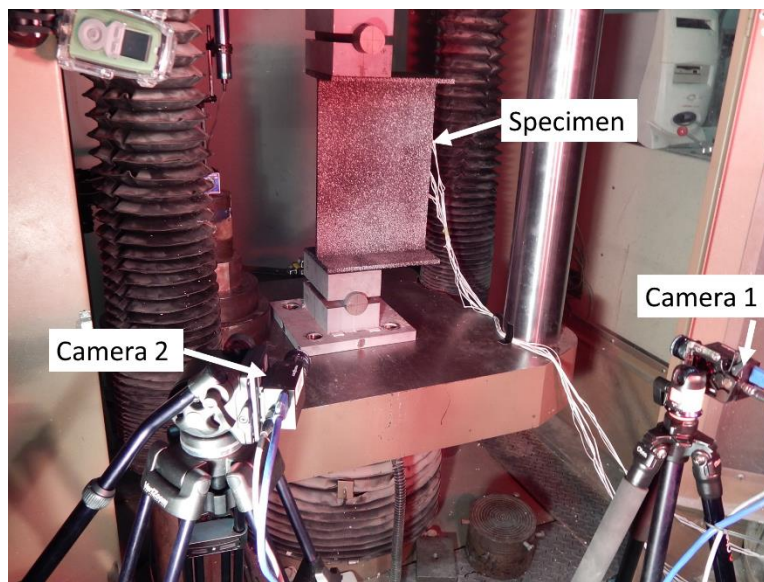


Figure 3.16: Setup of DIC cameras for experimental testing of corroded girders

Temperature gauges will also be used on the steel plate girder (foil type) and embedded in the UHPC repair panel (probes). These gauges will be used to monitor fluctuations in curing temperature from casting to testing.

4 Bearing Corrosion Analysis

4.1 3D SCANNER FOR CORROSION DETECTION

Research was conducted to determine the feasibility of using a 3D scanner to accurately measure the extent of corrosion damage. Corrosion damage is typically non-uniform in size, depth, and shape. However, field inspection reports typically record the maximum length, height, and depth of corrosion damage these may prove to be extremely conservative and inaccurate. 3D scanning corrosion damage could provide a precise depiction of the corrosion with millions of data points rather than taking selected measurements with a caliper and interpolating a surface between them. It allows for surface mapping of the scanned section to be imported into Finite Element software in order to create models with an accurate depiction of the geometry. A refined, accurate model is key to understanding the performance of the structure and determining the correct way to repair damage.

An Artec Eva 3D scanner was purchased (Figure 4.1). This scanner is capable of producing a complete 3D rendering of a scanned section with an accuracy of ≤ 0.5 -mm. The scanner is portable and may be used to measure corrosion damage of deficient, in-service bridges (Figure 4.2). This will allow engineers to determine the extent and pattern of corrosion damage in the field. For the experimental testing, this will allow for the replication of corrosion damage by removing similar volume and patterns of extreme damage from each of the experimental specimens (Figure 4.3). The damage may then be imported into finite element models to more accurately represent the specimens and capture their performance. The loss in section computed by the scanner could be used to more accurately predict girder capacity loss due to corrosion damage rather than current methods of field measurements and the assumption of a uniform reduction of cross sectional area. 3D scanning has the potential to be powerful tool for inspectors in measuring corrosion damage of structures in the field. The technology is accurate and provides a thorough understanding of the corrosion damage pattern and depth.



Figure 4.1: Artec Eva 3D Scanner



Figure 4.2: 3D Scanning using the Artec Eva

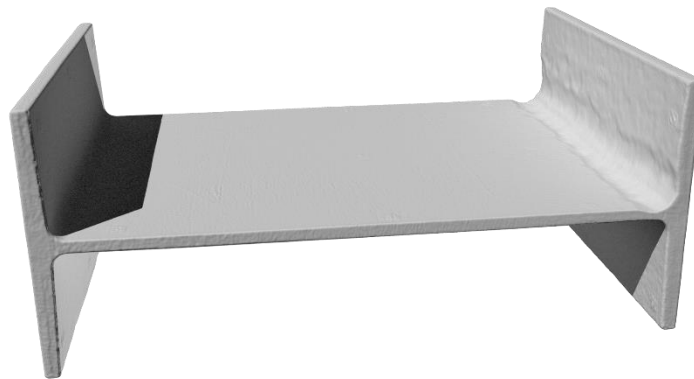


Figure 4.3: 3D point cloud of corroded girder

4.2 IMPORTING 3D SCAN DATA TO FINITE ELEMENT MODELS

To be able to accurately represent corrosion damage, methods are needed to accurately model non-uniform corrosion in Finite Element Models. Importing 3D scan data into finite element programs would provide an accurate geometry of the damaged section. Scans were taken of sections of corroded steel rolled girders from the old Q-Bridge in New Haven, CT. Several programs were used to convert the point cloud collected from the 3D scanner to a finite element mesh. Gmsh is open source software that was used to obtain finite element geometry from 3D scan data. An example of the finite element mesh is shown in Figure 4.4. A finite element simulation of the corroded section was run in Abaqus with the proper boundary conditions to determine the failure mode of the section. The deformed shape of the beam is shown in Figure 4.5 and Figure 4.6. The results of the model were found to be accurate as precise stress contours and buckling patterns were captured.



Figure 4.4: Finite Element 3D scanned mesh

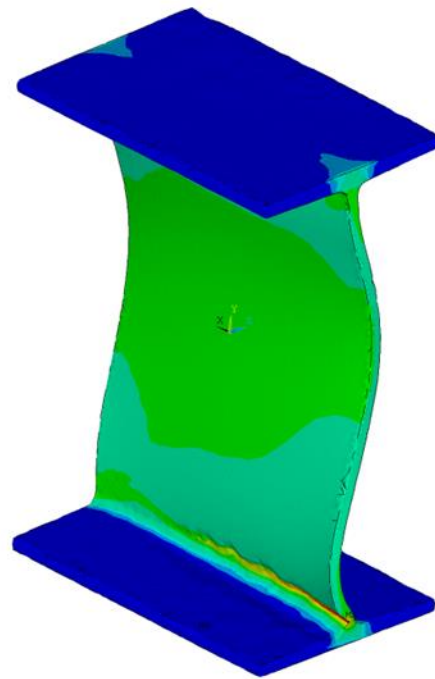


Figure 4.5: Overall deformed shape of the corroded steel girder

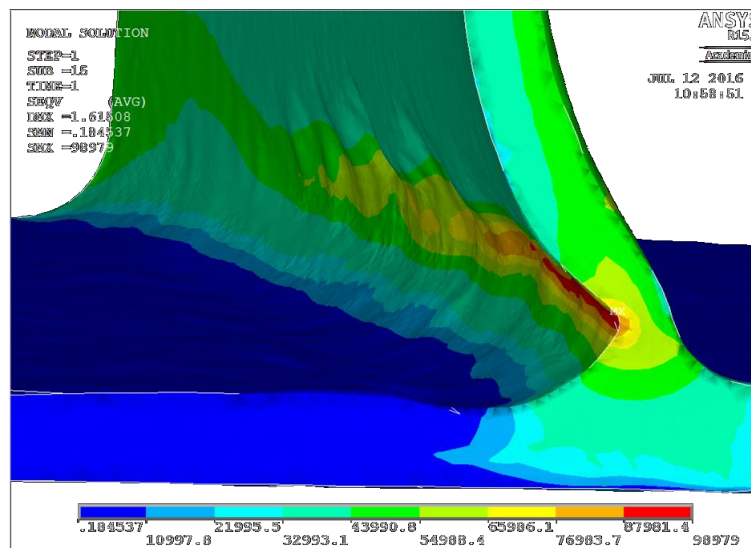


Figure 4.6: Stress contour of the corrosion damaged section of the steel girder

Additional beam sections were also scanned to acquire the exact geometry of the corroded section. Several changes were made to the finite element models for advanced analysis. A mass scaling sensitivity study was conducted to compare CPU time vs. deviation in the model. A parametric study was conducted to investigate deformed shape and load vs. displacement relationships to compare with upcoming experiment test that will be completed on the sections of corroded rolled-steel girders. The study varies element types and FEM characteristics. Hybrid models were also created for this study, which use only the 3D scanned geometry of the portion of the

girder with corrosion damage. The intact portion was replaced with an idealized model based on the geometry of the rolled-steel shape in order to improve computational efficiency. Figure 4.7 shows the finite element geometry with the scanned corroded area and the idealized geometry for the intact rolled-steel shape. Figure 4.8 shows the deformed shape of the girder section. Table 4.1 shows the progression of each of the four rolled-steel girder sections from the 3D scan to FEM geometry to analysis, and the results.

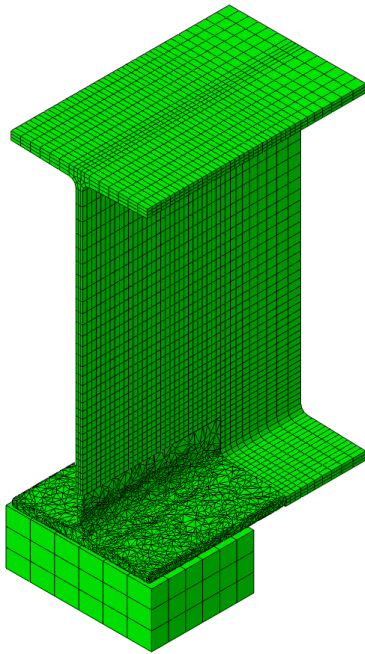


Figure 4.7: FE geometry with the scanned corroded area and the idealized geometry for the intact rolled-steel shape

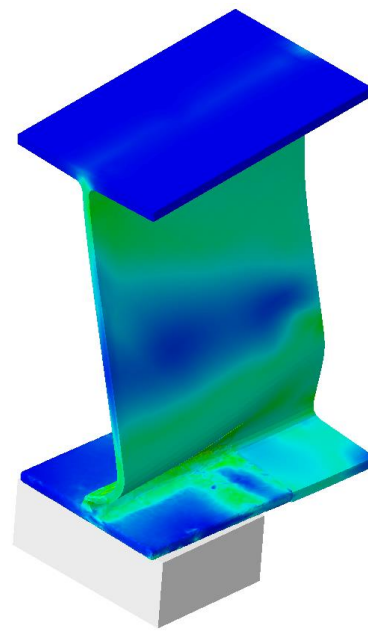



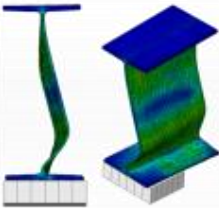
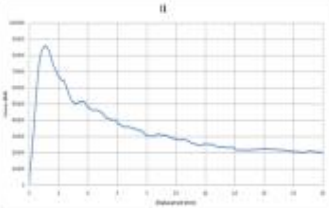



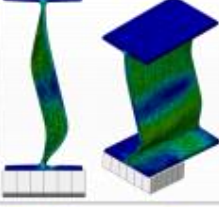
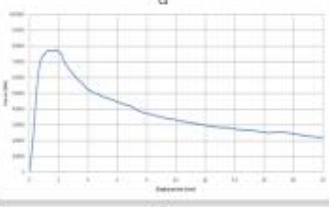



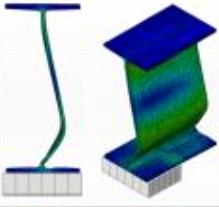
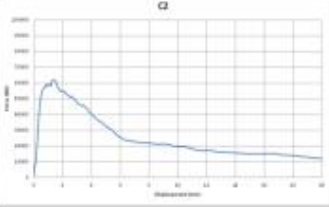



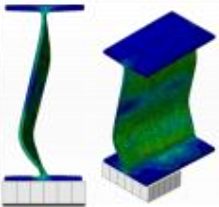
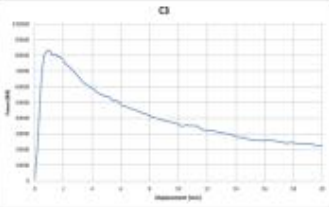


Figure 4.8: Deformed shape for corroded rolled-steel girder

Table 4.1: Steps for finite element analysis of corroded beams using 3D scanned geometry

Specimen	Picture	3D Scan	FEM	Deformed Shape	Force Displacement Relationship
Intact I1 Volume loss: 0 mm ³					
Corroded C1 Volume loss: 23536 mm ³					
Corroded C2 Volume loss: 39346 mm ³					
Corroded C3 Volume loss: 9508 mm ³					

4.3 EXPERIMENTAL TESTING OF CORRODED STEEL GIRDER SECTIONS

Experimental Tests will be conducted on the four corroded rolled-steel girder sections that were salvaged from the old Q-Bridge in New Haven, CT. The results of these tests will be used to validate the finite element models of the corroded girder sections. Similar results will show that the 3D scanned geometry of the corroded area could be used to accurately model to the structural section. The 3D DIC system explained in Section 3.5 will also be used to capture the strain field on the surface of the girder under loading. The results from the DIC will be used to compare with the results of the finite element models. Figure 4.9 shows the layout for the experimental testing of the corroded girder specimens. A bearing load was applied directly at the location of maximum corrosion of the beam. Two roller bearings were used to apply the load to the rolled girder.

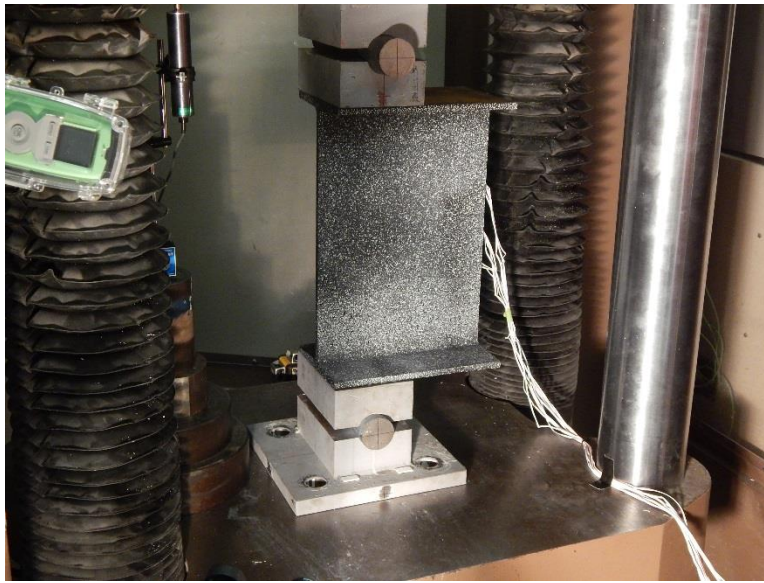


Figure 4.9: Experimental test setup for corroded beam ends

5 Design of Field Repair

Representatives from the University of Connecticut, Connecticut Department of Transportation, CME Associates, and GM2 Associates are working together to coordinate and design a field repair for Bridge No. 03094 in New Haven, CT using UHPC encasement. Several meetings were held to discuss the scope of the project, delegation of tasks, logistics, and the complete design. It was decided to begin the preliminary design for the bridge using UHPC to encase the corroded beam ends. The material presented below details the development of design guidelines, a set of calculations for the repair capacity and stud strength, and design drawings.

5.1 BRIDGE NO. 3094 IN NEW HAVEN, CT

Bridge No. 3094, constructed in 1965, is located in New Haven, CT. The bridge carries I-91 Northbound and Southbound over an Amtrak Railroad (AI-Engineers 2016; CME 2015). The bridge is located between exits 7 and 8. The bridge has a rolled-steel girder superstructure with a reinforced concrete deck with four simply supported spans. The span lengths vary due to a variety of different skew angles. The substructure consists of two reinforced concrete abutments and three reinforced concrete piers. The bearings are elastomeric expansion bearings and steel fixed bearings. Figure 5.1 shows Bridge No. 03094.



Figure 5.1: Bridge No. 03094 in New Haven, CT, servicing I-91 over Amtrak Railroad

Field inspection of the bridge superstructure showed that the girders are in poor condition as the girder ends exhibit extensive rust. The webs have a maximum section loss of 5/16 inch and the bottom flange has a maximum section loss of 1/4 inch. This resulted in a maximum bearing capacity loss of 58.3% and a maximum shear capacity loss of 21%. Figure 5.2 shows portions of the corrosion damage to girder ends. The superstructure was deemed structurally deficient and requires extensive repairs for corrosion damage.



Figure 5.2: Severe corrosion damage of girder ends

Repairs of the I-91 Bridge will occur over night with only temporary lane closures to minimize traffic disruption. All repair operations will be coordinated with Amtrak. This will likely limit the duration and extent of closures while work is completed. CME Associates completed a rehabilitation study to determine the proper course of action for repairing this structurally deficient bridge. Recommendations were provided to use UHPC encasement to repair the corroded girder ends. This repair option was recommended over the conventional method of plated steel repair because of lower cost estimates, shorter construction duration and lane closures, and lower impact to the railroad traffic.

5.2 DESIGN METHODS TO DETERMINE REPAIR CAPACITY

Three different design methods were studied for the repair of corroded beam ends with UHPC encasement: Strength Design, Fatigue Design, and Capacity Design. These methods were completed to determine the number of shear studs needed to restore adequate capacity. Complete calculations for all design methods may be found in Appendix F.

Strength Design

The Strength Design method was used to determine the number of studs needed for the repair. This could be done for two different situations: 1) Live Load only, HL-93, where the Dead Load is carried by the remaining steel section, or 2) Strength 1 design where the studs are designed to carry all gravity loads applied to the beam. For the live load only case, the total shear carried by the repair panel was taken as the HL-93 loading multiplied by the dynamic load factor of 1.75. This particular design method generated the lowest design capacity. This method may be used in situations where it is difficult to weld studs and/or when the repair is only temporary and is not necessary to over design the repair. The second controlling scenario would follow the Strength I design where the shear studs are designed to carry all gravity loads applied to the girder. For this design method, the shear demand on the girder end was calculated for dead load (both components and wearing components) and live load based on load factors and load combinations from the AASHTO Bridge Design Code (AASHTO 2012). The shear demand for strength design was determined based on distribution factors of both live load and dead load for exterior beams, interior beams, skewed, beams, and additional components. Shear demands at girder end calculations are shown in Appendix F.

Fatigue Design

The second method for the design of the repair method was the fatigue design of the shear studs welded to the web of the girder. The shear studs are designed to carry shear and bearing forces from the girder to the UHPC repair panel. Due to live load traffic over the bridge, the shear studs are expected to experience extensive cycles of loading which may lead to fatigue failure. Based on the number of cycles the shear studs will experience (based on ADT of the bridge), fatigue design may be used to verify the strength of the shear studs. AASHTO's fatigue design for shear connectors was used to determine the fatigue capacity of each shear stud (AASHTO 2012). The fatigue demand load was determined according to AASHTO for a fatigue wheel load and the fatigue truck. The number of studs needed to provide acceptable fatigue strength of the repair was higher than for basic strength performance of the repair. Therefore, for situations where the bridge experiences a high volume of traffic or where the repair has

a longer design life, fatigue strength of the repair is the controlling factor. Fatigue capacity calculations for shear studs are shown in Appendix F.

Capacity Design

Capacity design may be used to design the UHPC repair to restore the original as-built bearing and shear capacity of the girder end. For this type of capacity based design, the bearing and shear capacity of a new, uncorroded girder end must be determined. The compressive bearing strength of a girder end may be determined by the cross section of the web and bearing stiffeners at the girder end, as they create an effective column section which carries bearing loads to the bearing and substructure. The shear capacity of the girder may be determined by the effective web area and the end panel shear strength. Capacity design is the most conservative design method. This method restores the capacity of the corroded girder end to the original capacity of an uncorroded girder. This design would have the largest number of studs and may lead to constructability issues for tight spaces. Shear and bearing capacity calculations for girder ends are shown in Appendix F.

5.3 DESIGN OF GIRDER END UHPC REPAIR

The design for each girder is based on the number of shear studs needed to provide sufficient capacity. There is no requirement for the pattern or placement of shear studs on the web of the girders. The only requirement is that the studs be welded to the uncorroded portions of the web. The studs should not be spaced closer than $3d_b$, where d_b is the diameter of the stud shank. This drastically simplifies field application of the repair because welding contractors do not need to individually measure and mark out the location of each stud. They only need to verify that the correct numbers of studs are welded to the web with sufficient spacing. Recommendations may be provided on placement to avoid back-to-back studs on the web. This would improve the load transfer path from the web, through the studs, and to the UHPC repair panel. The results of the push-off tests validate the flexibility of stud spacing and location to generate the desired stud capacity. Further tests are required to verify this design parameter, but current results satisfy this design. Figure 5.3 shows the design for the potential shear stud layout on the web of a corroded girder end. The location and spacing of the studs could vary for different repairs. Figure 5.4 shows the full height UHPC repair which encases the bearing stiffeners and the corroded web and flange. Sample Design drawings for the UHPC repair of Bridge No. 3094 may be found in Appendix G.

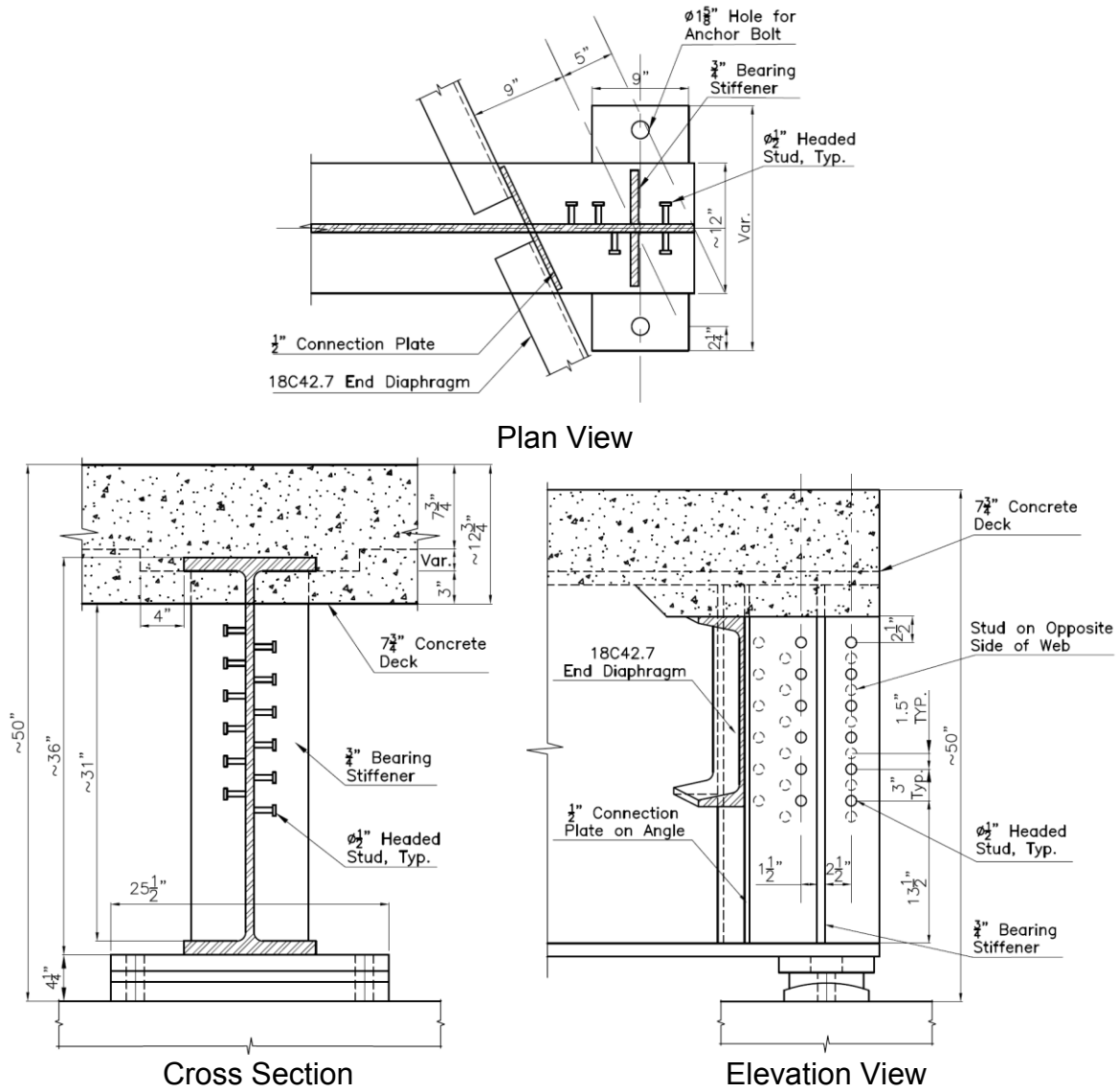


Figure 5.3: Design of potential shear stud layout for a corroded girder end

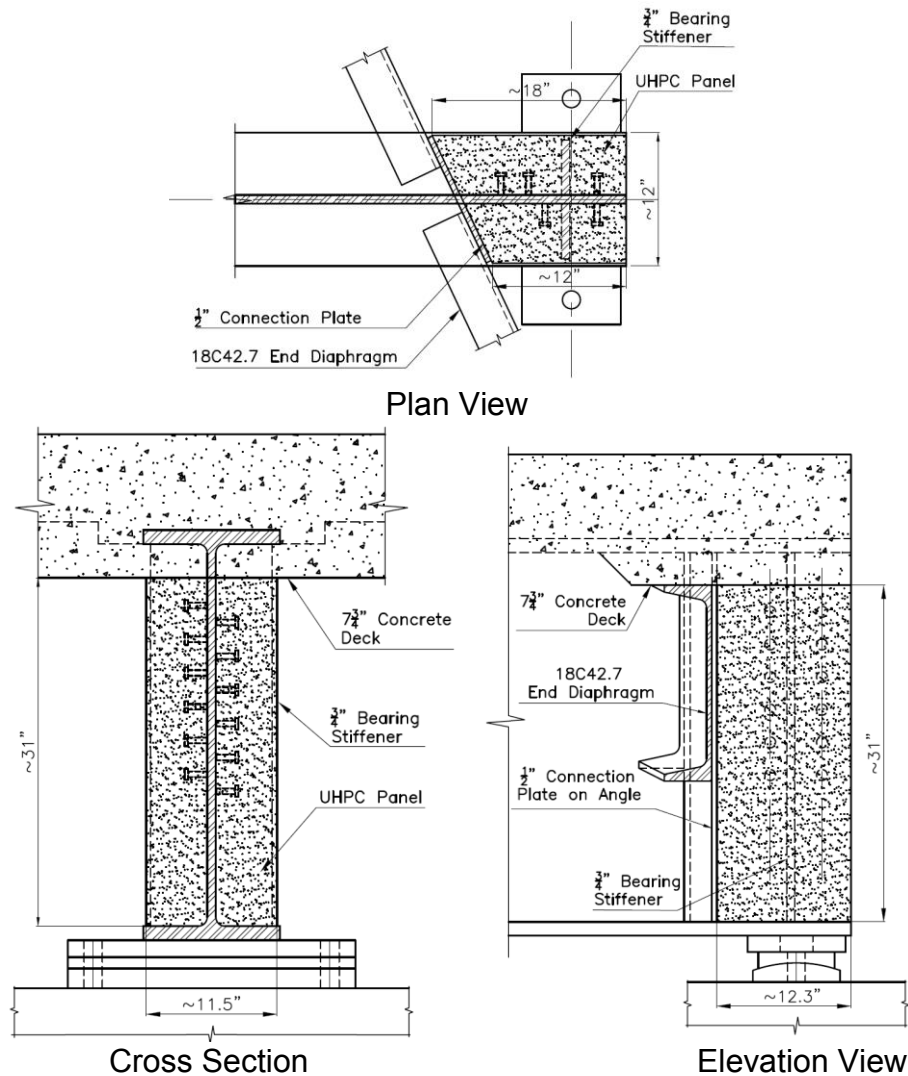


Figure 5.4: Proposed UHPC repair panel for corroded steel girder

Finite Element models of the complete bridge will be created to determine how the UHPC repair affects the performance of the bridge under live load. The model will include the girder with all stiffeners, cross bracing, composite deck, and bearings. The model will be simplified to improve the efficiency by providing geometric symmetry and realistic boundary conditions. Figure 5.5 shows the finite element model-create for Bridge No. 3094.

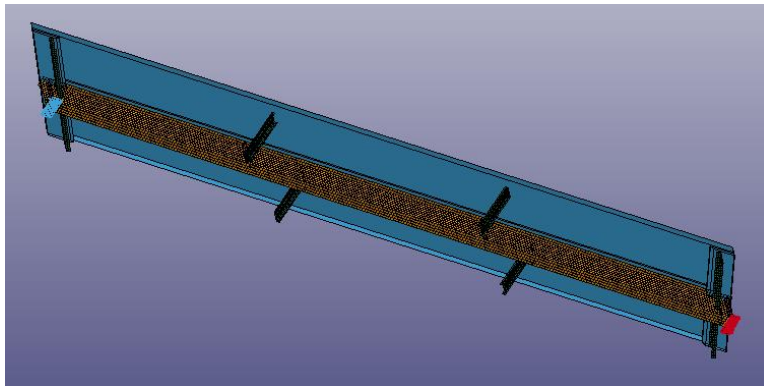


Figure 5.5: Finite Element model of Bridge No. 3094

REFERENCES

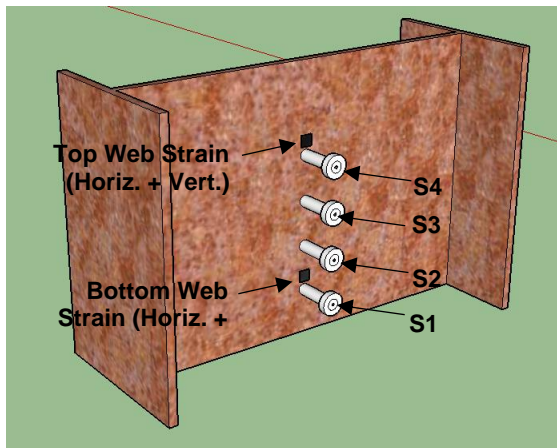
- AASHTO (2012). *AASHTO LRFD Bridge Design Specifications*, American Association of State Highway and Transportation Officials, Washington, DC 20001.
- Abbas, S., Nehdi, M. L., and Saleem, M. A. (2016). "Ultra-High Performance Concrete: Mechanical Performance, Durability, Sustainability, and Implementation Challenges." *International Journal of Concrete Structures and Materials*, 10(3), 271-295.
- Ahn, J.-H., Kainuma, S., and Kim, I.-T. (2013). "Shear Failure Behaviors of a Web Panel with Local Corrosion Depending on Web Boundary Conditions." *Thin-Walled Structures*, 73, 302-317.
- Ahn, J.-H., Kainuma, S., Yasuo, F., and Takehiro, I. (2013). "Repair Method and Residual Bearing Strength Evaluation of a Locally Corroded Plate Girder at Support." *Engineering Failure Analysis*, 33, 398-418.
- AI-Engineers (2016). "Routine and Special Inspection: Bridge No. 03094." Connecticut Department of Transportation, New Haven, CT. January 26, 2016.
- AISC (2011). "Steel Construction Manual." American Institute of Steel Construction. Fourteenth Edition.
- Albrecht, P., and Hall Jr, T. T. (2003). "Atmospheric Corrosion Resistance of Structural Steels." *Journal of Materials in Civil Engineering*, 15, 2-24.
- ASCE (2014). "2013 Report Card for America's Infrastructure." American Society of Civil Engineers.
- ASM-International (2000). "Introduction and Overview of Electrochemical Corrosion." *Fundamentals of Electrochemical Corrosion*.
- Brockenbrough, R. (2002). "AISC Rehabilitation and Retrofit Guide." American Institute of Steel Construction, Pittsburgh, PA.
- Chang, L. M., and Lee, Y.-J. (2001). "Evaluation and Policy for Bridge Deck Expansion Joints." Indiana Department of Transportation and Federal Highway Administration. Purdue University. SPR-2198.
- Classen, M., Gallwoszus, J., and Stark, A. (2016). "Anchorage of Composite Dowels in UHPC Under Fatigue Loading." *Structural Concrete*, 17(2), 183-193.
- Close, J., and Miller, P.C. (2011). "Preliminary Design Report - Putnam Bridge, Bridge NO. 00417." Connecticut Department of Transportation. Glastonbury and Wethersfield. Project No. 53-175.
- CME (2015). "Rehabilitation Study Report: Bridge No. 03094 in New Haven." Connecticut Department of Transportation. CME Associates, State Project No. 92-675. New Haven, CT.
- Elnashai, A. S., Takanashi, K., Elghazouli, A. Y., and Dowling, P. J. (1991). "Experimental Behaviour of Partially Encased Composite Beam-Columns Under Cyclic and Dynamic." *Proceedings Institute of Civil Engineers*, 2(91), 259-272.
- Esmaili Zaghi, A., Wille, K., Zmetra, K., and McMullen, K. (2015). "Repair of Steel Beam/Girder Ends with Ultra High Strength Concrete (Phase I)." Connecticut Department of Transportation. University of Connecticut. SPR-2282(Report #CT-2282-F-15-2).
- Eurocode-4 (2004). "Design of Composite Steel and Concrete Structures." European Committee for Standardization., Brussels, Belgium.
- Feldmann, M., Hechler, O., and Hegger, J. (2011). "Fatigue Behavior of Shear Connectors in High Performance Concrete." *Composite Construction in Steel and Concrete VI*, 310-321.
- FHWA (2014). "Bridges By Structure Type." <<http://www.fhwa.dot.gov/bridge/struct.cfm>>.
- FLDOT (2011). "Bridge Maintenance and Repair Handbook." *Steel Beam & Girder Repair*, Florida Department of Transportation. 4.6, 78-83.

- Graybeal, B. (2014). "Design and Construction of Field-Cast UHPC Connections." Federal Highway Administration. FHWA-HRT-14-084.
- Grünberg, J., Lohaus, L., Ertel, C. W., and Wefer, M. "M.: Multi-Axial and Fatigue Behaviour of ultra-high-performance concrete (UHPC)." *Proc., Proceedings of the 2nd International Symposium on Ultra-High Performance Concrete*.
- He, J., Liu, Y., Chen, A., and Yoda, T. (2012a). "Shear behavior of partially encased composite I-girder with corrugated steel web: Experimental study." *Journal of Constructional Steel Research*, 77, 193-209.
- He, J., Liu, Y., Lin, Z., Chen, A., and Yoda, T. (2012b). "Shear behavior of partially encased composite I-girder with corrugated steel web: Numerical study." *Journal of Constructional Steel Research*, 79, 166-182.
- Hegger, J., Sedlacek, G., Döinghaus, P., Trumpf, H., and Eligehausen, R. "Studies on the ductility of shear connectors when using high-strength steel and high-strength concrete." *Proc., International Symposium on Connections between Steel and Concrete, University of Stuttgart*, 1025-1045.
- Hyashi, K., Ono, S., and Nakamura, S. (2003). "Experimental Studies on Retrofit by Partially Encased Concrete to the Steel I-Girder Subjected to Buckling Deformation." *Technical Memorandum of Public Works Research Institute*(3920), 229-236.
- Kayser, J. R., and Nowak, A. S. (1989). "Capacity Loss Due to Corrosion in Steel-Girder Bridges." *Journal of Structural Engineering*, 115(6), 1525-1537.
- Khurram, N., Sasaki, E., Katsuchi, H., and Yamada, H. (2014b). "Experimental and Numerical Evaluation of Bearing Capacity of Steel Plate Girder Affected by End Panel Corrosion." *International Journal of Steel Structures*, 14(3), 659-676.
- Khurram, N., Sasaki, E., Kihira, H., Katsuchi, H., and Yamada, H. (2014a). "Analytical Demonstrations to Assess Residual Bearing Capacities of Steel Plate Girder Ends with Stiffeners Damaged by Corrosion." *Structure and Infrastructure Engineering*, 10, 69-79.
- Kim, J. S., Kawark, J., Joh, C., Yoo, W., and Lee, K. (2015). "Headed stud shear connector for thin ultra-high performance concrete bridge deck." *Journal of Constructional Steel Research*.
- Koch, G. H., Brongers, M. P., Thompson, N. G., Virmani, Y. P., and Payer, J. H. (2002). "Corrosion Cost and Preventive Strategies in the United States." Federal Highway Association & CC Technologies Laboratories, Inc. NACE International. FHWA-RD-01-156.
- Lam, D., and El-Lobody, E. (2005). "Behavior of Headed Stud Shear Connectors in Composite Beam." *Journal of Structural Engineering*. ASCE.
- Li, A., and Kristen, C. (1996). "Push-out tests on studs in high strength and normal strength concrete." *Journal of Constructional Steel Research*.
- Liu, C., Miyashita, T., and Nagai, M. (2011). "Analytical Study on Shear Capacity of Steel I-Girders with Local Corrosion Nearby Supports." *Procedia Engineering*, 14, 2276-2284.
- Miyashita, T., Wakabayashi, D., Hidekuma, Y., Kobayashi, A., Okuyama, Y., Koide, N., Horimoto, W., and Nagai, M. "CFRP Repair Method for Corroded Steel Girder Ends." *Proc., IABSE Symposium Report, International Association for Bridge and Structural Engineering*, 1-7.
- Miyashita, T., Wakabayashi, D., Hidekuma, Y., Kobayashi, A., Okuyama, Y., Koide, N., Horimoto, W., and Nagai, M. "Repair Method for Corroded Steel Girder Ends using CFRP Sheet." *Proc., IABSE-JSCE Conference on Advances in Bridge Engineering, International Association for Bridge and Structural Engineering*, 1-7.
- Nakamura, S., Momiyama, Y., Hosaka, T., and Homma, K. (2002). "New Technologies of Steel/Concrete Composite Bridges." *Journal of Construction Steel Research*, 58, 99-130.
- Nakamura, S., and Narita, N. (2003). "Bending and Shear Strength of Partially Encased Composite I-Girders." *Journal of Constructional Steel Research*, 59, 1435-1453.

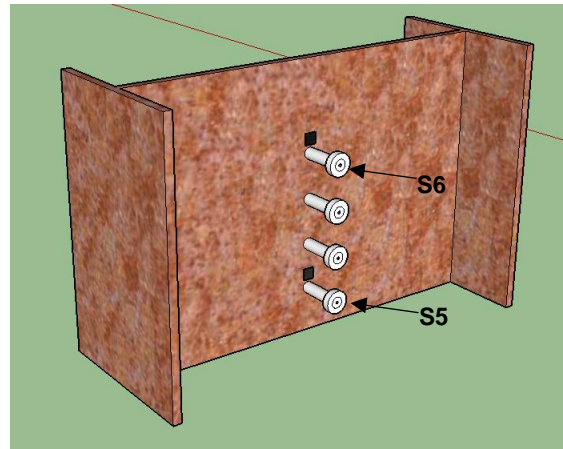
- Ogami, H., Fujii, K., Yamada, T., and Iwashaki, H. (2015). "Renovation of Corroded Girder End in Plate Girder Bridge with Resin and Rebars." *Implementing Innovative Ideas in Structural Engineering and Project Management*, ISEC Press, 1-6.
- Revie, R. W., and Uglig, H. H. (2008). "Corrosion and Corrosion Control: An Introduction to Corrosion Science and Engineering." Wiley Interscience.
- Rossow, M. (2003). "FHWA Bridge Maintenance: Superstructure." Continuing Education and Development, Inc., Federal Highway Association.
- Russell, H., and Graybeal, B. (2013). "Ultra-High Performance Concrete: A State-of-the-Art Report for the Bridge Community." Federal Highway Administration, McLean, VA. FHWA-HRT-13-060.
- Shaheen, E., and Shrive, N. (2008). "Cyclic Loading and Fracture Mechanics of Ductal Concrete." *Springer Science & Business Media*.
- Shi, X., Fay, L., Yang, Z., Nguyen, T. A., and Liu, Y. (2009). "Corrosion of Deicers to Metals in Transportation Infrastructure: Introduction and Recent Developments." *Corrosion reviews*, 27(1-2), 23-52.
- Usukura, M., Yamaguchi, T., Suzuki, Y., and Mitsugi, Y. "Strength Evaluation for a Corroded Damaged Steel Girder End Considering its Collapse Mechanism." *Proc., Proceedings of the Thirteenth East Asia-Pacific Conference on Structural Engineering and Construction (EASEC-13)*.
- Van de Lindt, J., and Pei, S. (2006). "Buckling Reliability of Deteriorating Steel Beam Ends." *Electronic Journal of Structural Engineering*(6), 1-7.
- Wipf, T. J., Fanous, F. S., Klaiber, F. W., and Eapen, A. S. (2003). "Evaluation of Appropriate Maintenance, Repair, and Rehabilitation Methods for Iowa Bridges." Iowa Department of Transportation. Iowa State University. Project TR-429.
- WisDOT (2015). "Bridge Manual: Ch. 40 - Bridge Rehabilitation." *Superstructure Inspection*, Wisconsin Department of Transportation. 40.14, 24-26.
- Yamaguchi, E., and Akagi, T. "Degradation of Load-Carrying Capacity of Steel I-Girder End due to Corrosion." *Proc., Proceedings of the Thirteenth East Asia-Pacific Conference on Structural Engineering and Construction (EASEC-13)*.
- Yaun, J., and Graybeal, B. (2014). "Bond Behavior of Reinforcing Steel in Ultra-High Performance Concrete." Federal Highway Administration. FHWA-HRT-14-090.
- Zmetra, K. (2015). "Repair of Corrosion Damaged Steel Bridge Girder Ends By Encasement in Ultra-High Performance Concrete." Ph.D., University of Connecticut Storrs, CT.
- Zmetra, K., Zaghi, A., and Wille, K. (2015). "Rehabilitation of Steel Bridge Girders with Corroded Ends Using Ultra-High Performance Concrete." *Structures Congress 2015*, 1411-1422.

APPENDIX A Experimental Push-Off Data

A1 GRAPH TERMINOLOGY

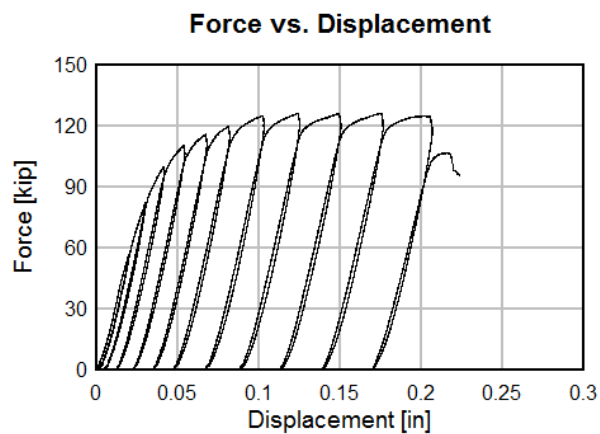


Front Side

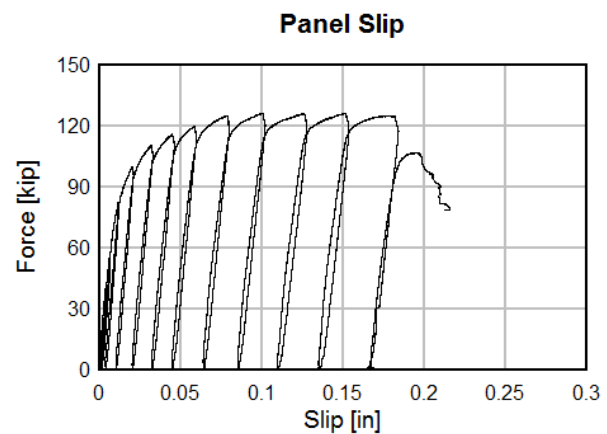


Back Side

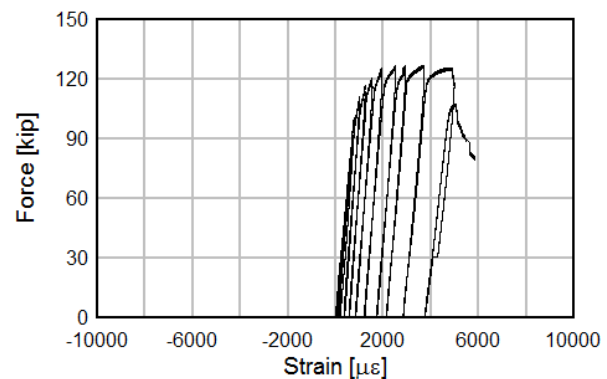
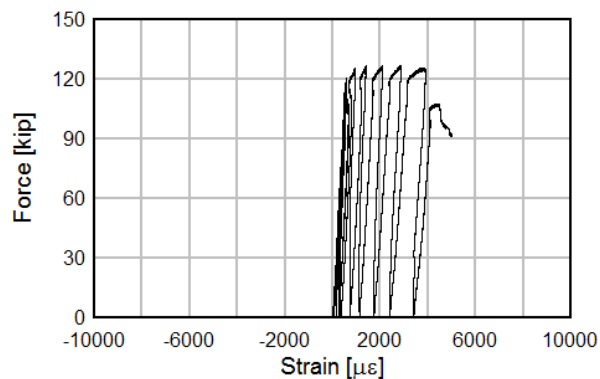
A2 S1-8-2-NS-1/2 – BENCHMARK SPECIMEN

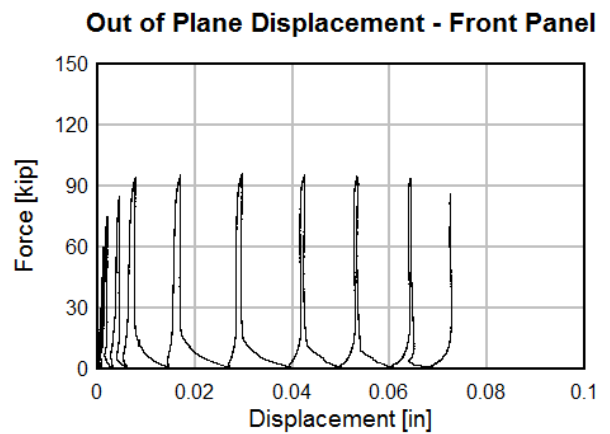
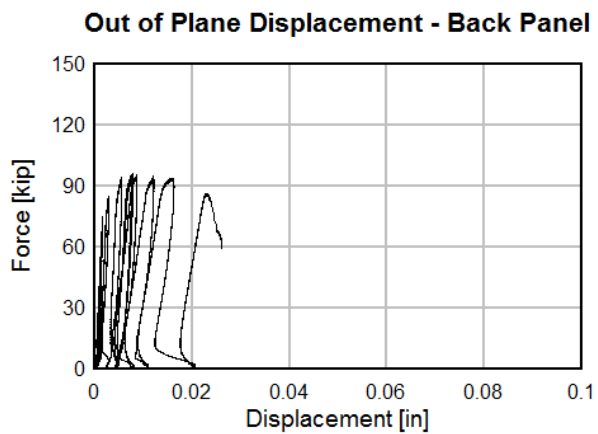
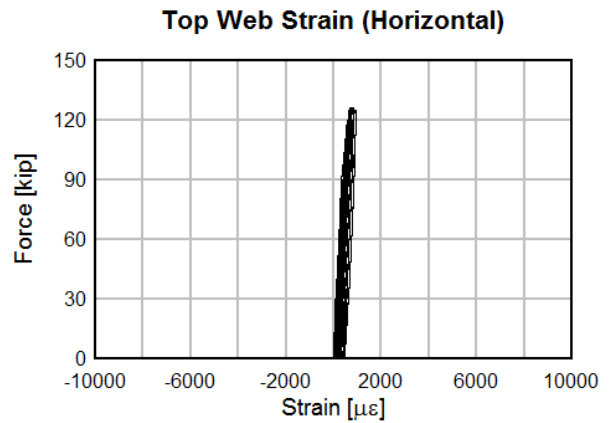
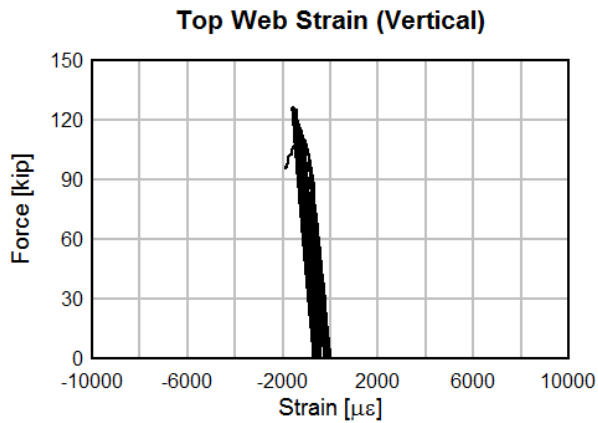
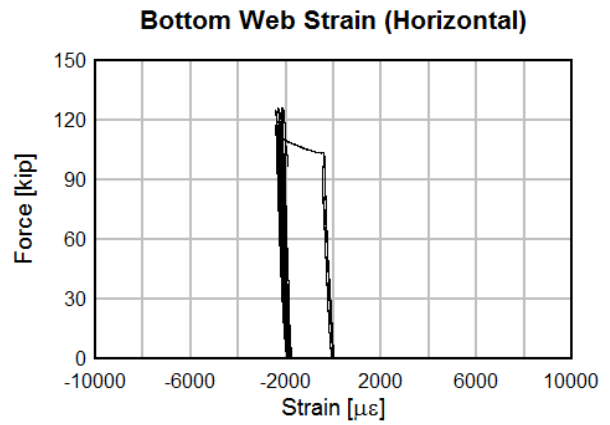
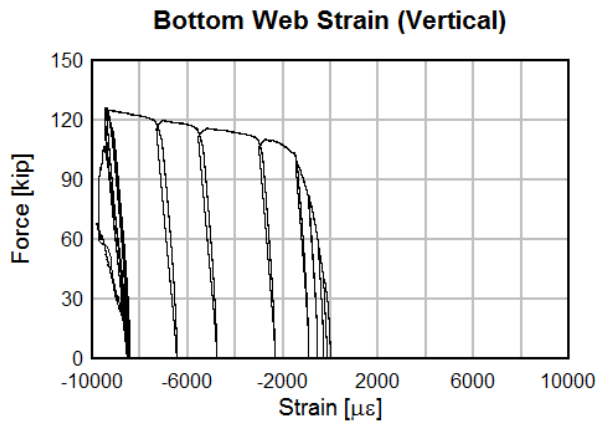
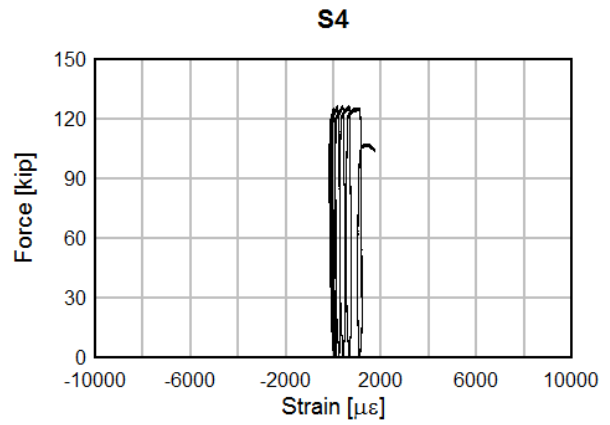
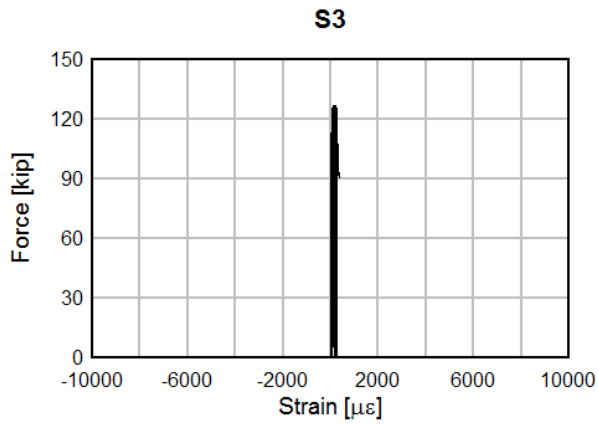


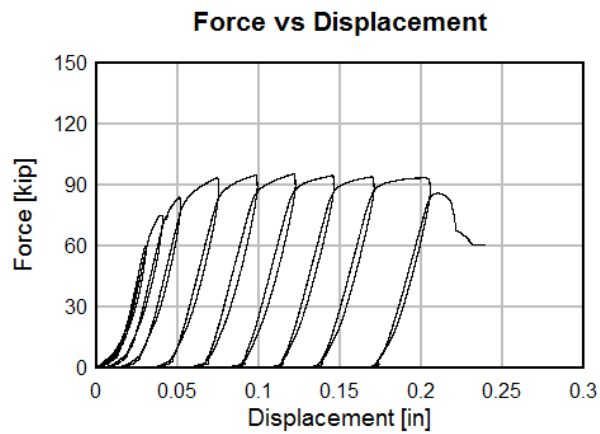
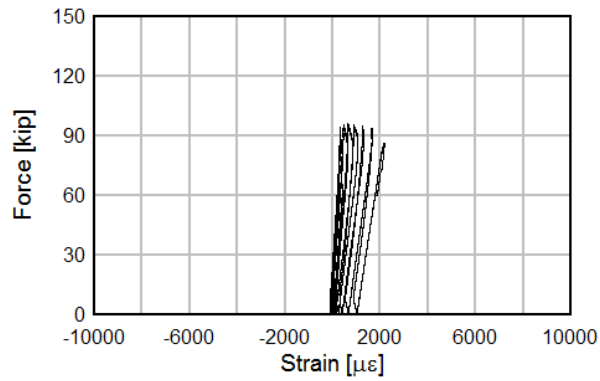
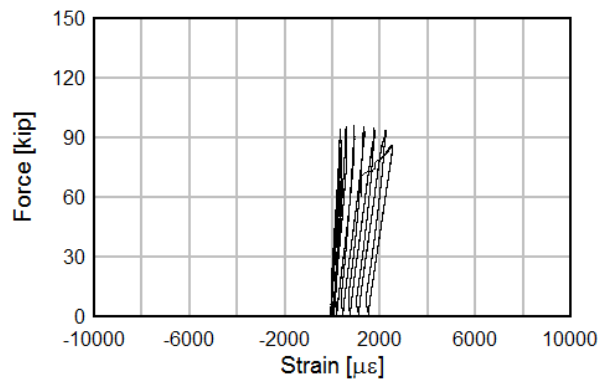
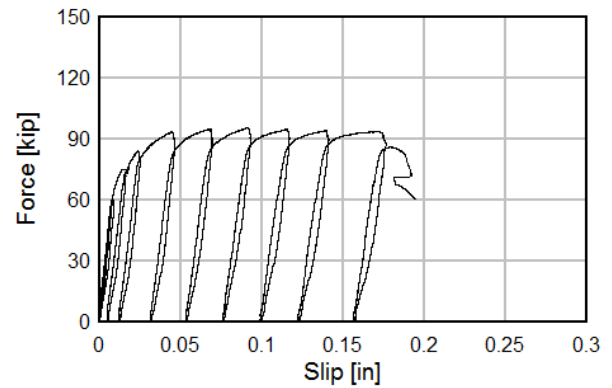
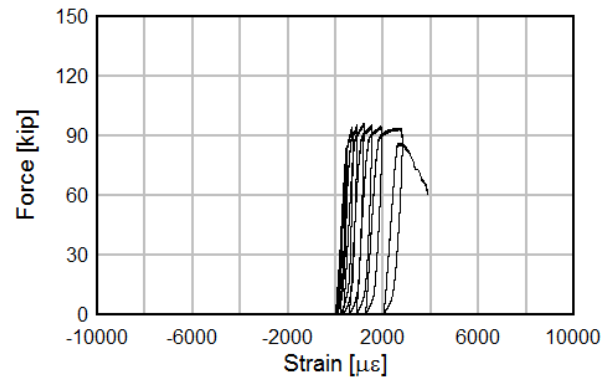
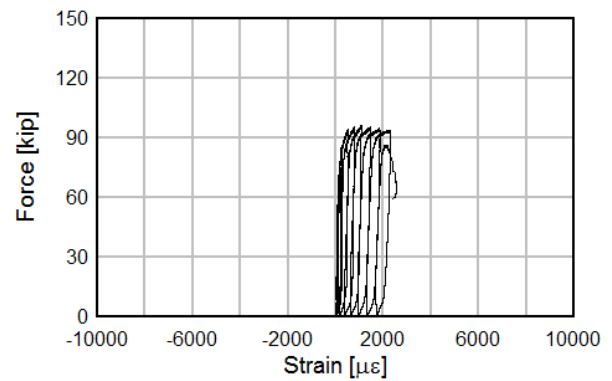
S1

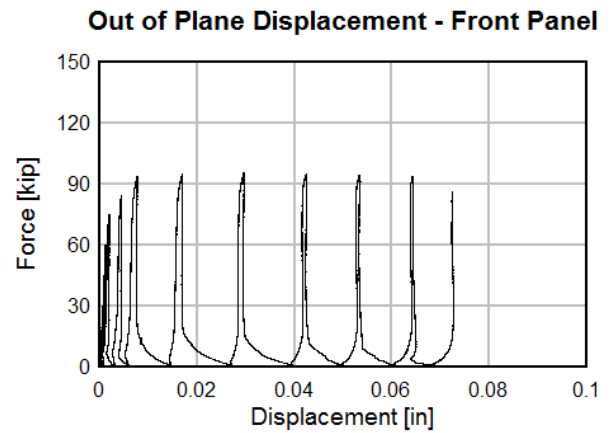
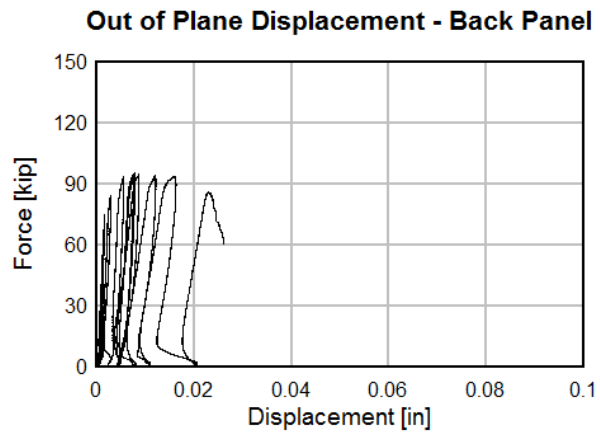
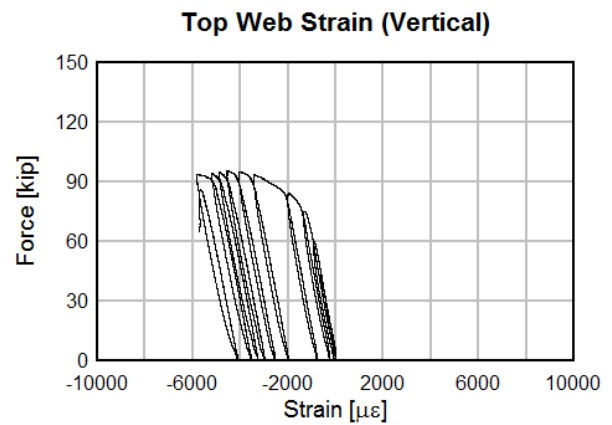
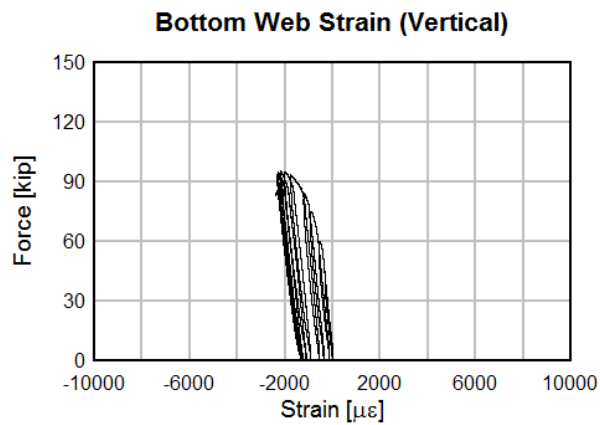
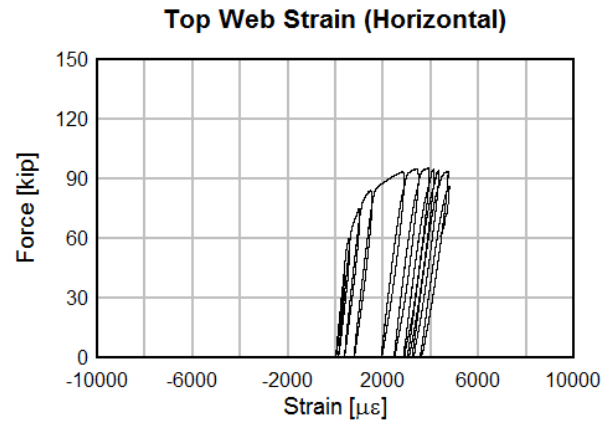
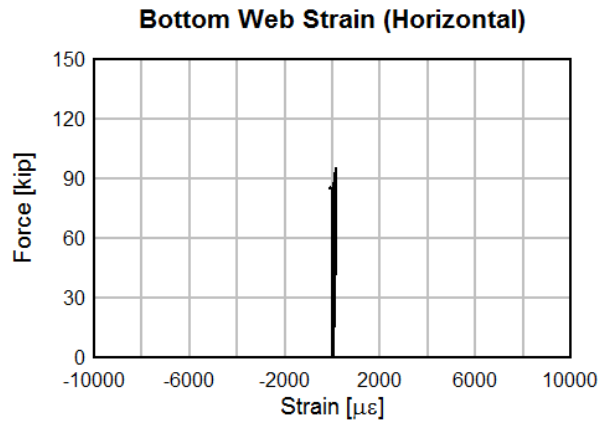


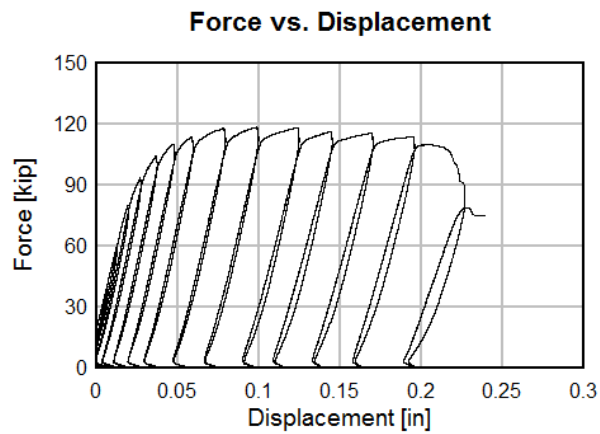
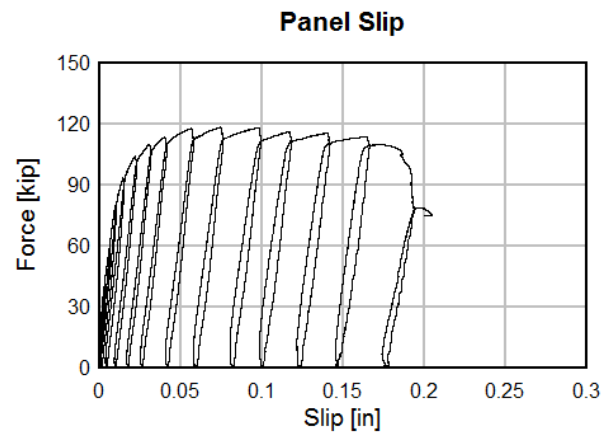
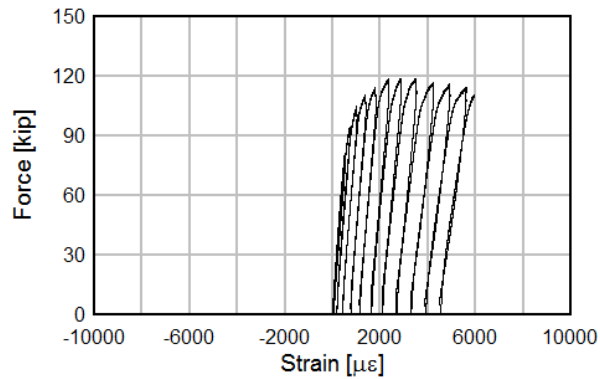
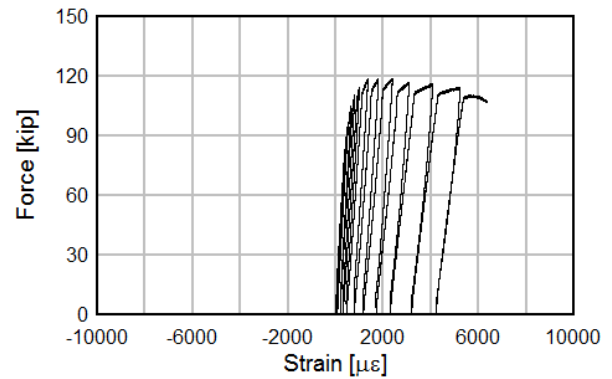
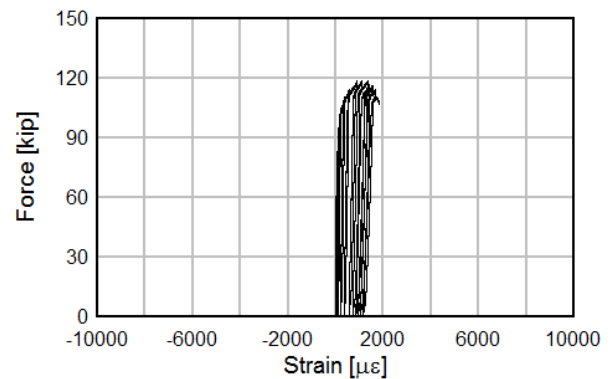
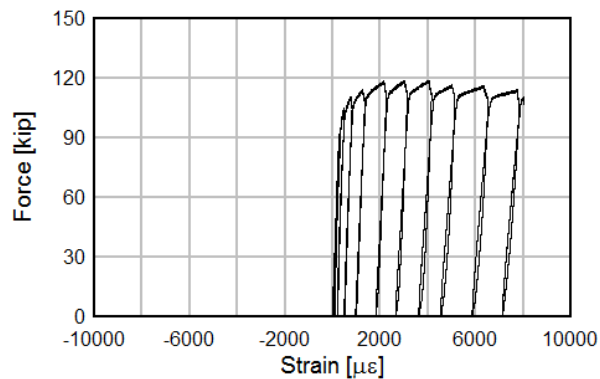
S2

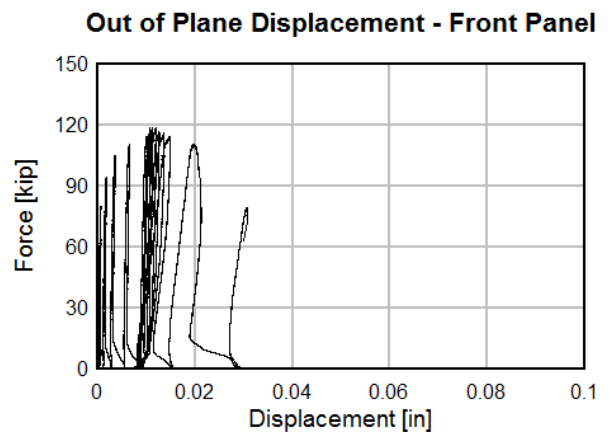
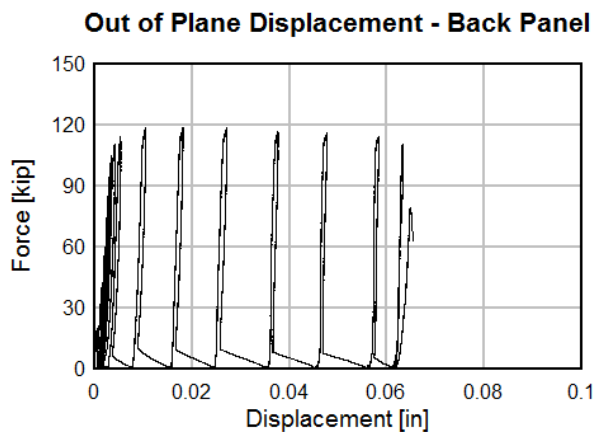
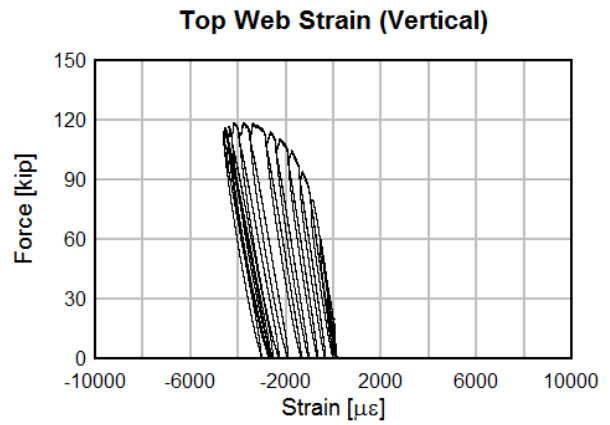
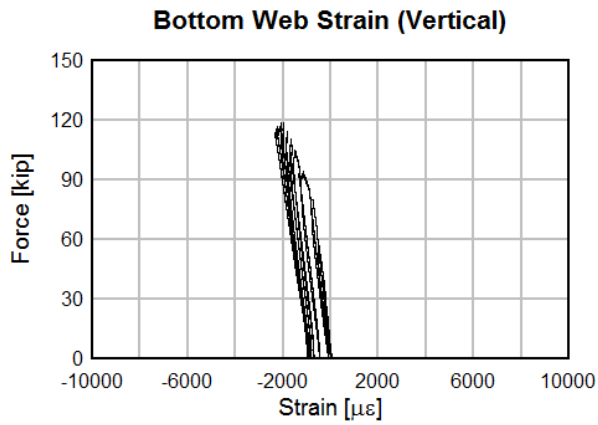
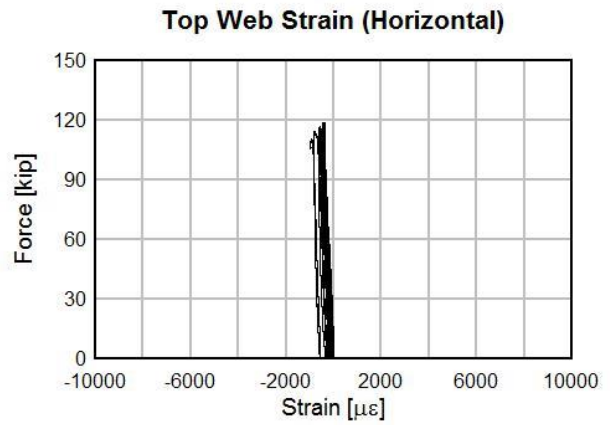
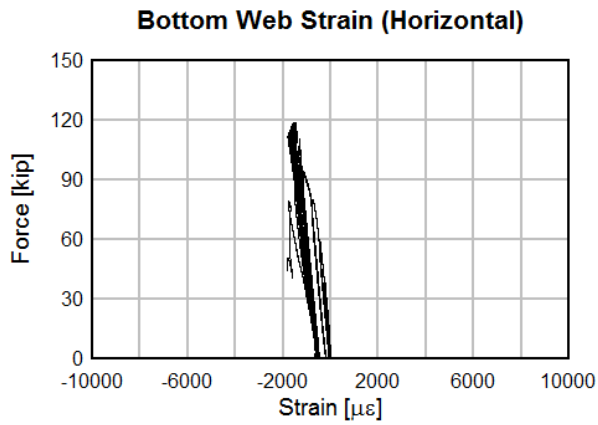
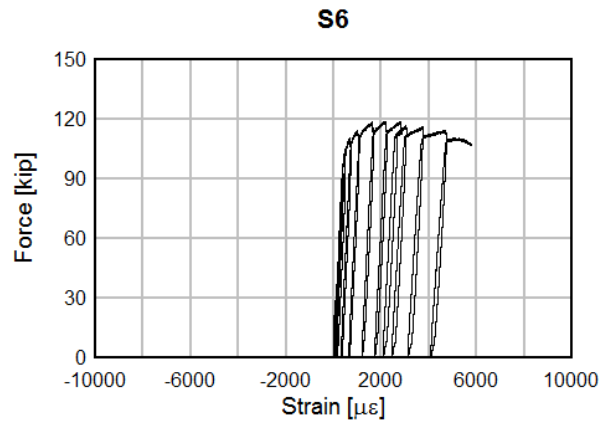
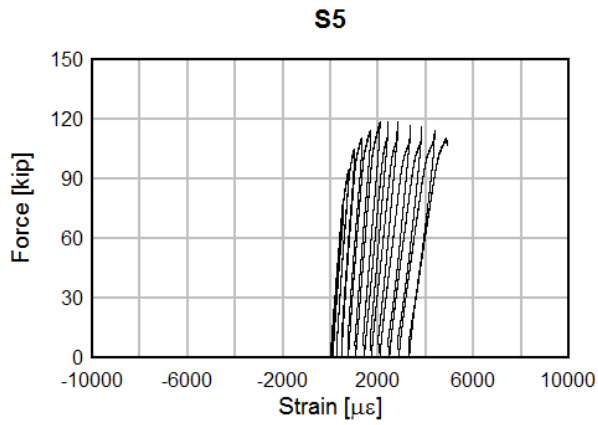


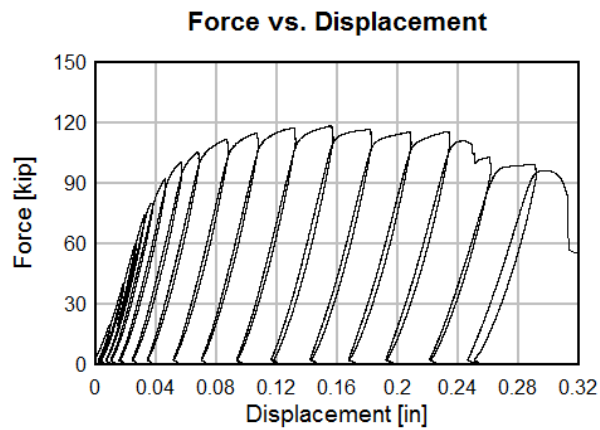
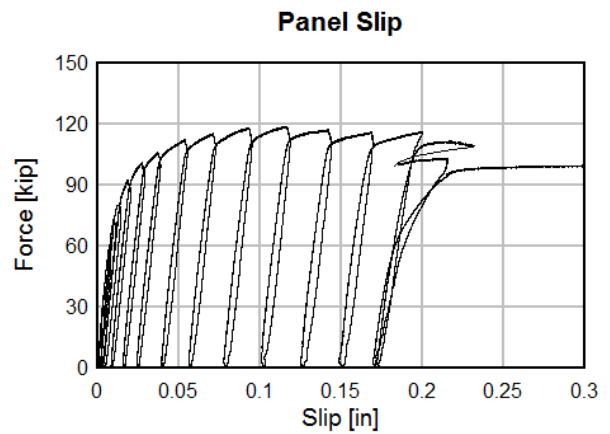
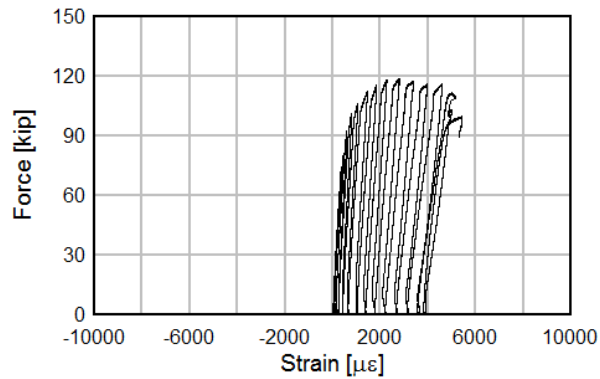
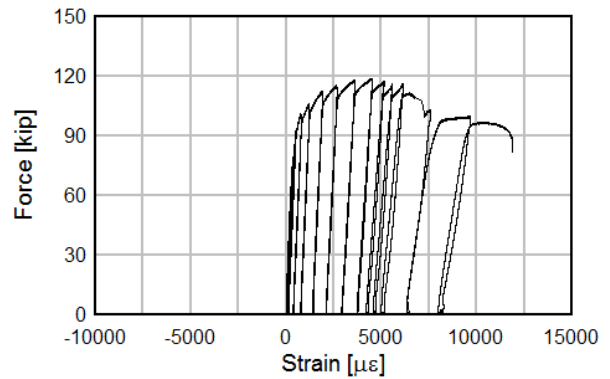
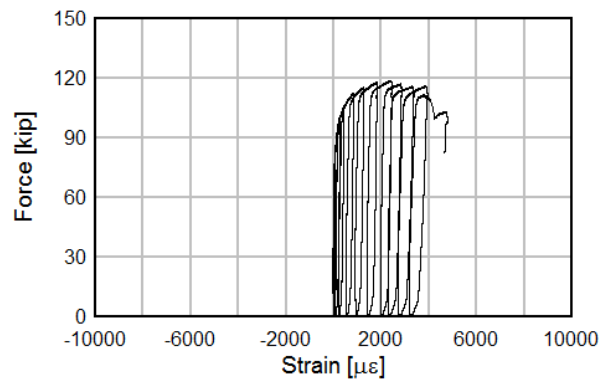
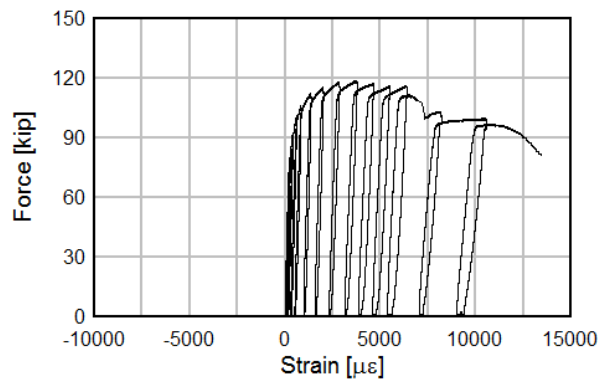


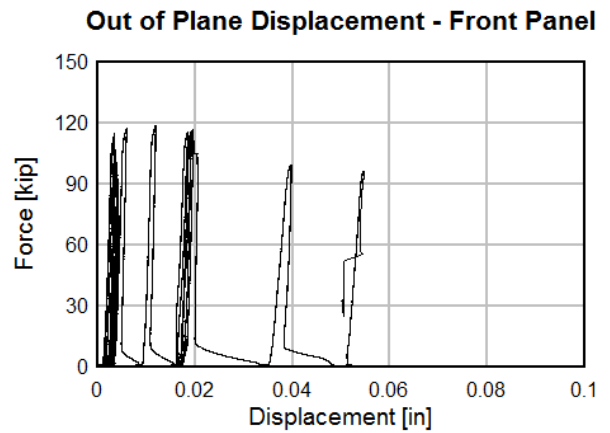
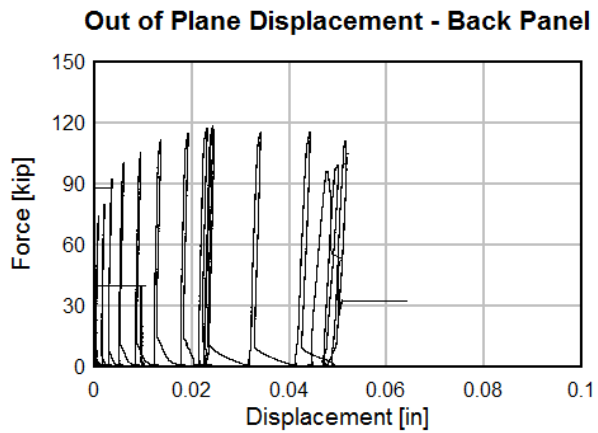
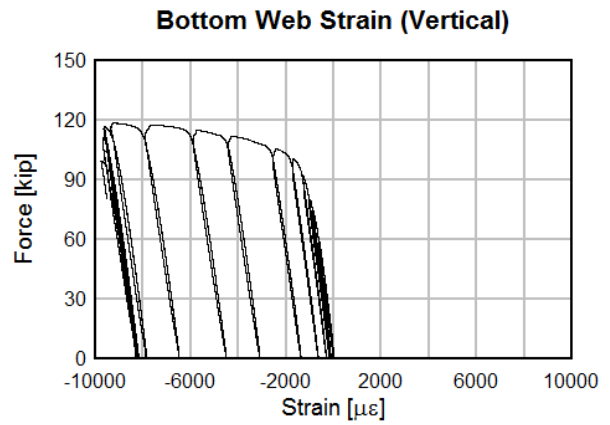
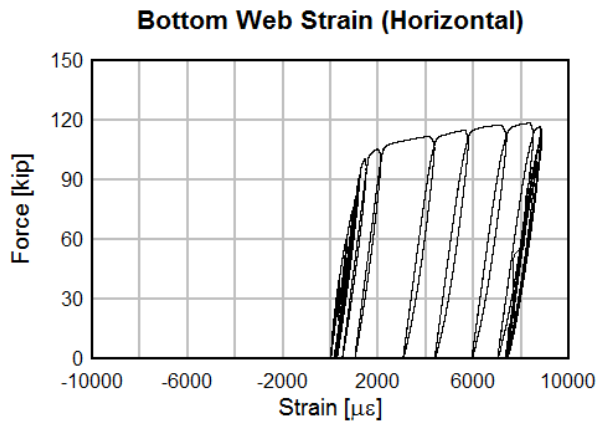
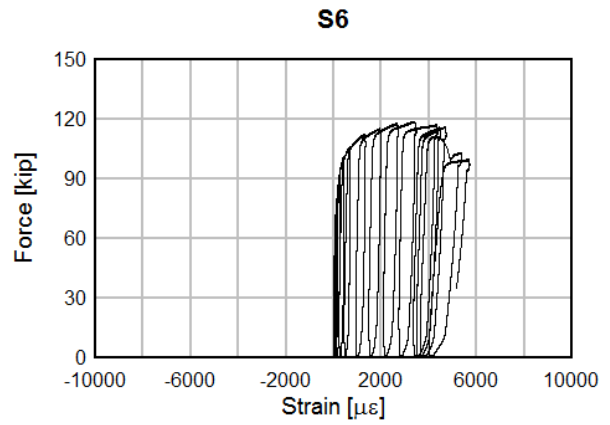
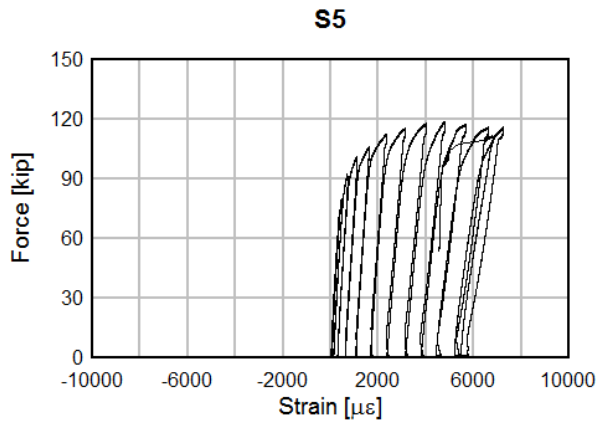
A3 S2-4-2.5-NS-5/8 – 5/8" STUDS**S1****S3****Panel Slip****S2****S4**

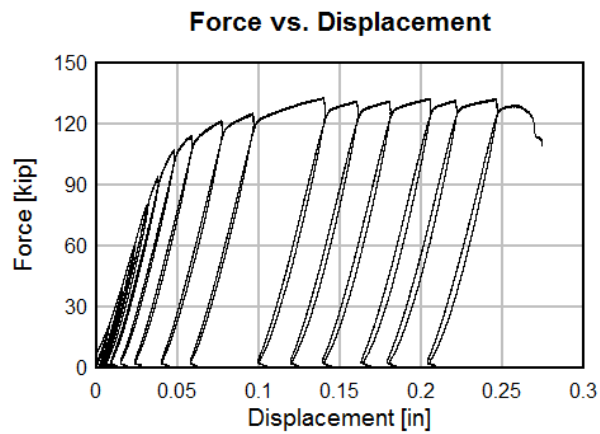
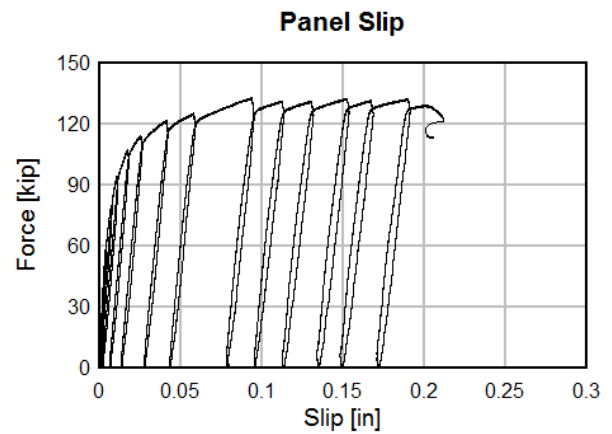
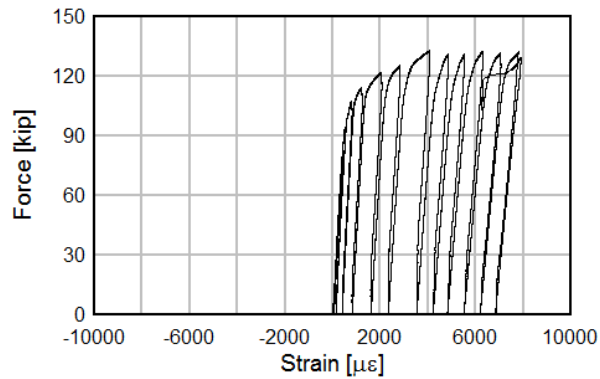
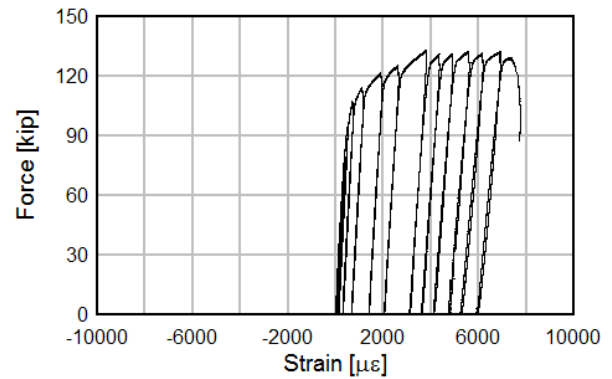
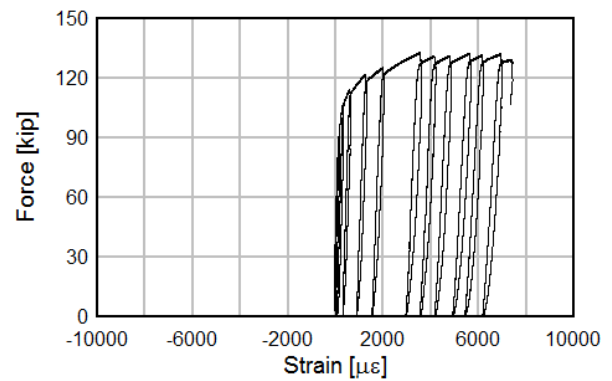
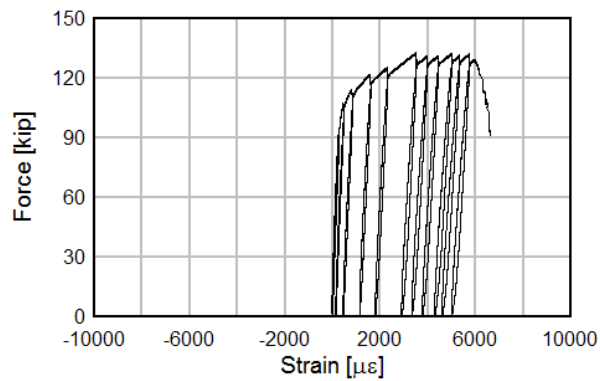


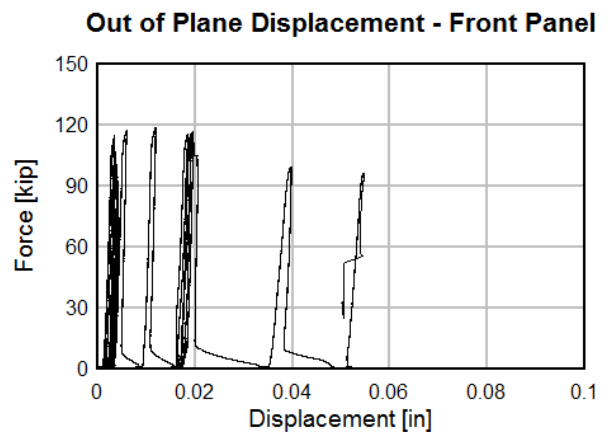
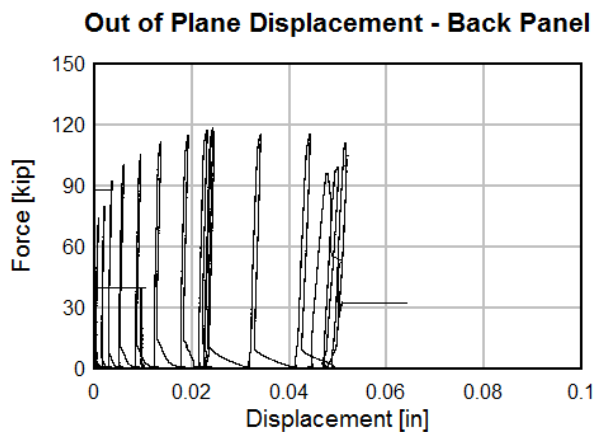
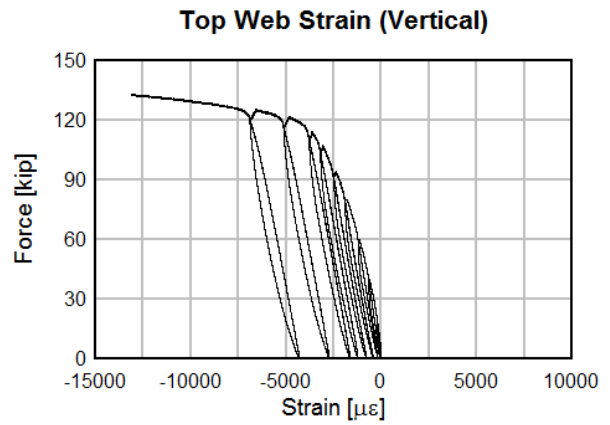
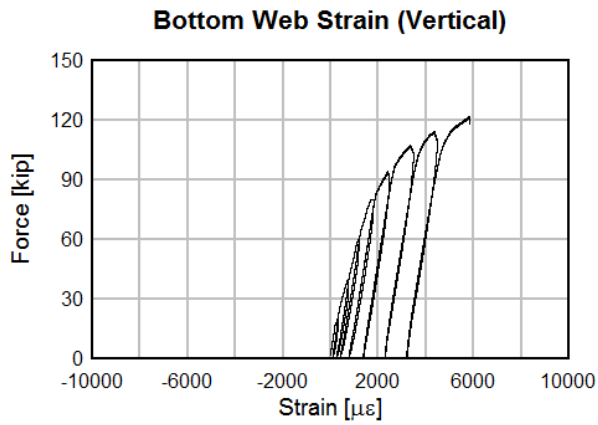
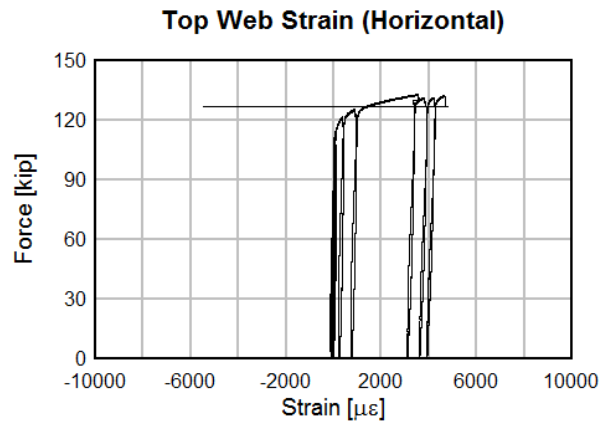
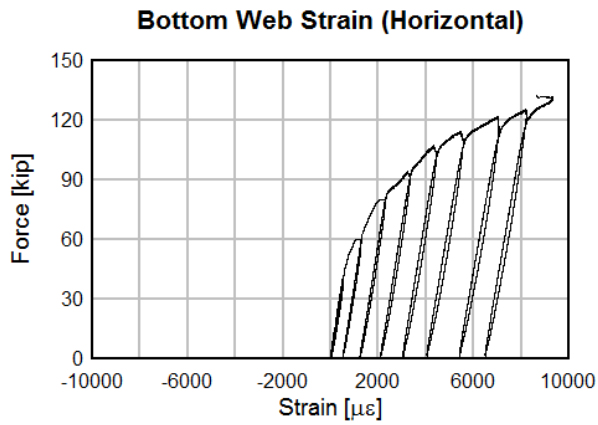
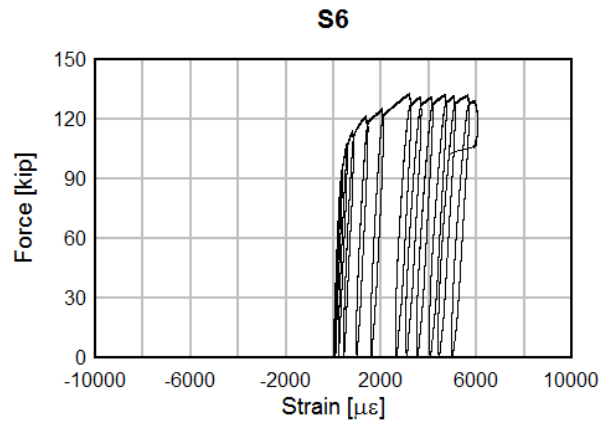
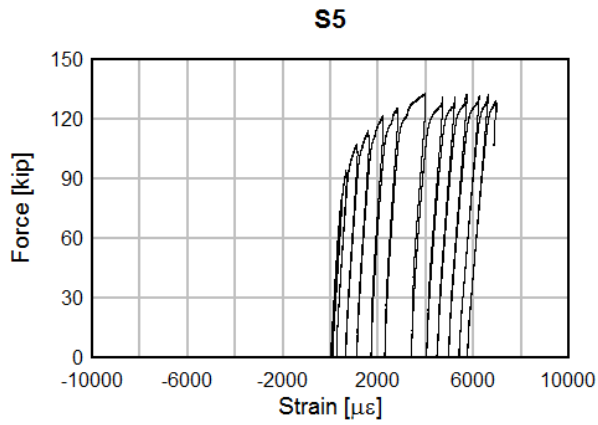
A4 S3-8-2-VHS-1/2 – VERTICAL AND HORIZONTAL STAGGER**S1****S2****S3****S4**



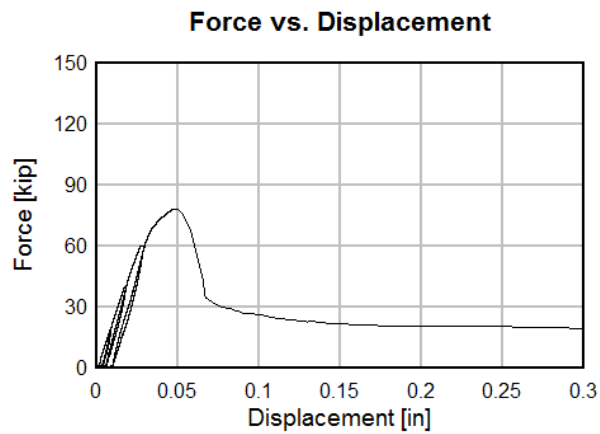
A5 S4-8-1.5-NS-1/2 – 3D_B STUD SPACING**S1****S2****S3****S4**



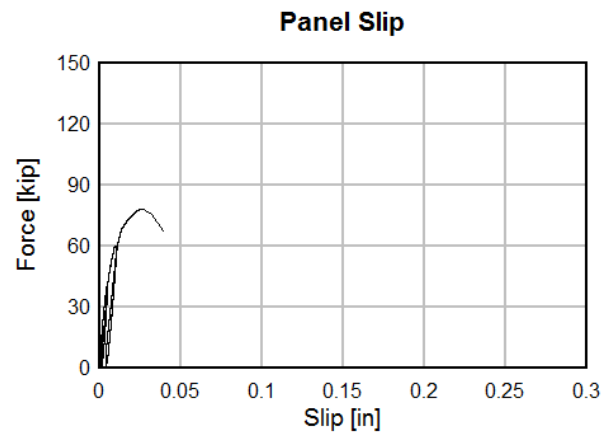
A6 S5-8-2-VS-1/2 – VERTICAL STAGGER**S1****S2****S3****S4**



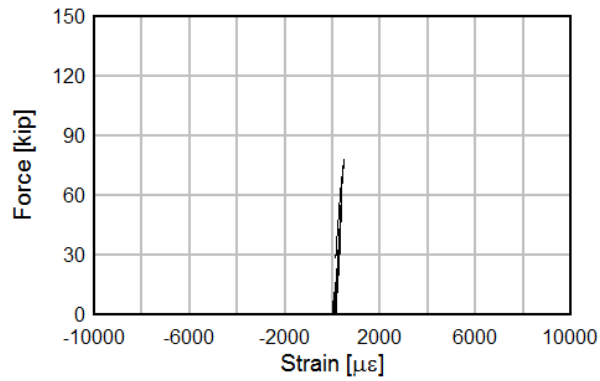
A7 S6-8-2-NS-1/2 – REGULAR STRENGTH CONCRETE



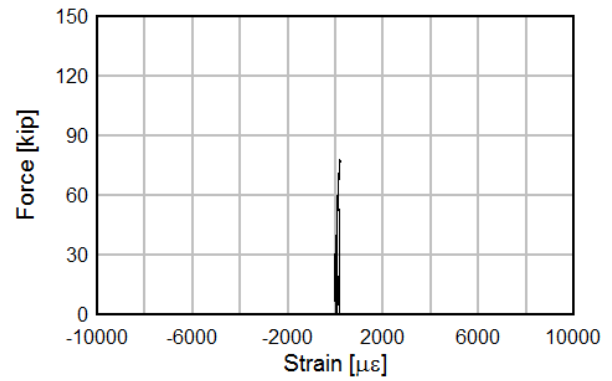
S1



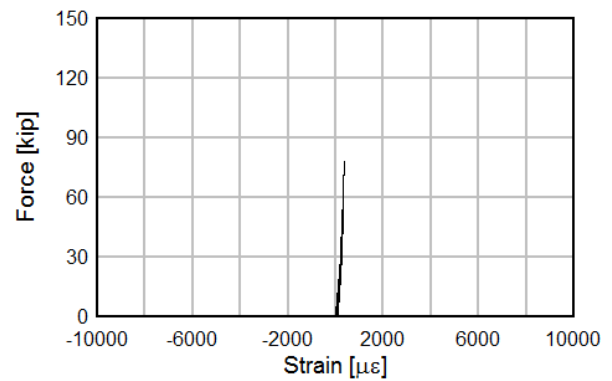
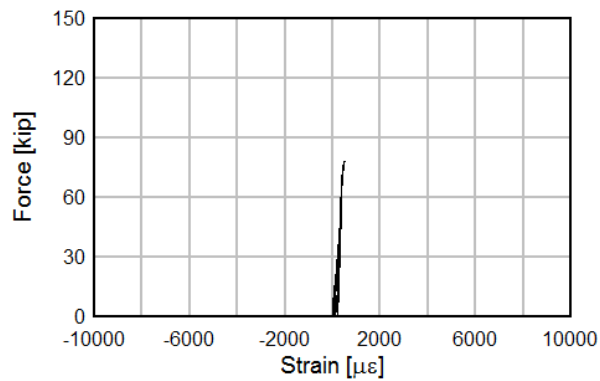
S2

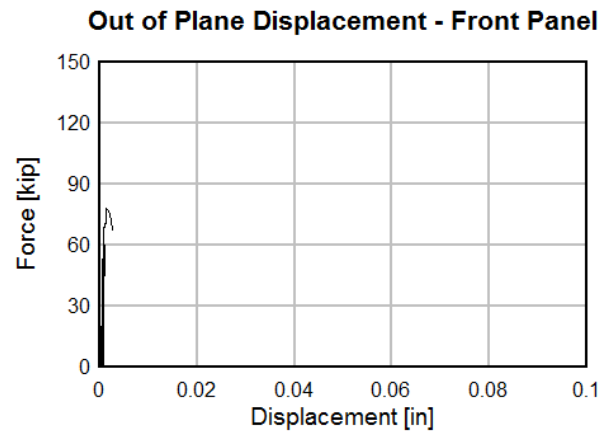
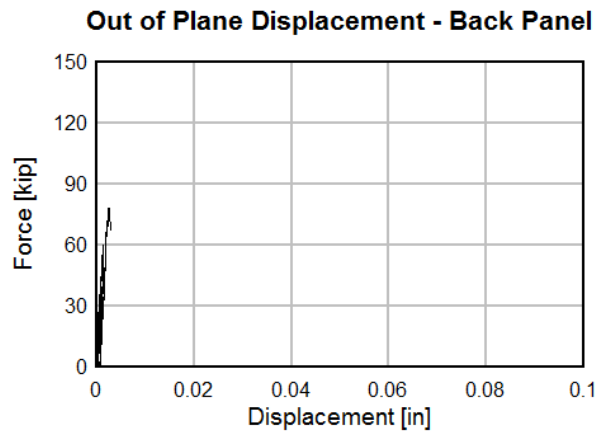
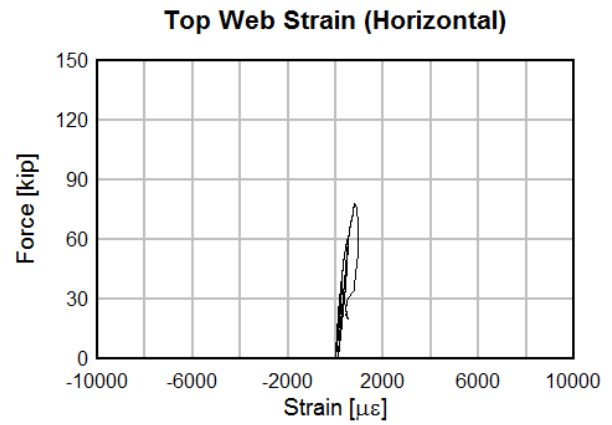
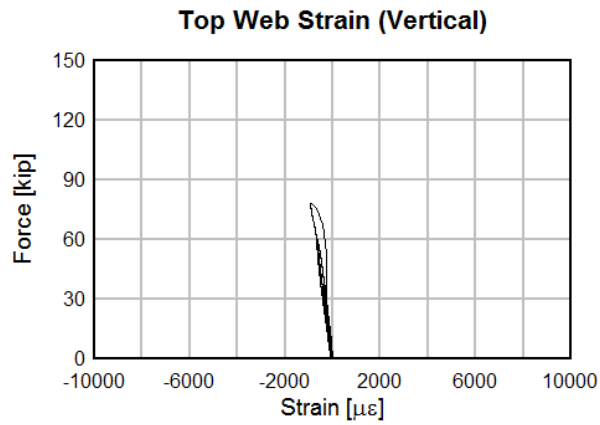
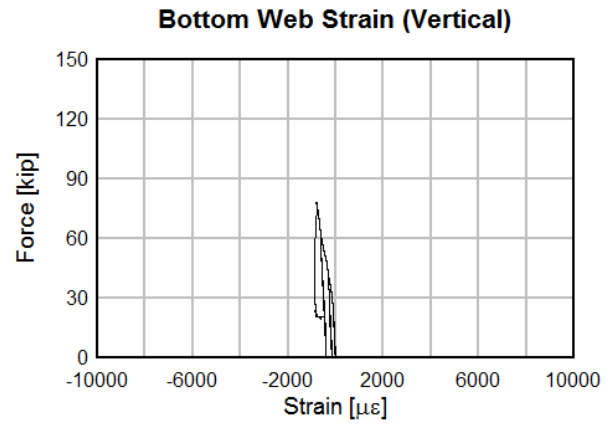
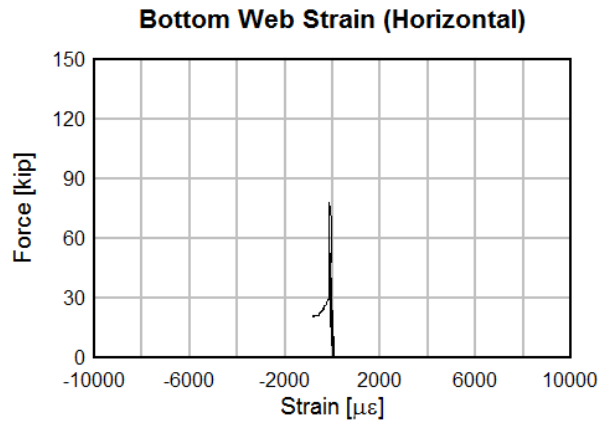


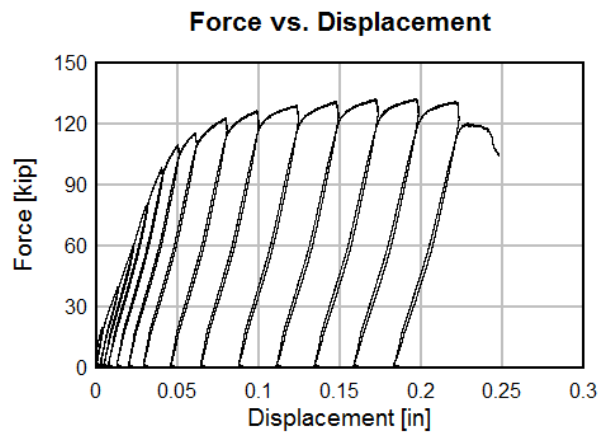
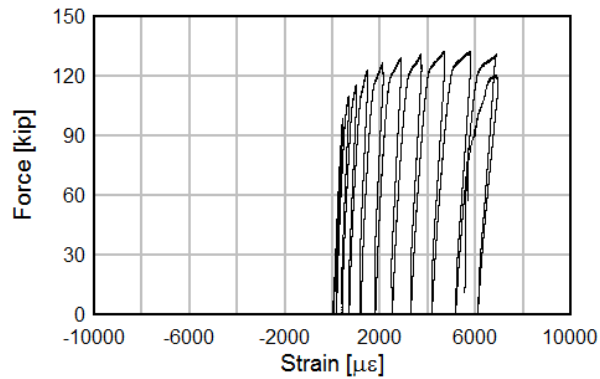
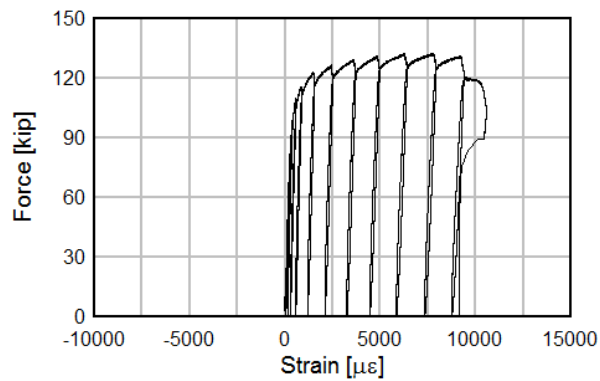
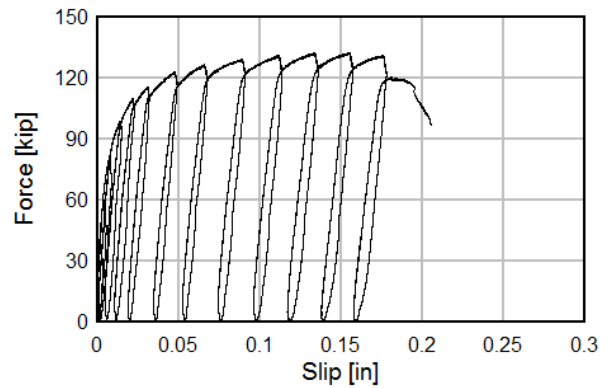
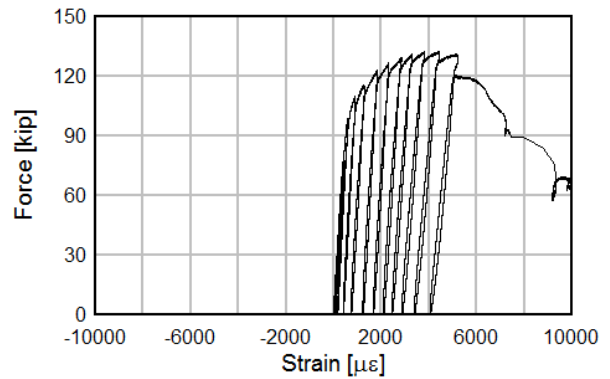
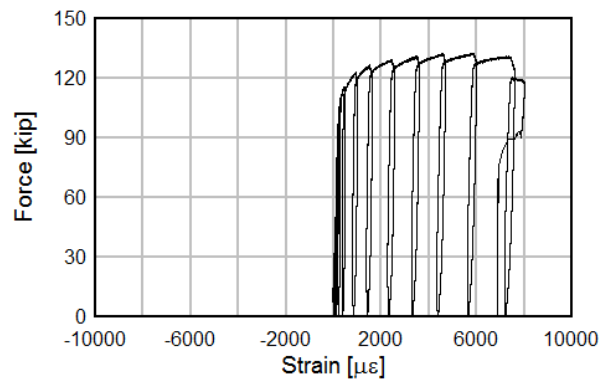
S3

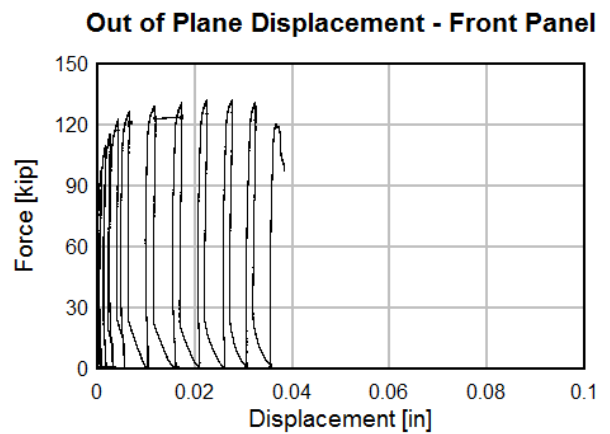
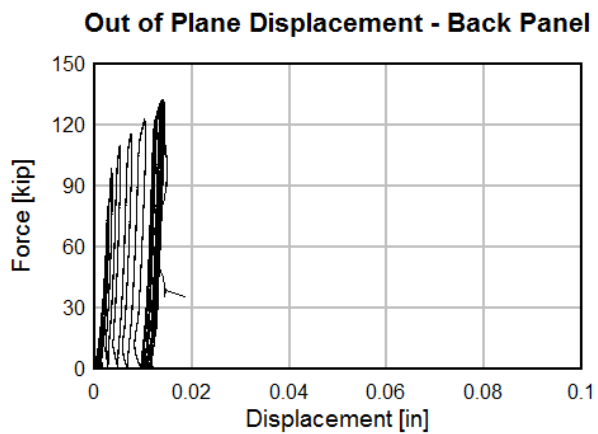
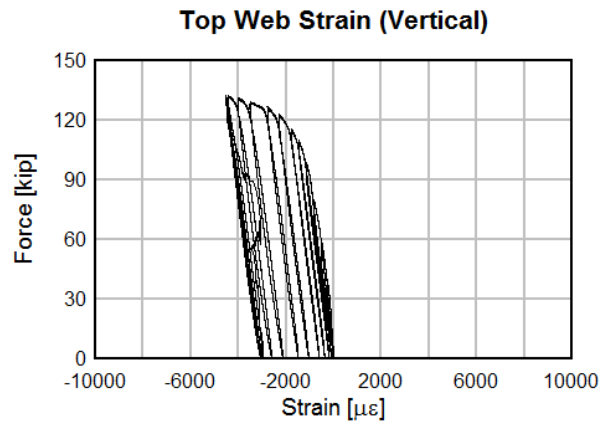
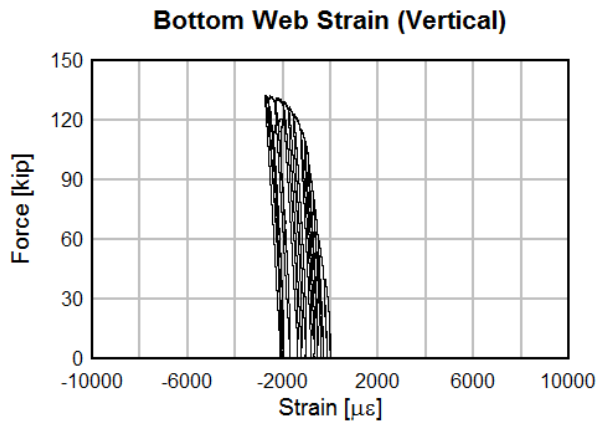
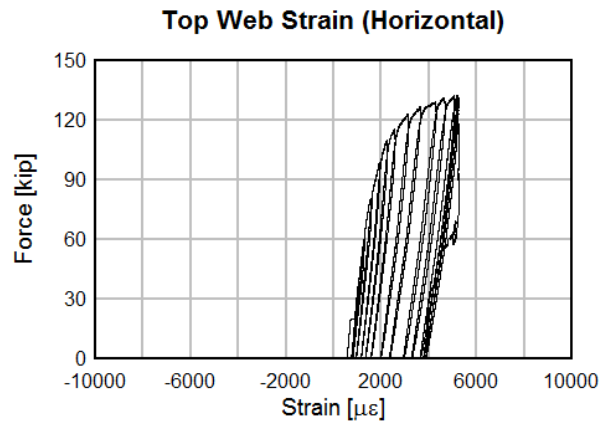
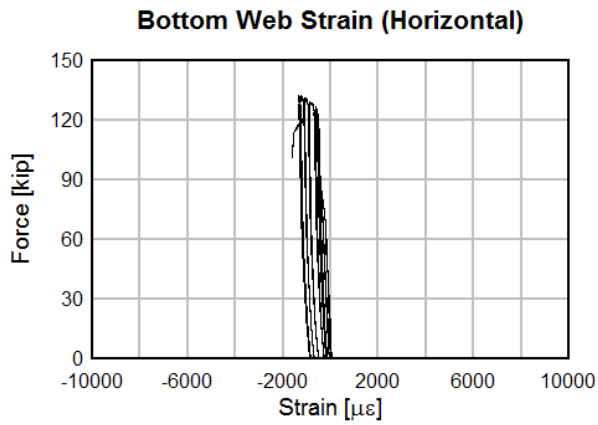
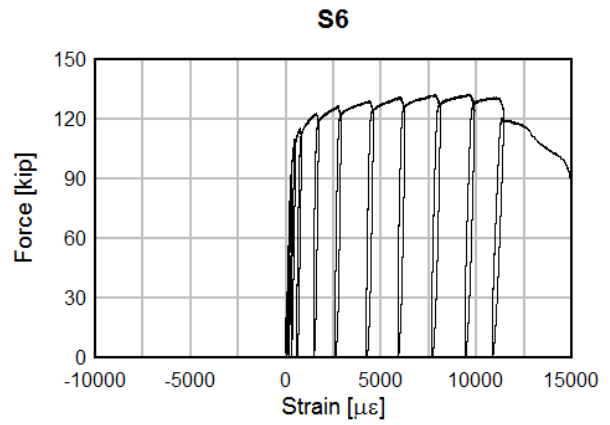
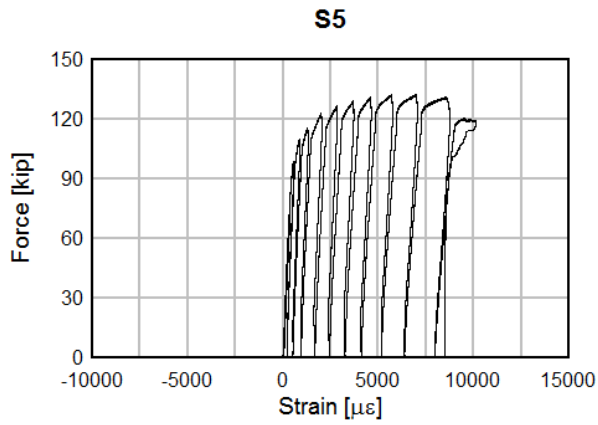


S4

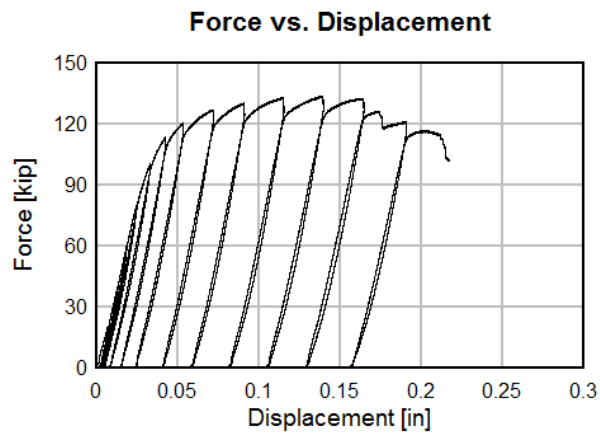




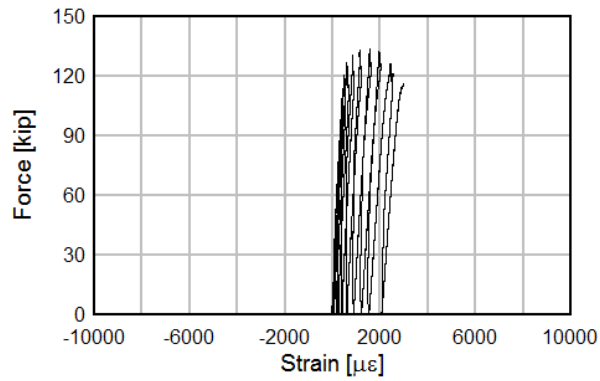
A8 S7-8-2-NS-1/2 – REDUCED COVER (1/4")**S1****S3****Panel Slip****S2****S4**



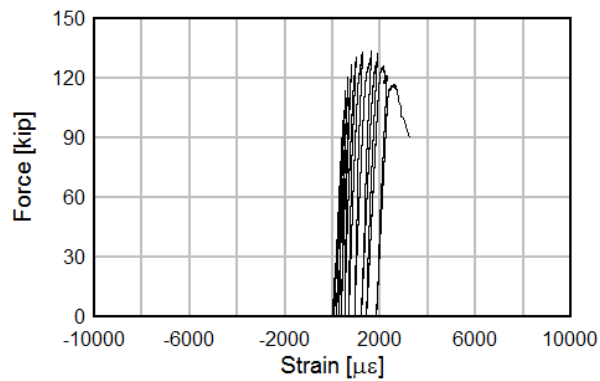
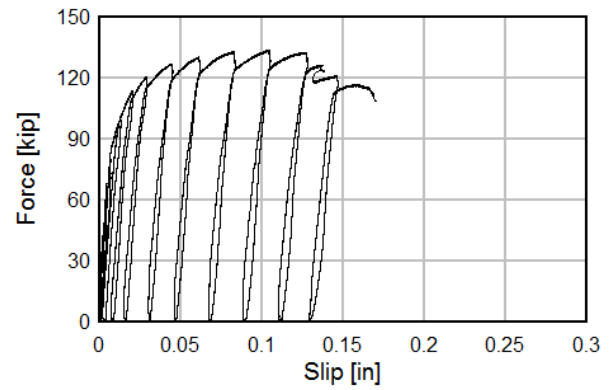
A9 S8-8-2-NS-1/2 – F'C = 28-KSI



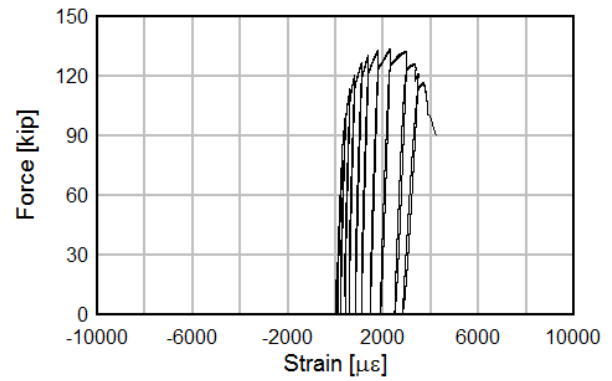
S1



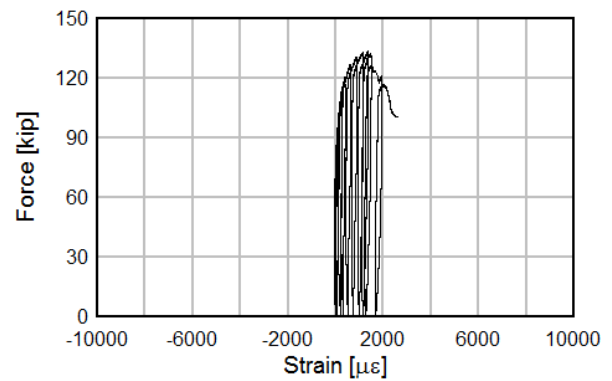
S3

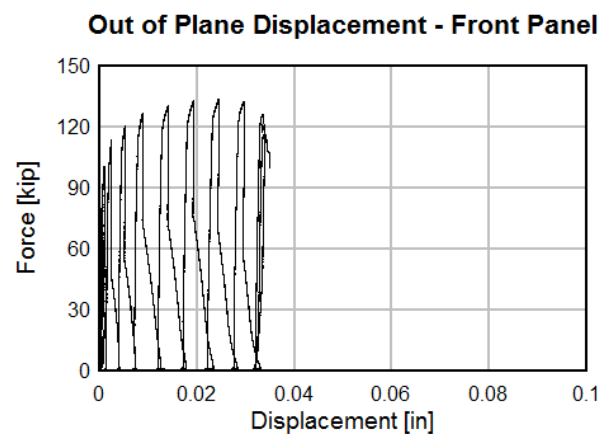
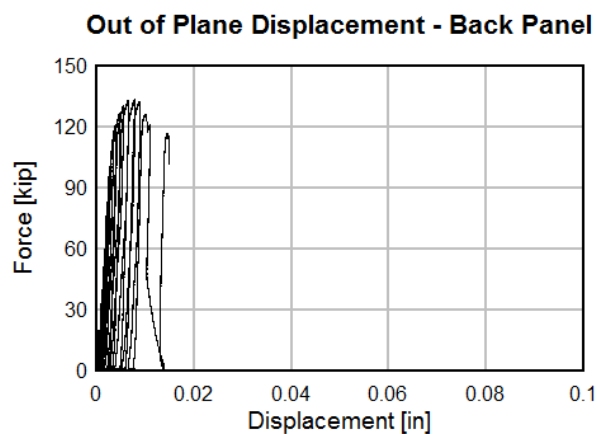
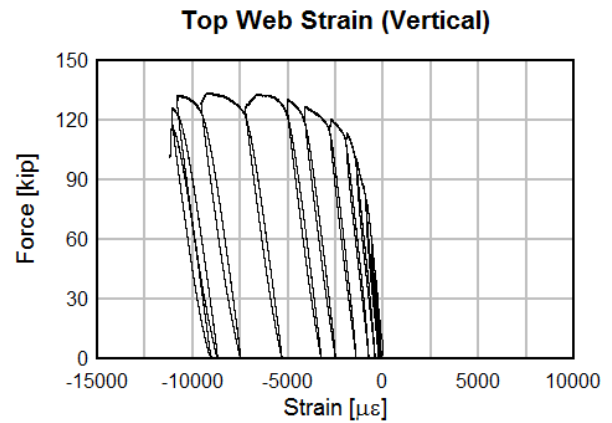
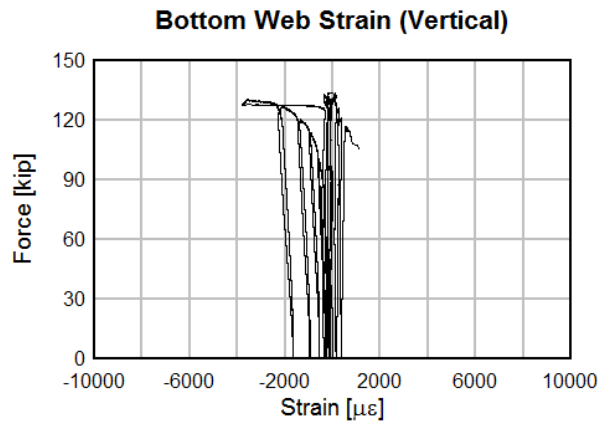
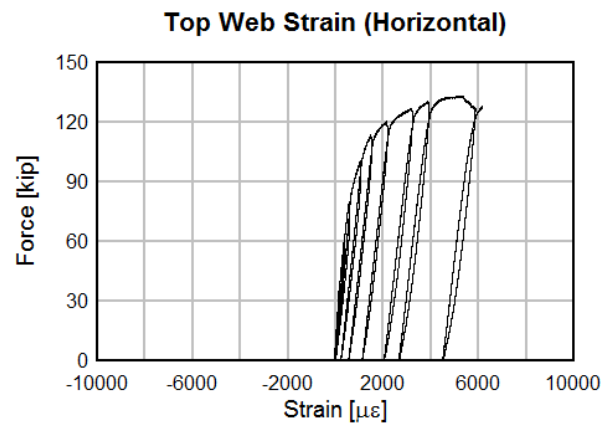
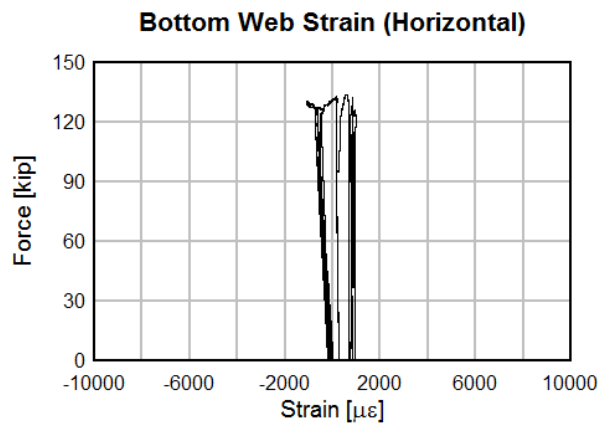
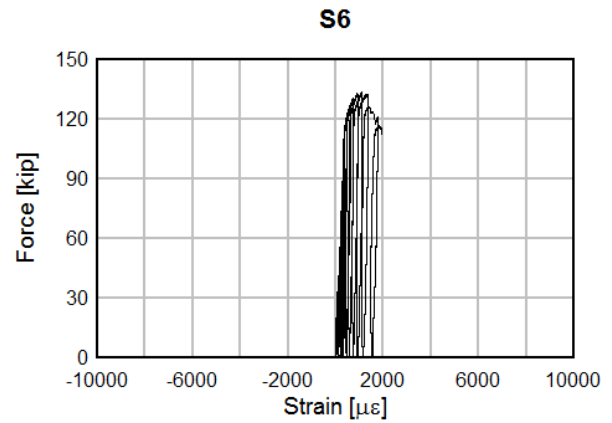
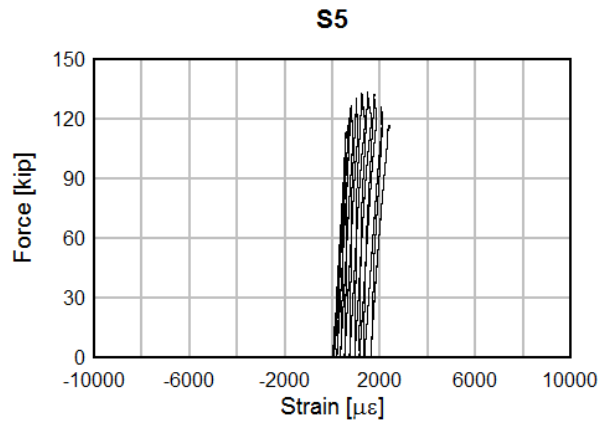
**Panel Slip**

S2

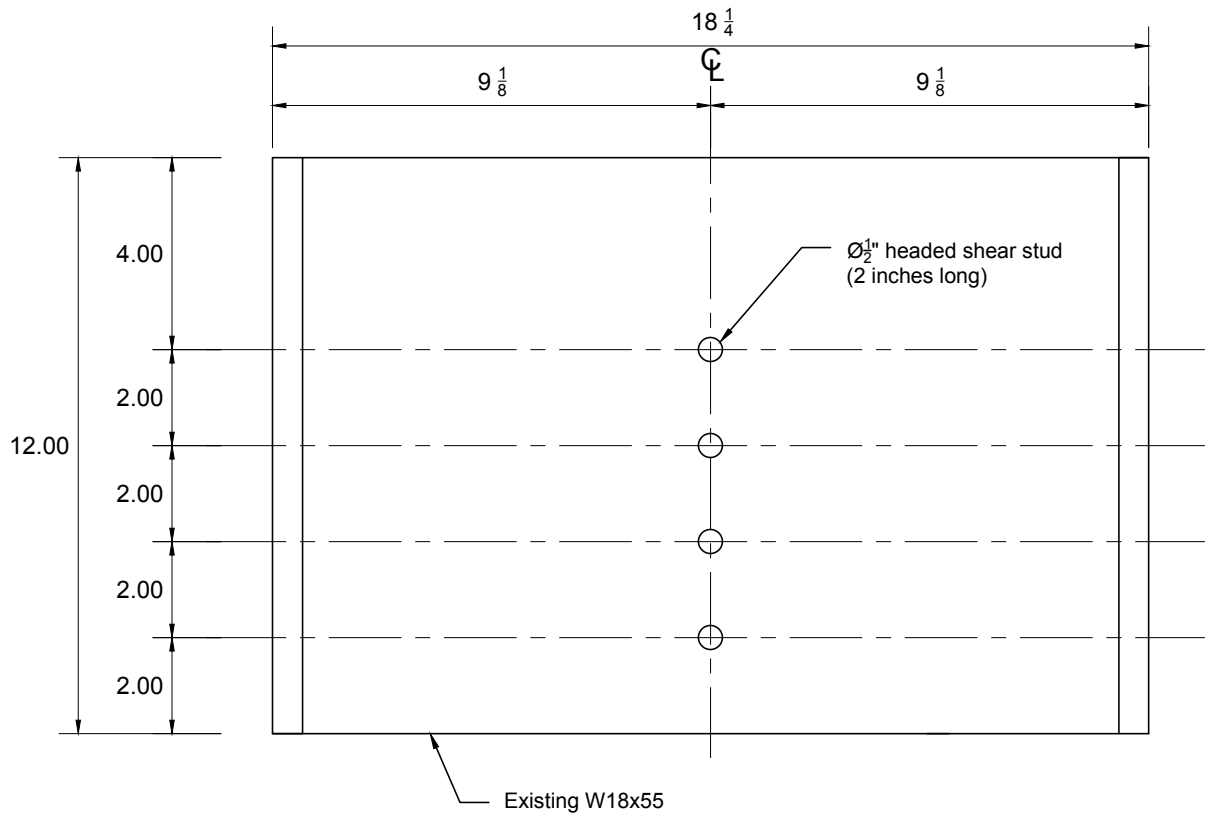


S4





**Appendix B Shop Drawings of Push-off
Specimens**



S1-1: Benchmark - 4db
Scale - 1:4



University of Connecticut



Connecticut Dept. of Transportation

Project: Girder-End Repair

Title: Push Out Specimen - Benchmark

Drawn by: Dominic Kruszewski

Approved by:

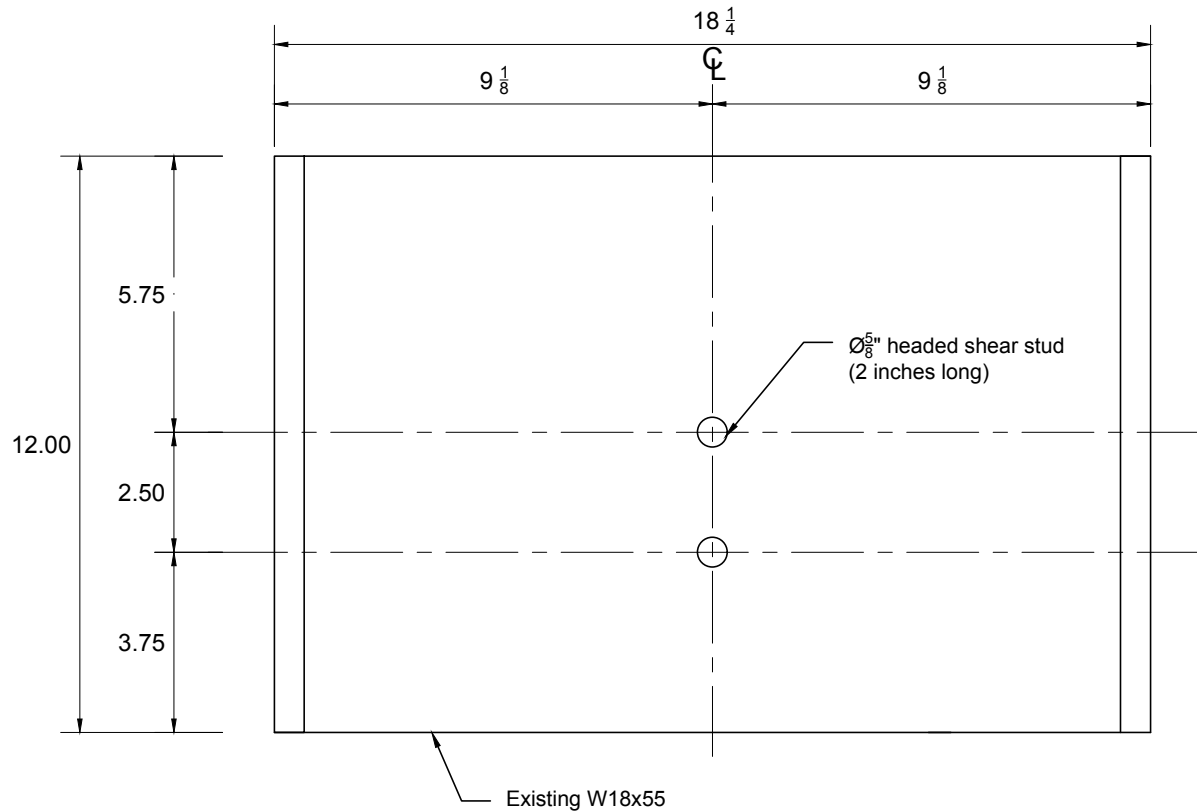
Scale: As noted

Sheet Number: S1

Date: 04/20/2016

Notes

1. All units in inches.
2. All welding to be performed in accordance with AWS standards.
3. Stud location tolerance: $\frac{1}{32}$ "
4. Number of specimens: 2



S3-1: No Stagger Pattern - 5/8" studs
Scale - 1:4



University of Connecticut



Connecticut Dept. of Transportation

Project: Girder-End Repair

Title: Push Out Specimen - 5/8" Studs

Drawn by: Dominic Kruszewski

Approved by:

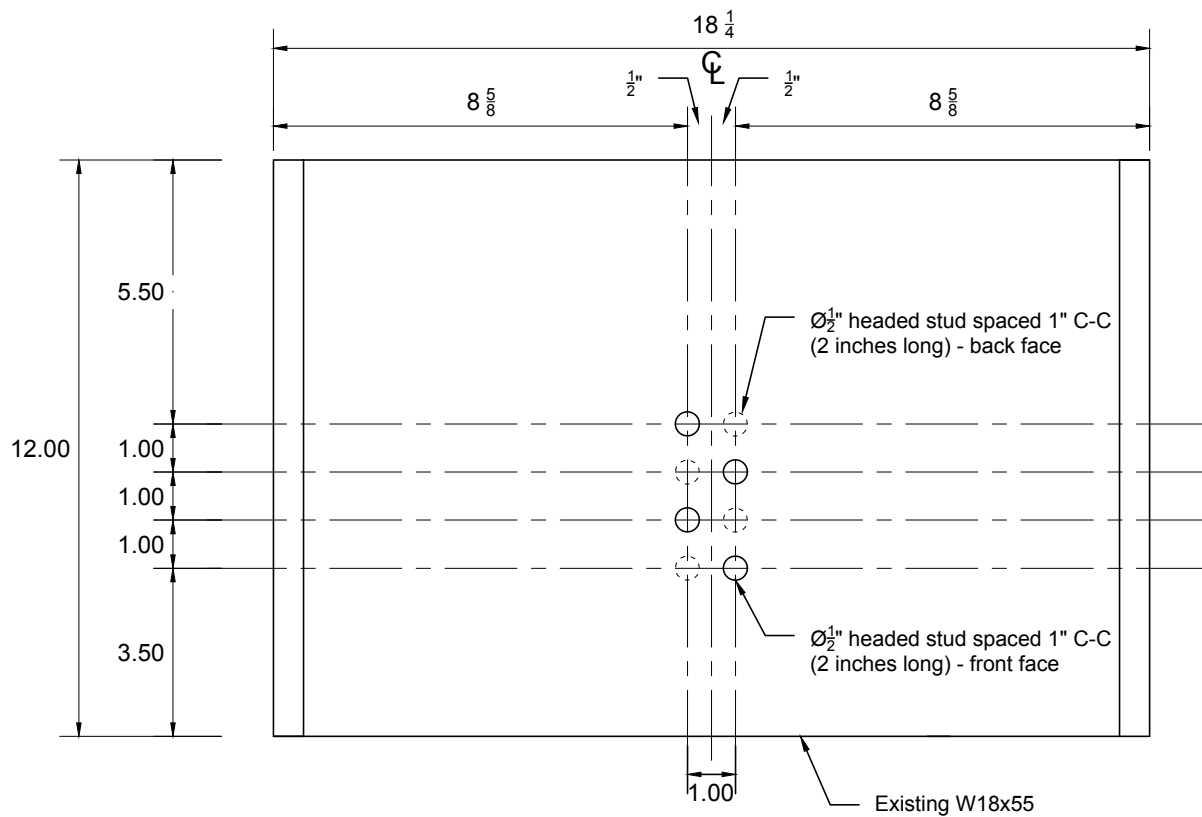
Scale: As noted

Sheet Number: S3

Date: 04/20/2016

Notes

1. All units in inches.
2. All welding to be performed in accordance with AWS standards.
3. Stud location tolerance: $\frac{1}{32}$ "
4. Number of specimens: 1



S4-1: Horizontal and Vertical Stagger Pattern
Scale - 1:4



University of Connecticut



Connecticut Dept. of Transportation

Project: Girder-End Repair

Title: Push Out Specimen - V+H Stagger

Drawn by: Dominic Kruszewski

Approved by:

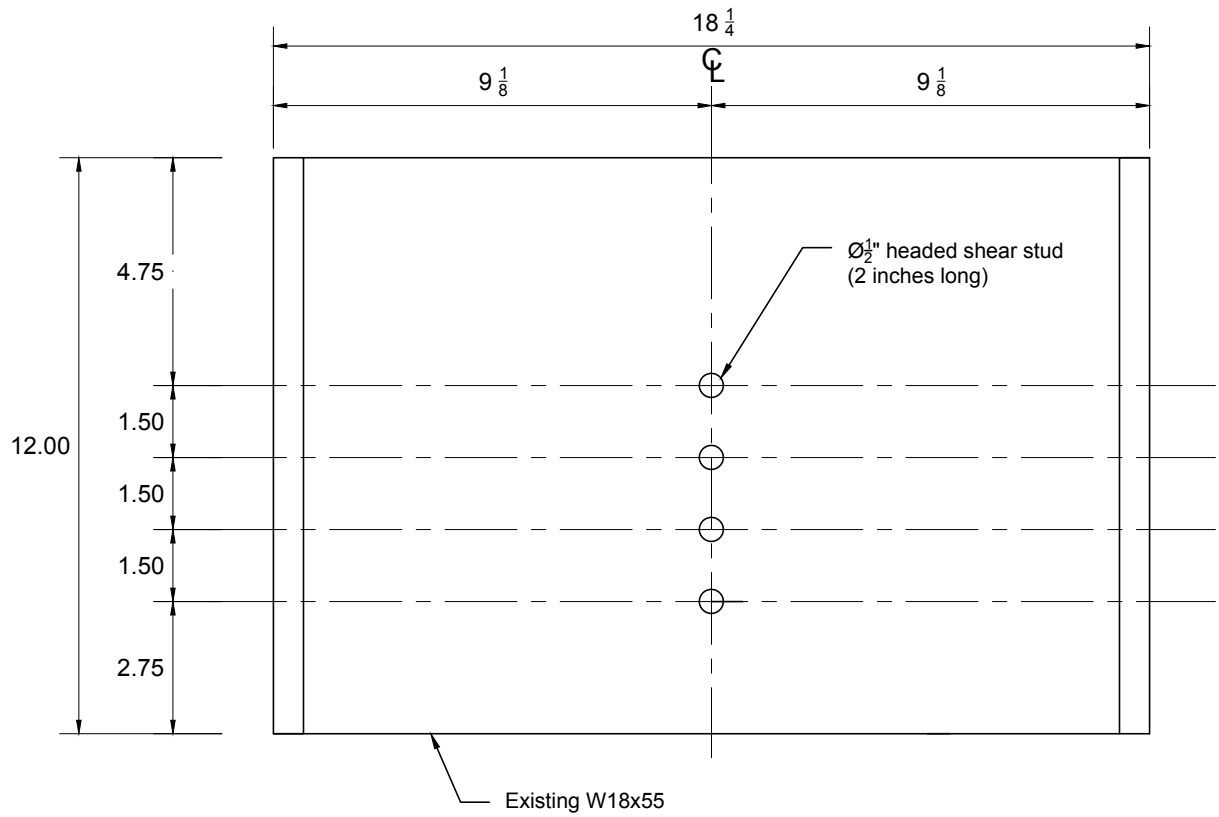
Scale: As noted

Sheet Number: S4

Date: 04/20/2016

Notes

1. All units in inches.
2. All welding to be performed in accordance with AWS standards.
3. Stud location tolerance: $\frac{1}{32}$ "
4. Number of specimens: 1



S2-1: 3db Stud Spacing
Scale - 1:4



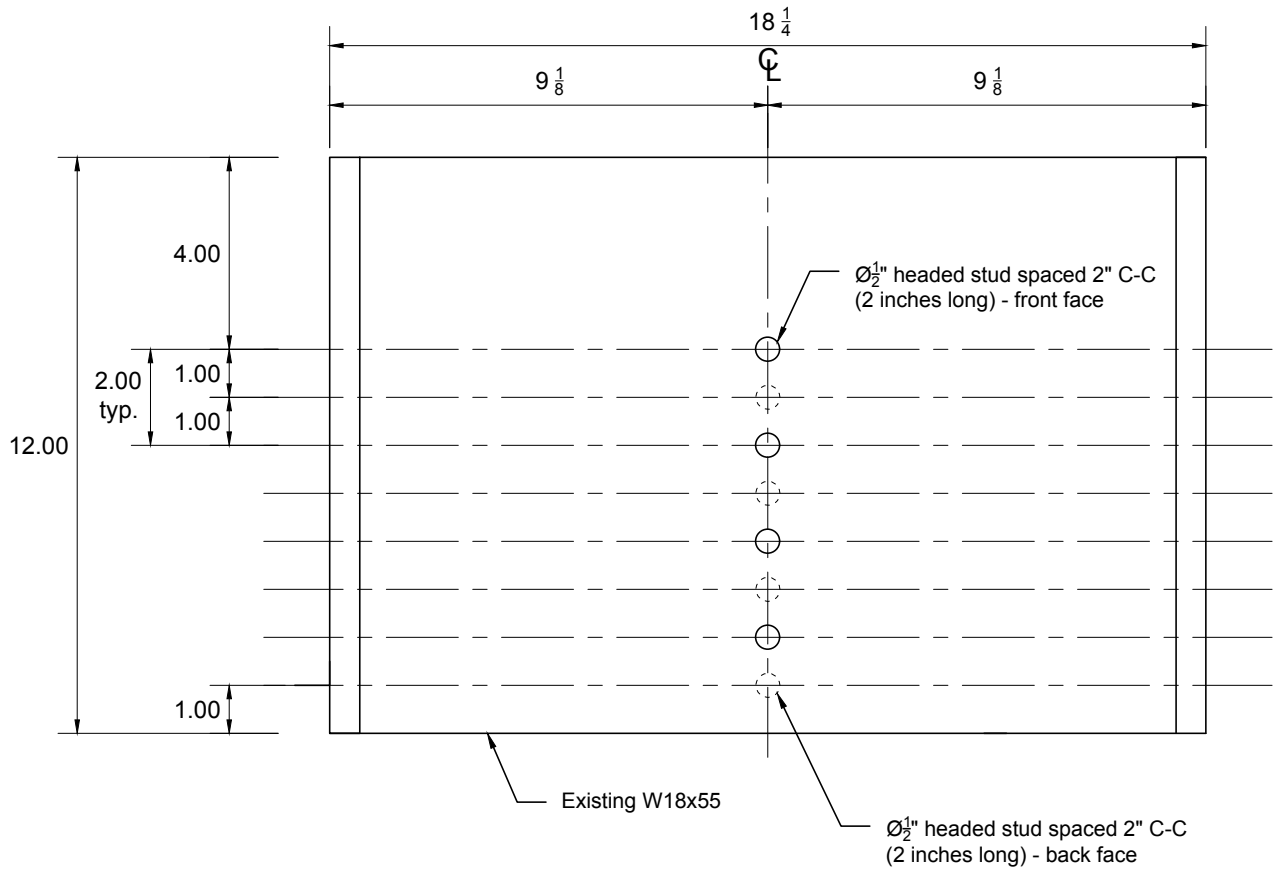
University of Connecticut





Connecticut Dept. of Transportation

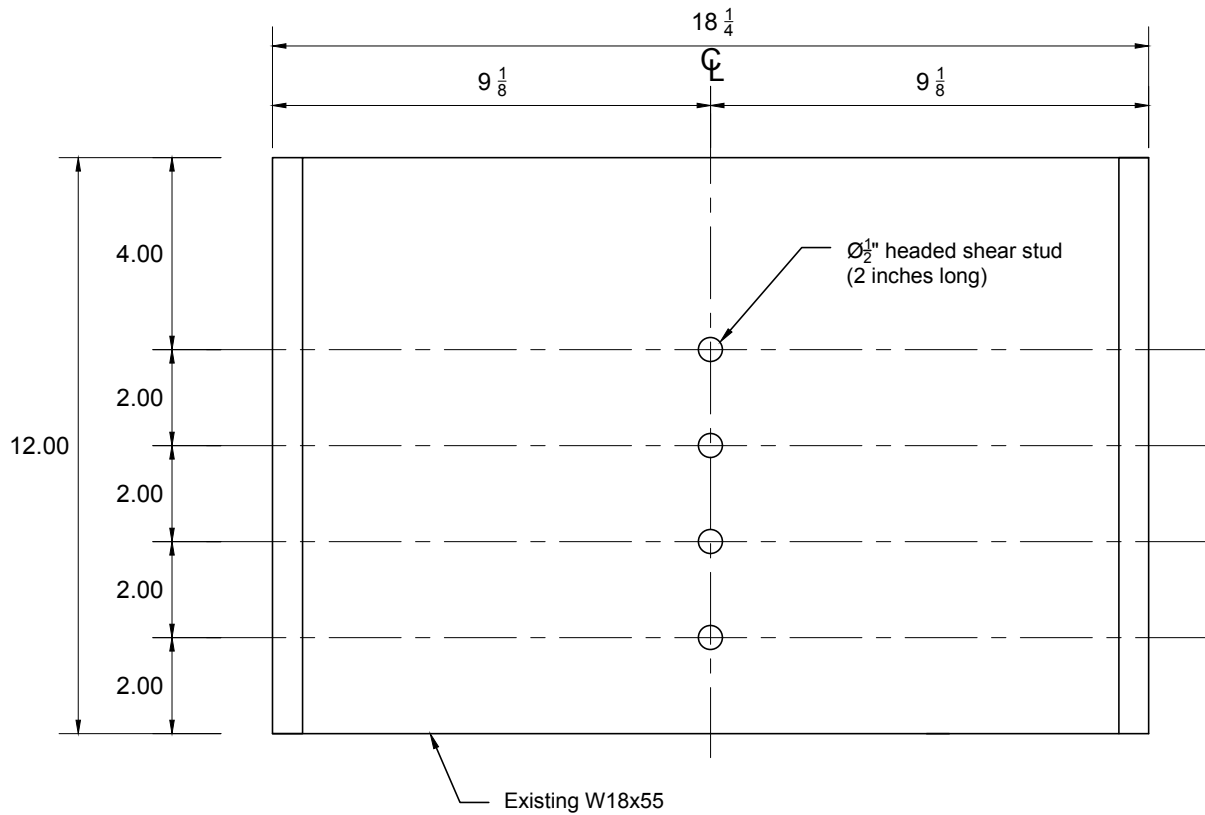
Project: Girder-End Repair		
Title: Push Out Specimen - 3db Stud Spacing		
Drawn by: Dominic Kruszewski	Approved by:	
Scale: As noted	Sheet Number: S2	Date: 04/20/2016

- Notes**
1. All units in inches.
 2. All welding to be performed in accordance with AWS standards.
 3. Stud location tolerance: $\frac{1}{32}$ "
 4. Number of specimens: 1



S5-1: Vertical Stagger Pattern
Scale - 1:4

 University of Connecticut	 Connecticut Dept. of Transportation	Project: Girder-End Repair			Notes 1. All units in inches. 2. All welding to be performed in accordance with AWS standards. 3. Stud location tolerance: $\frac{1}{32}$ " 4. Number of specimens: 1
		Title: Push Out Specimen - Vertical Stagger			
		Drawn by: Dominic Kruszewski	Approved by:		
		Scale: As noted	Sheet Number: S5	Date: 04/20/2016	



S6-1: Benchmark - RSC Sample
 Scale - 1:4



University of Connecticut



Connecticut Dept. of Transportation

Project: Girder-End Repair

Title: Push Out Specimen - Benchmark - RSC Sample

Drawn by: Dominic Kruszewski

Approved by:

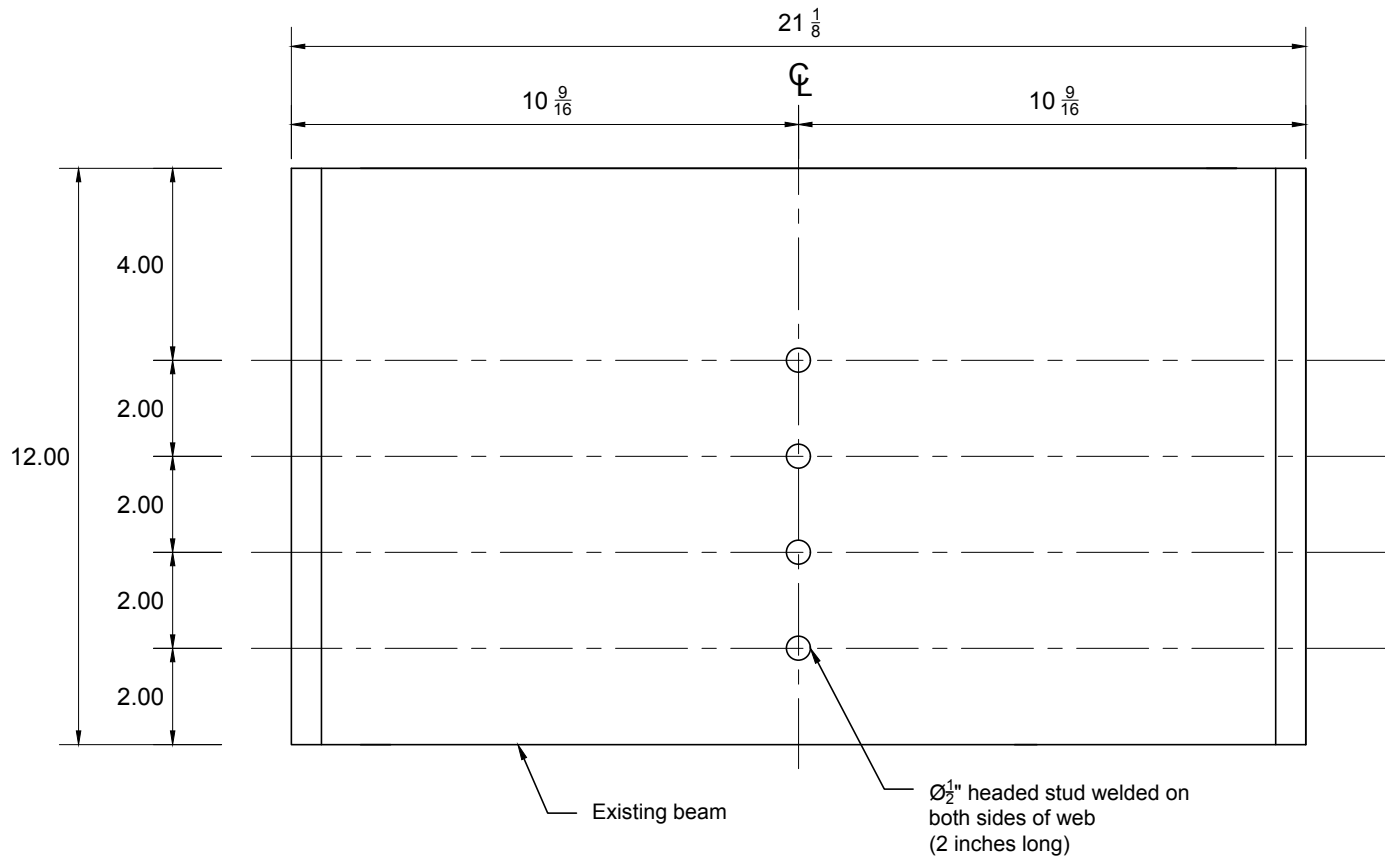
Scale: As noted

Sheet Number: S6

Date: 04/20/2016

Notes

1. All units in inches.
2. All welding to be performed in accordance with AWS standards.
3. Stud location tolerance: $\frac{1}{32}$ "
4. Number of specimens: 2



S7-1: Reduced Cover Specimen
 Scale - 1:4



University of Connecticut



Connecticut Dept. of Transportation

Project: Girder-End Repair

Title: Push Out Specimen - Reduced Cover

Drawn by: Dominic Kruszewski

Approved by:

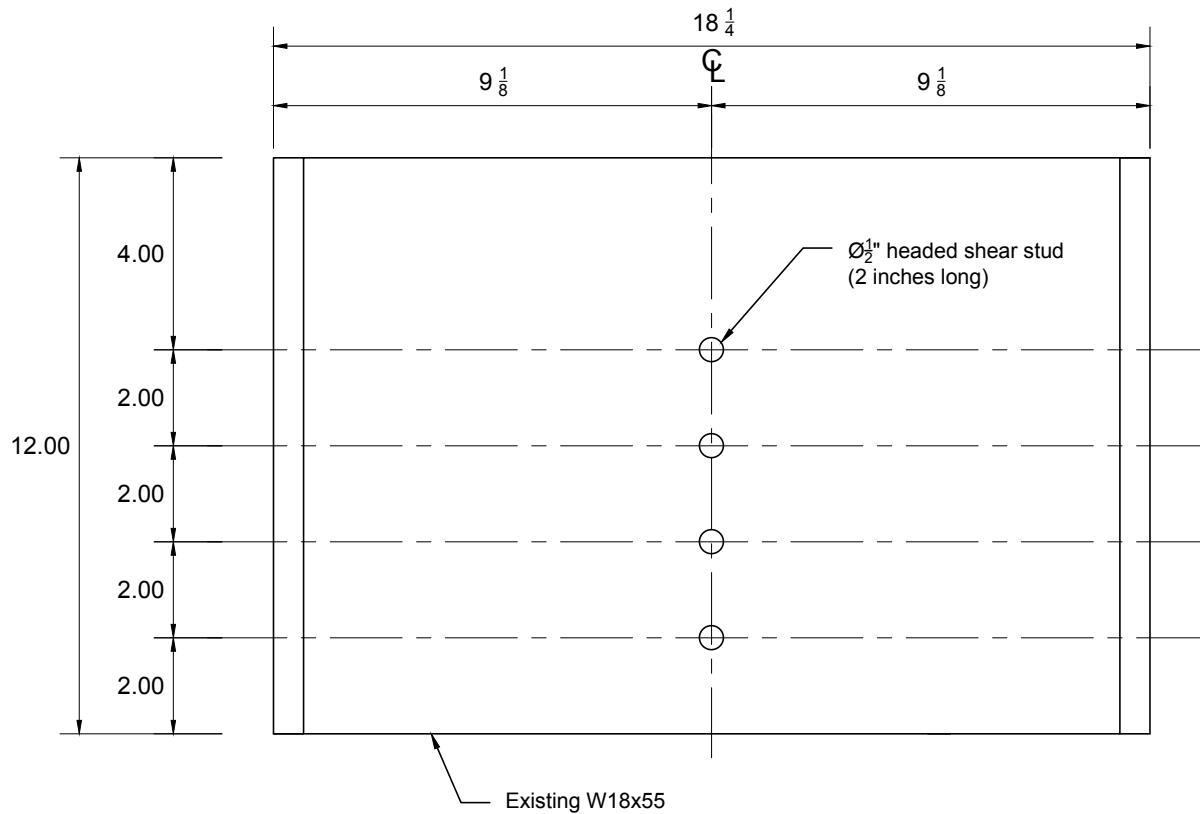
Scale: As noted

Sheet Number: S7

Date: 04/20/2016

Notes

1. All units in inches.
2. All welding to be performed in accordance with AWS standards.
3. Stud location tolerance: $\frac{1}{32}$ "
4. Number of specimens: 1



S8-1: Ultimate Strength Specimen
Scale - 1:4



University of Connecticut



Connecticut Dept. of Transportation

Project: Girder-End Repair

Title: Push Out Specimen - Ultimate Strength Specimen

Drawn by: Dominic Kruszewski

Approved by:

Scale: As noted

Sheet Number: S8

Date: 04/20/2016

Notes

1. All units in inches.
2. All welding to be performed in accordance with AWS standards.
3. Stud location tolerance: $\frac{1}{32}$ "
4. Number of specimens: 1

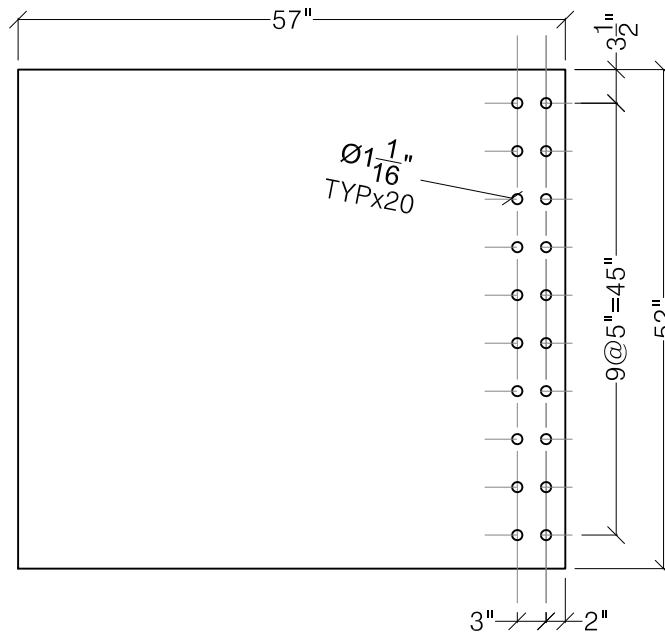
Appendix C Experimental Plate Girder Specimen Shop Drawings

Materials				
Item	Part #	Quantity	Size (in)	Weight (lb/item)
TS Top Flange	TSTF	4	PL1½x18x57	437.1
TS Web	TSW	4	PL¾x52x57	315.7
TS Bottom Flange	TSBF	4	PL1x18x57	291.4
PE Top Flange	PETF	1	PL1½x18x163½	1,253.7
PE Web	PEW	1	PL¾x52x163½	905.5
PE Bottom Flange	PEBF	1	PL1x18x163½	835.8
WS Stiffener	WS	14	PL¾x6x52	33.2
BS Stiffener	BS	8	PL½x6x52	44.3
LR Stiffeners	LR	6	PL1½x6x52	132.9
Web Splice PL	WSP	2	PL¾x14¼x49	74.4
Flange Splice PL 1	FSP1	2	PL¾x15¼x18	58.5
Flange Splice PL 2	FSP2	4	PL¾x8x15¼	26.0
Connection PL 1	CPL1	4	PL½x12x28	47.7
Connection PL 2	CPL2	2	PL2x16x16	145.4
Connection PL 3	CPL3	1	PL2x13½x16	122.7
Connection PL 4	CPL4	10	PL1x11¼x15	35.9
Triangular Brace	TB	20	PL½x8x8 Triangle	4.5
Bracket Tube	BT	10	HSS6x4x¼x48	62.5

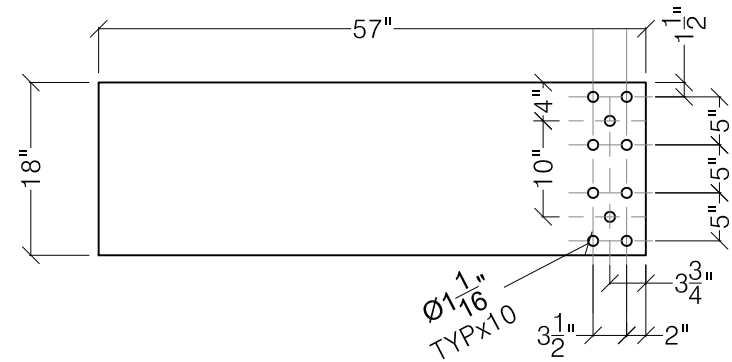


Notes

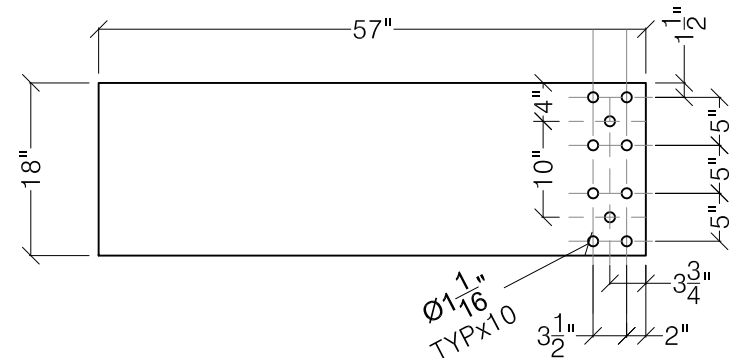
1. All steel plates are A36-Gr. 36,
Prefer Gr. 50 Steel for 2" Plates
2. All dimensions are inches.
3. All holes are standard, drilled
4. Spacing of holes is C-C
5. Stiffener spacing is C-C of plates
6. Stiffeners shall be welded on both sides of the top, bottom, and sides
7. Flanges shall be centered on the web
8. Tolerance is $\frac{1}{32}$ "



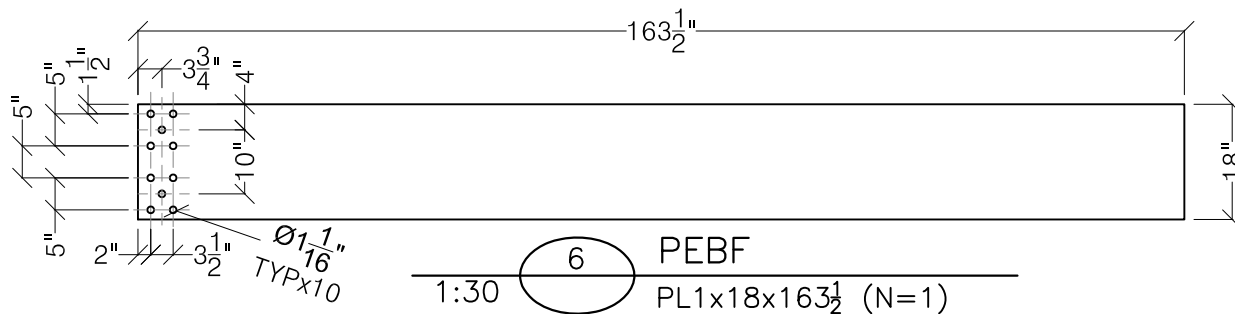
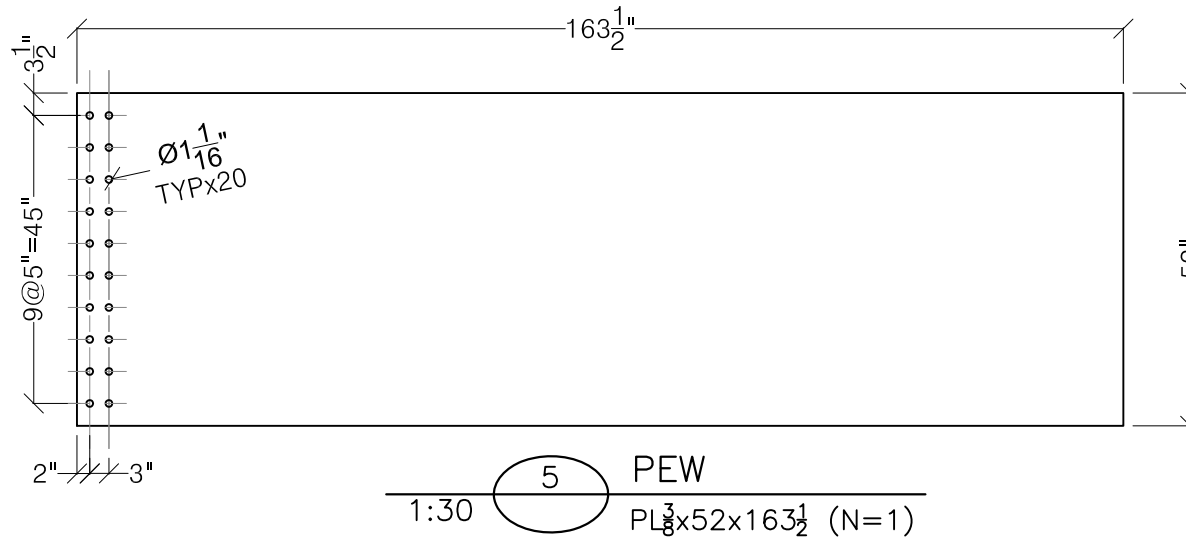
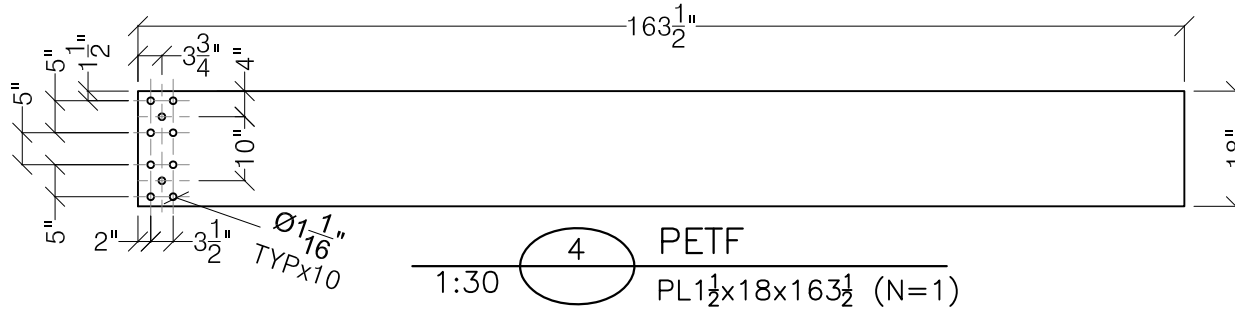
1:20 (2) TWS
PL $\frac{3}{8}$ x52x57 (N=4)



1:20 (1) TSTF
PL $1\frac{1}{2}$ x18x57 (N=4)



1:20 (3) TSBF
PL 1x18x57 (N=4)



UConn
SCHOOL OF ENGINEERING

University of Connecticut



Connecticut Department
of Transportation

Project: **ConnDOT Phase II**

Title: **Test Specimen - Permanent Girder**

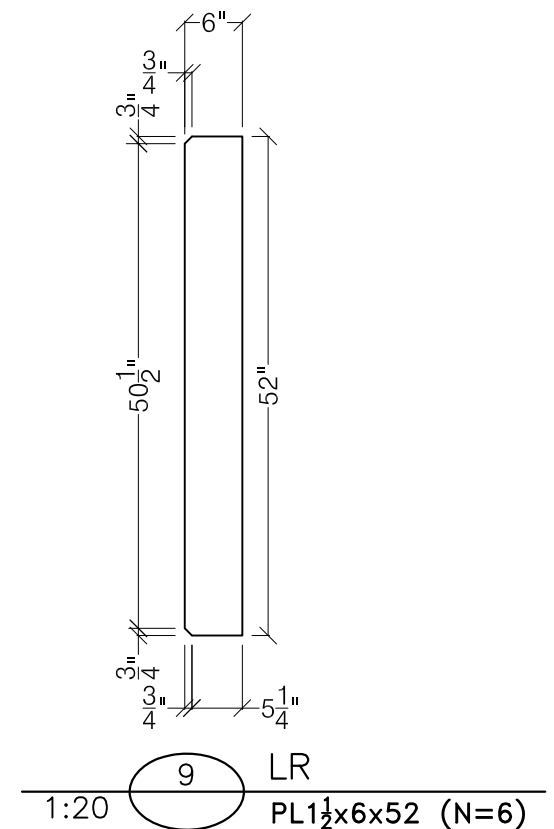
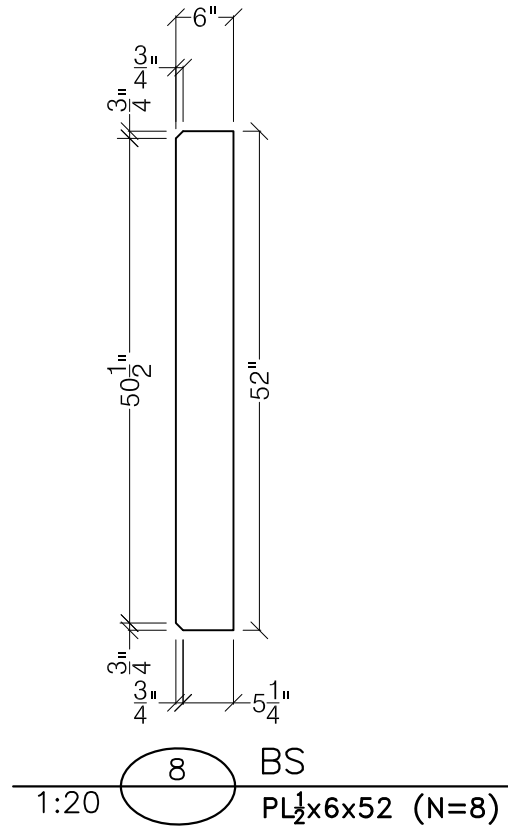
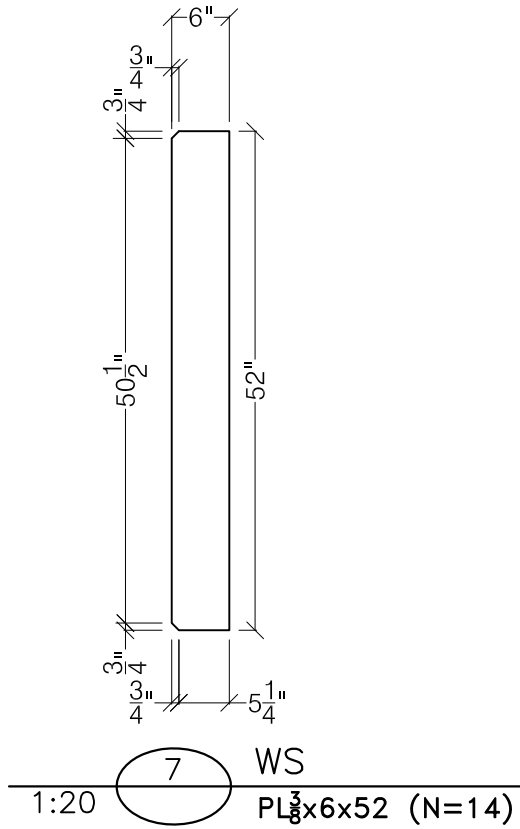
Drawn by: **Kevin McMullen**

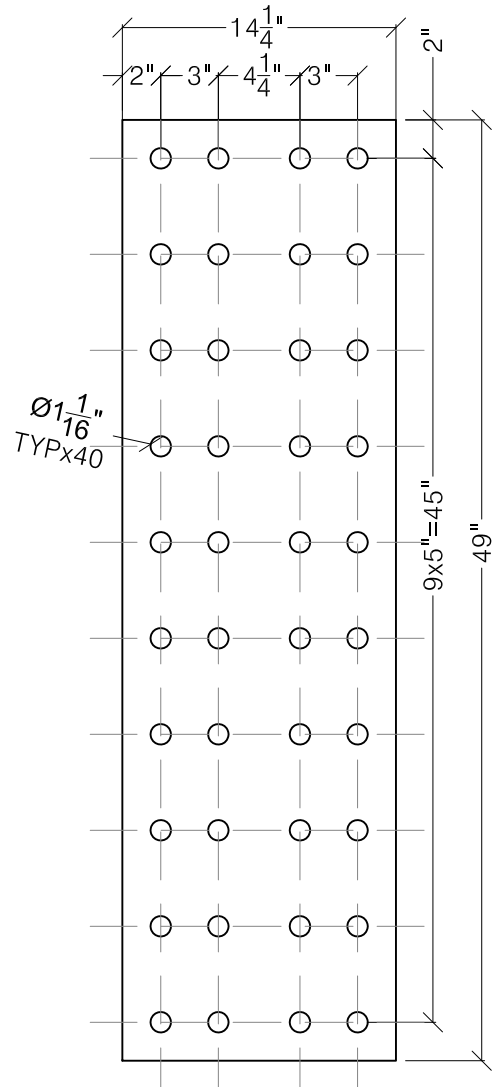
App. by: **Arash Zaghi, Prof.**

Scale: **As Shown**

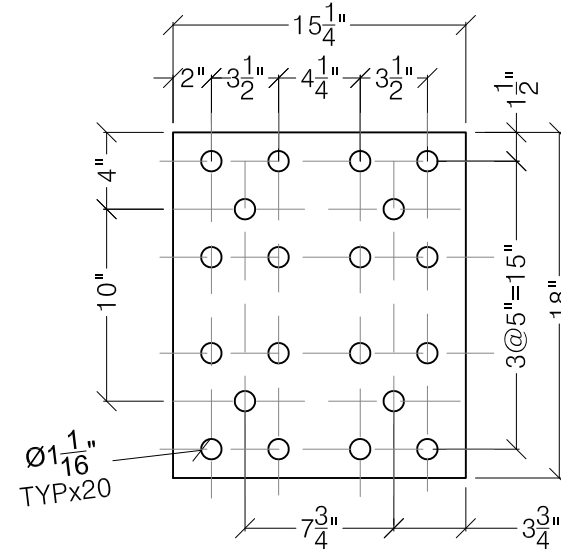
Sheet No: **S-02**

Date: **October 3, 2016**

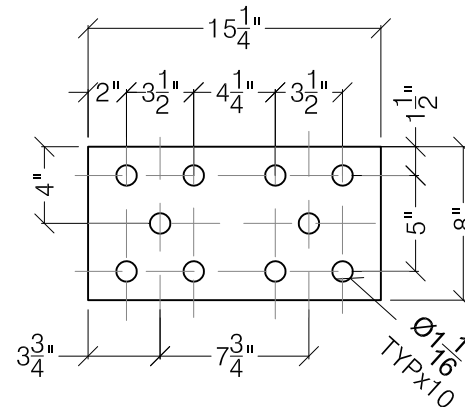




1:10 (10) WSP
 $PL_{\frac{3}{8}} \times 14\frac{1}{4} \times 49$ (N=2)



1:10 (11) FSP1
 $PL_{\frac{3}{4}} \times 15\frac{1}{4} \times 18$ (N=2)



1:10 (12) FSP2
 $PL_{\frac{3}{4}} \times 8 \times 15\frac{1}{4}$ (N=4)

UConn
 SCHOOL OF ENGINEERING

University of Connecticut



Connecticut Department
 of Transportation

Project: **ConnDOT Phase II**

Title: **Splice Plates**

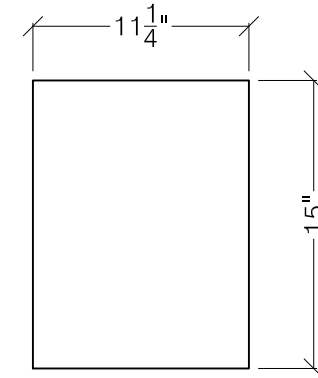
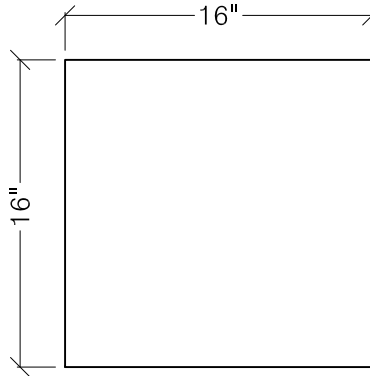
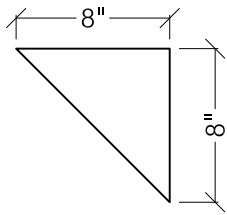
Drawn by: **Kevin McMullen**

App. by: **Arash Zaghi, Prof.**

Scale: **As Shown**

Sheet No: **S-04**

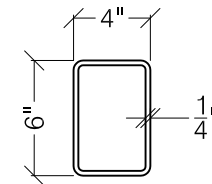
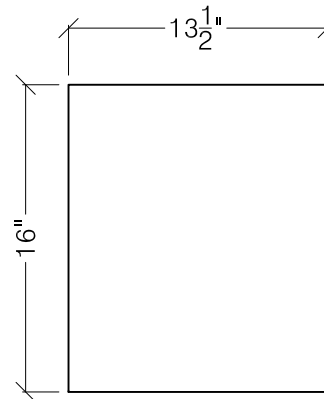
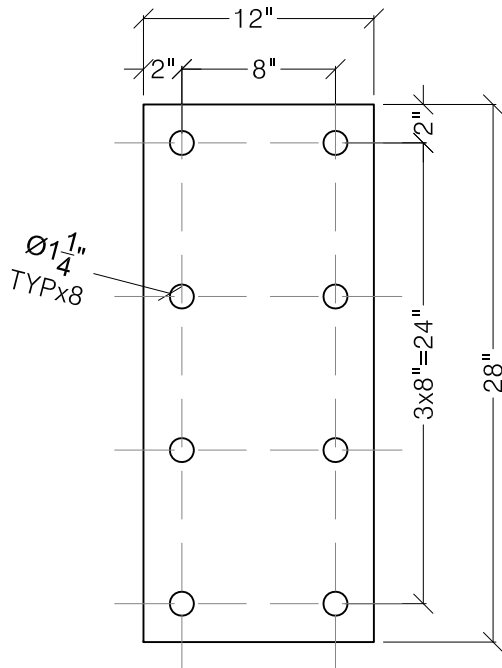
Date: **October 3, 2016**



1:10 (13) TB
PL $\frac{1}{2}$ x8x8 (Triangle)(N=20)

1:10 (15) CPL2
PL2x16x16 (N=2)

1:10 (17) CPL4
PL1x11 $\frac{1}{4}$ x15 (N=10)



1:10 (14) CPL1
PL $\frac{1}{2}$ x12x28 (N=4)

1:10 (16) CPL3
PL2x13 $\frac{1}{2}$ x16 (N=1)

1:10 (18) BT
HSS6x4x $\frac{1}{4}$ x48 (N=10)

UConn
SCHOOL OF ENGINEERING

University of Connecticut



Connecticut Department
of Transportation

Project: **ConnDOT Phase II**

Title: Connection Plates

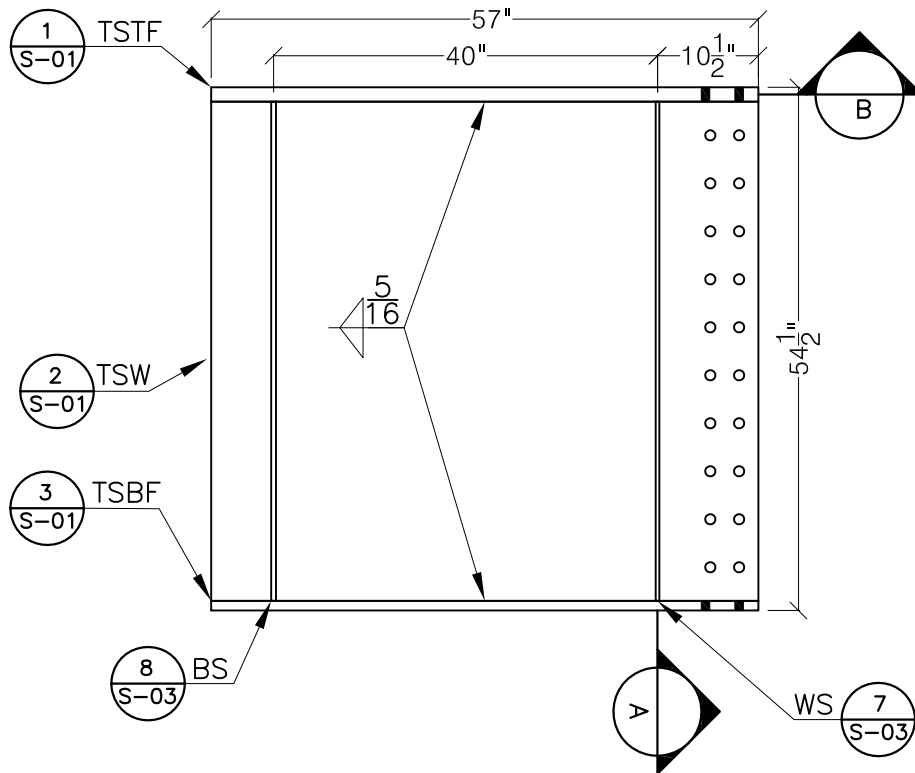
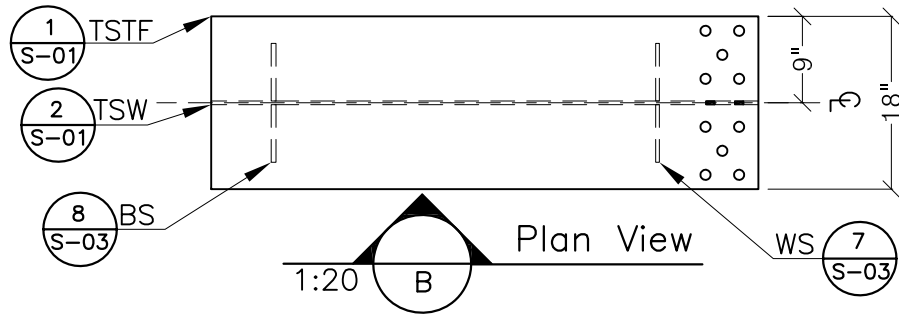
Drawn by: Kevin McMullen

App. by: Arash Zaghi, Prof.

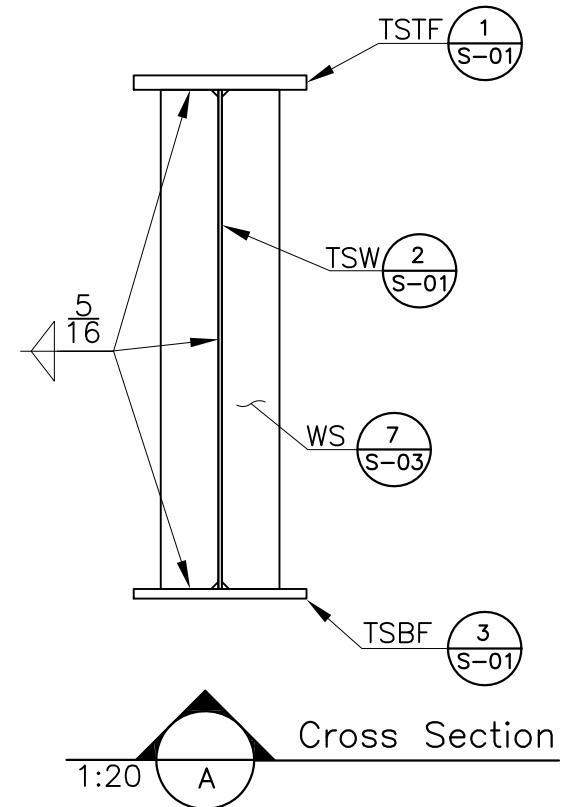
Scale: As Shown

Sheet No: S-05

Date: October 3, 2016



1 Test Specimen
1:20 N=4



UConn
SCHOOL OF ENGINEERING

University of Connecticut



Connecticut Department
of Transportation

Project: **ConnDOT Phase II**

Title: **Test Specimen**

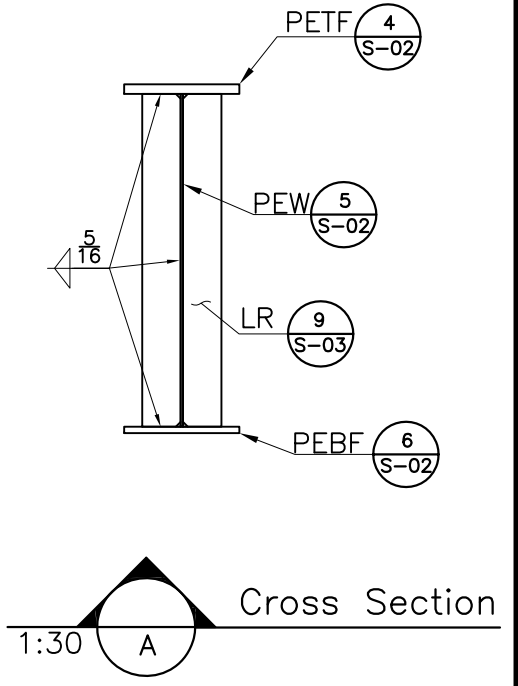
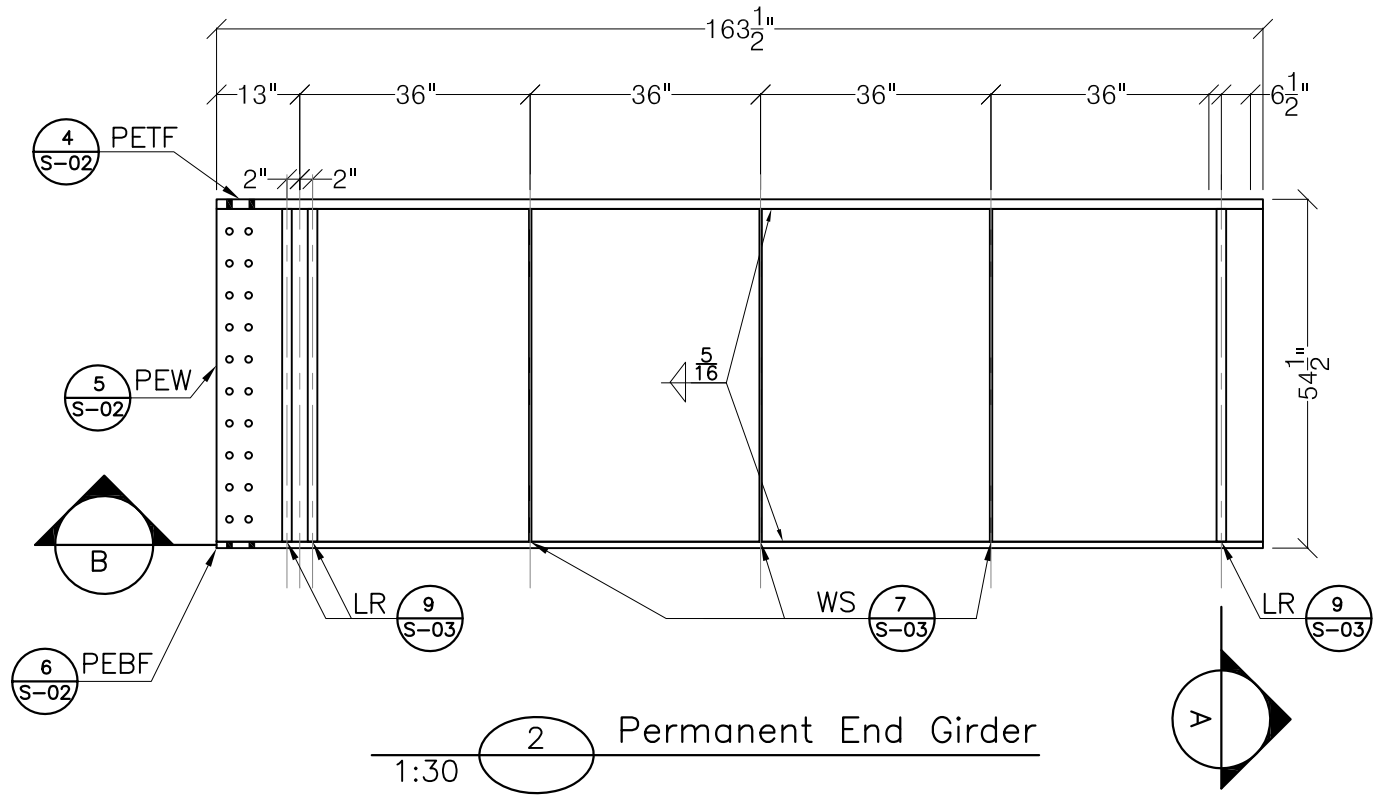
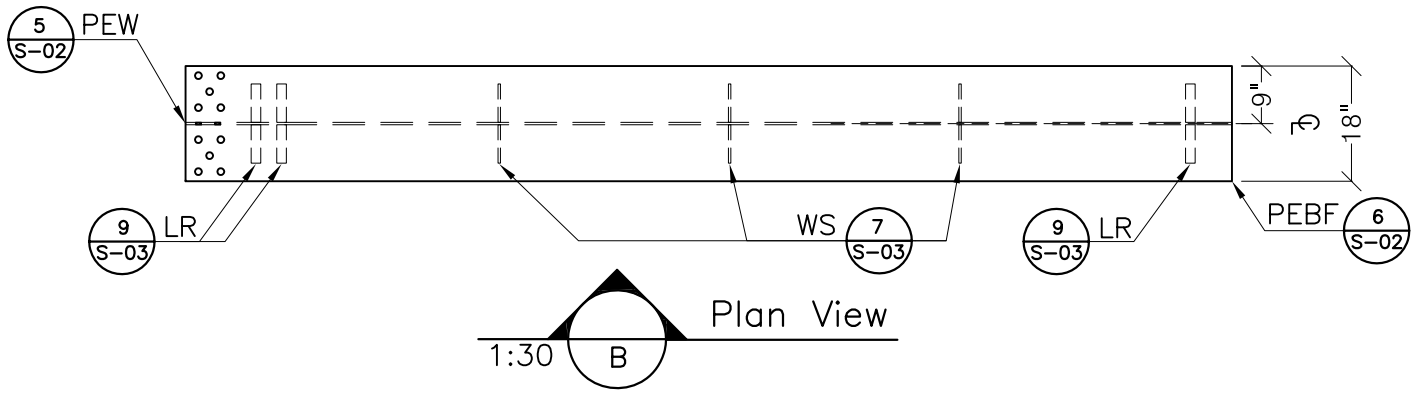
Drawn by: **Kevin McMullen**

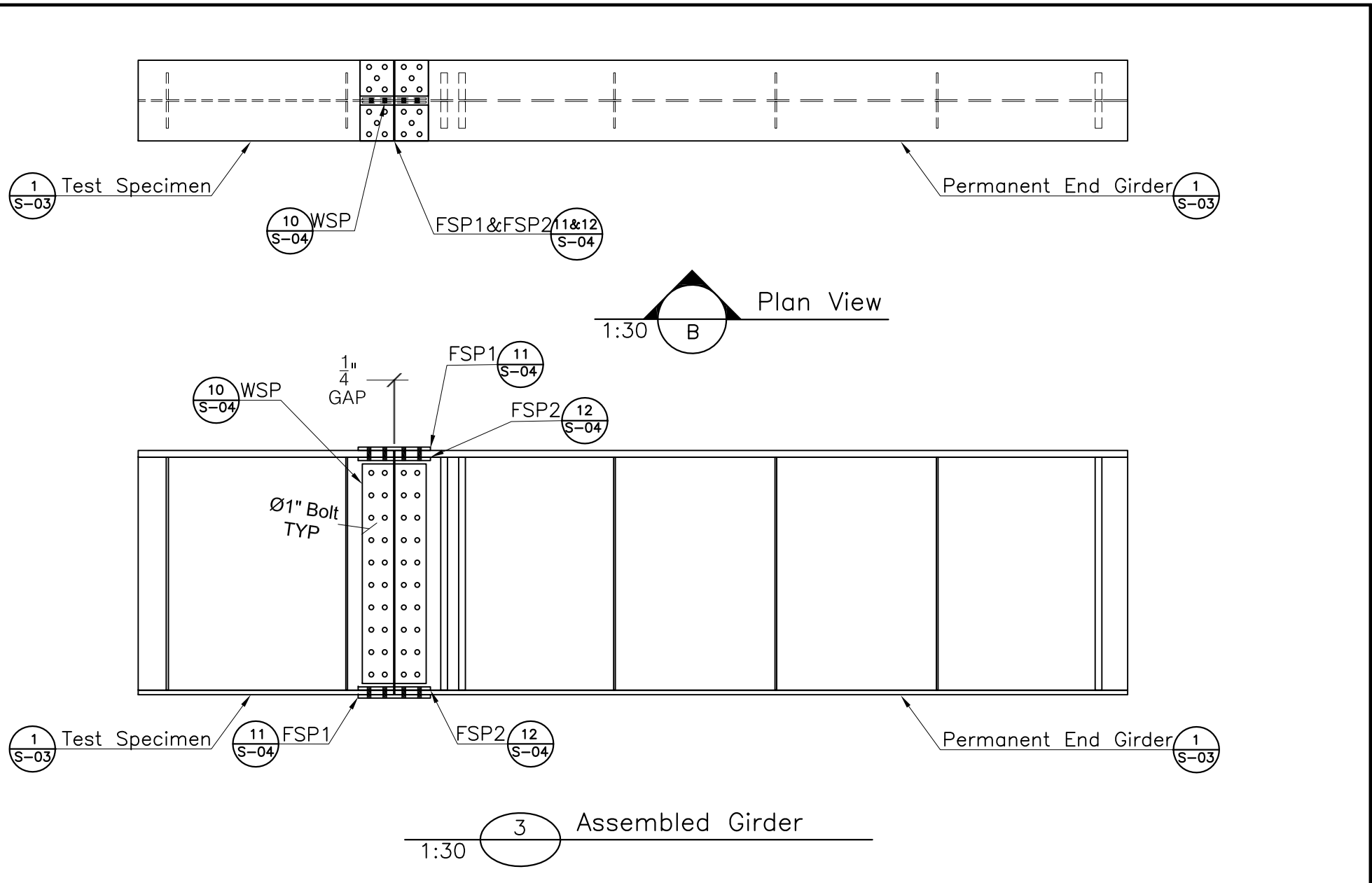
App. by: **Arash Zaghi, Prof.**

Scale: **As Shown**

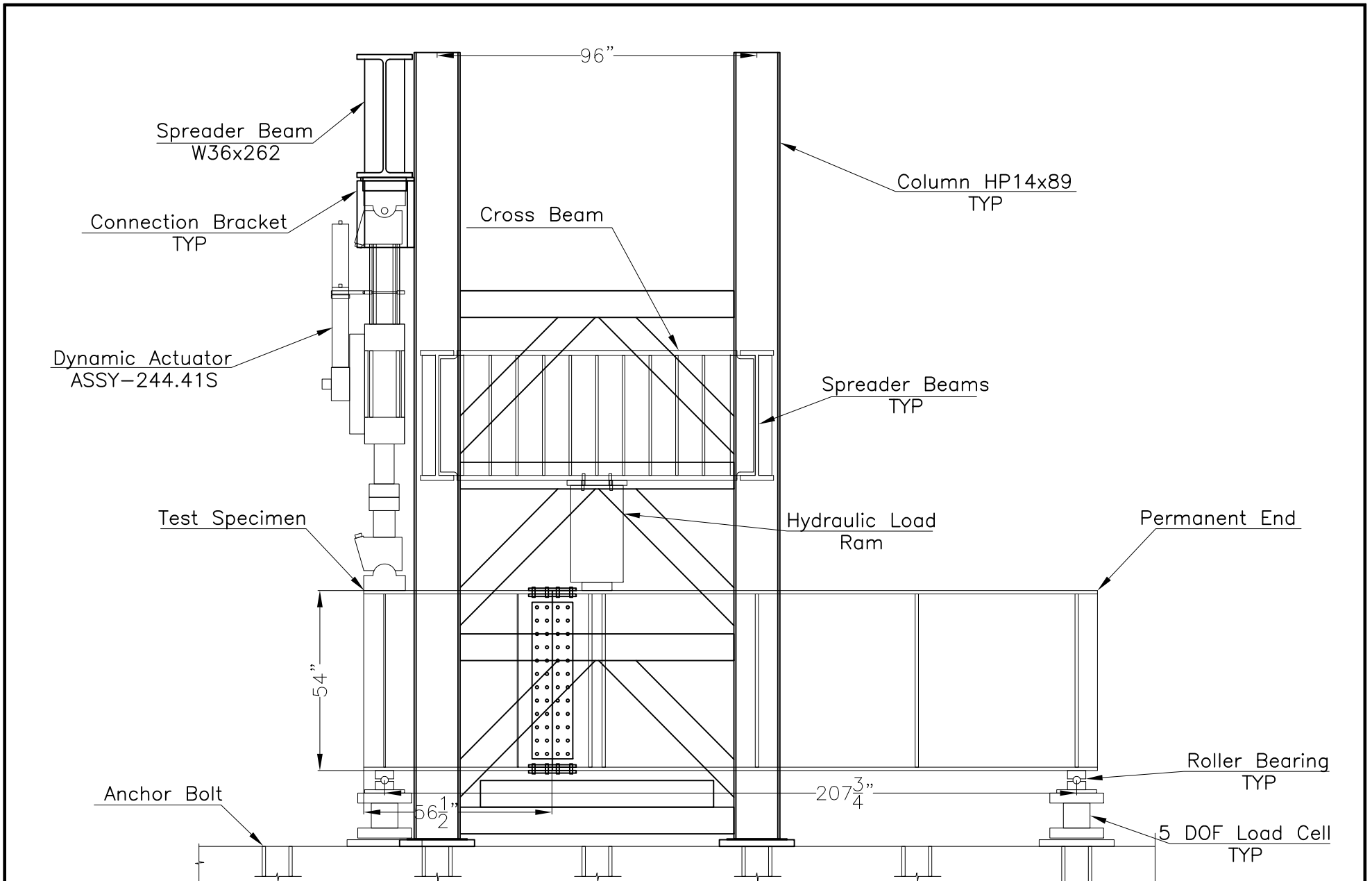
Sheet No: **S-07**

Date: **October 3, 2016**

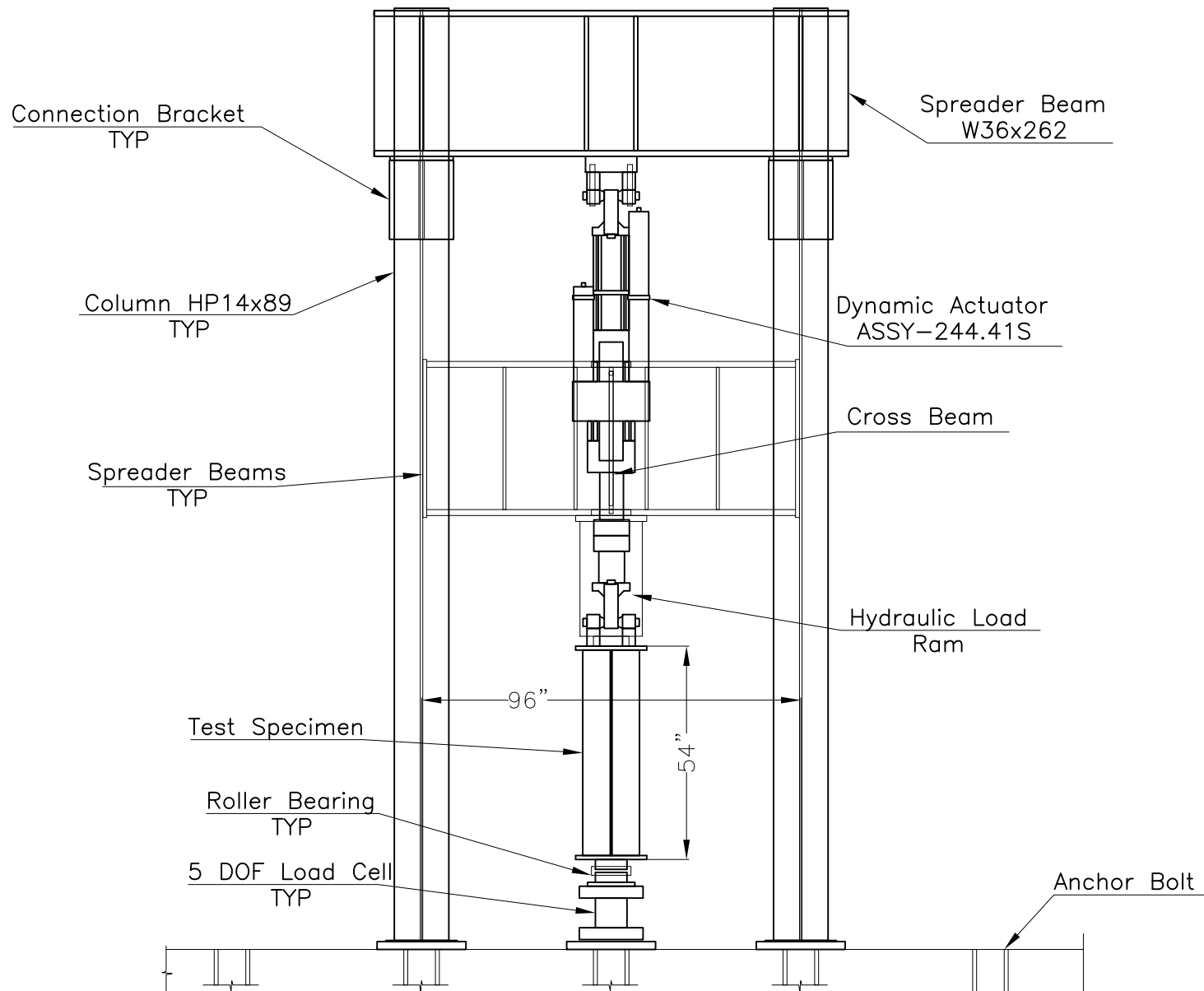


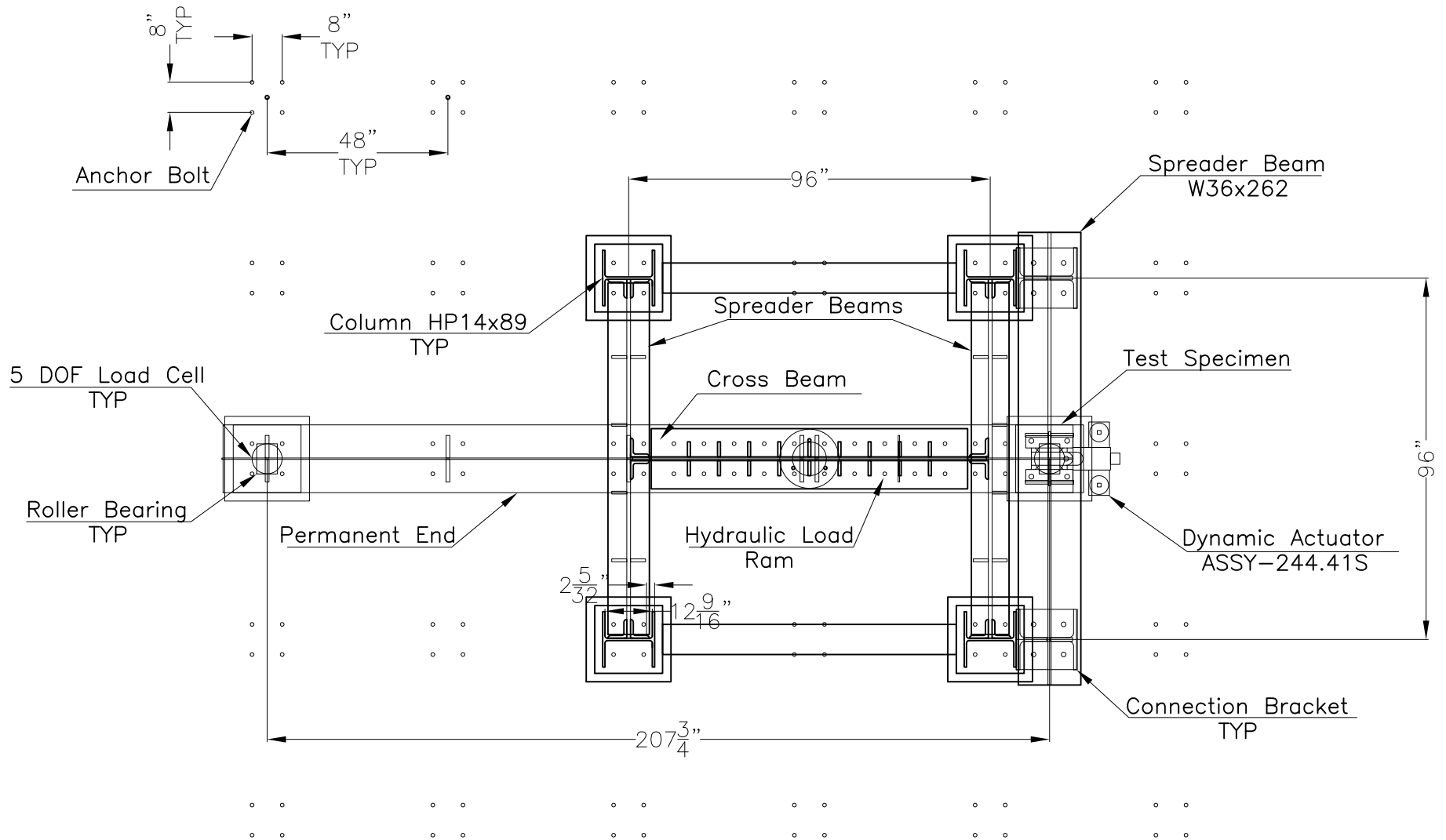


Appendix D Drawings of the Experimental Test Setup

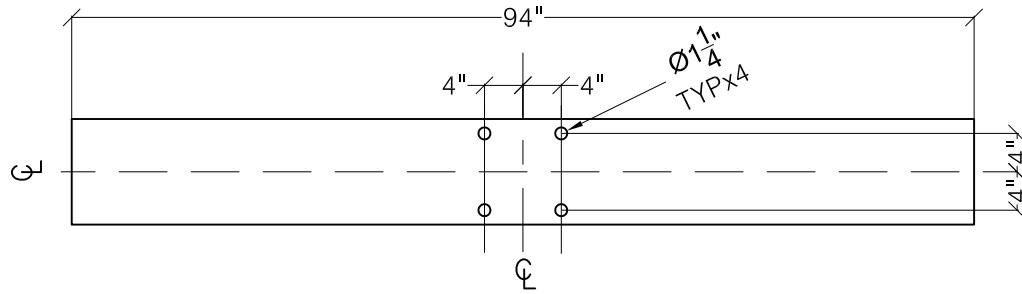


<p>University of Connecticut</p>	<p>Connecticut Department of Transportation</p>	Project: ConnDOT Phase II	
		Title: Large Scale Set Up - Elevation View	
Drawn by: Kevin McMullen		App. by:	
Scale: 1:40	Sheet No: S-01	Date: October 27, 2016	



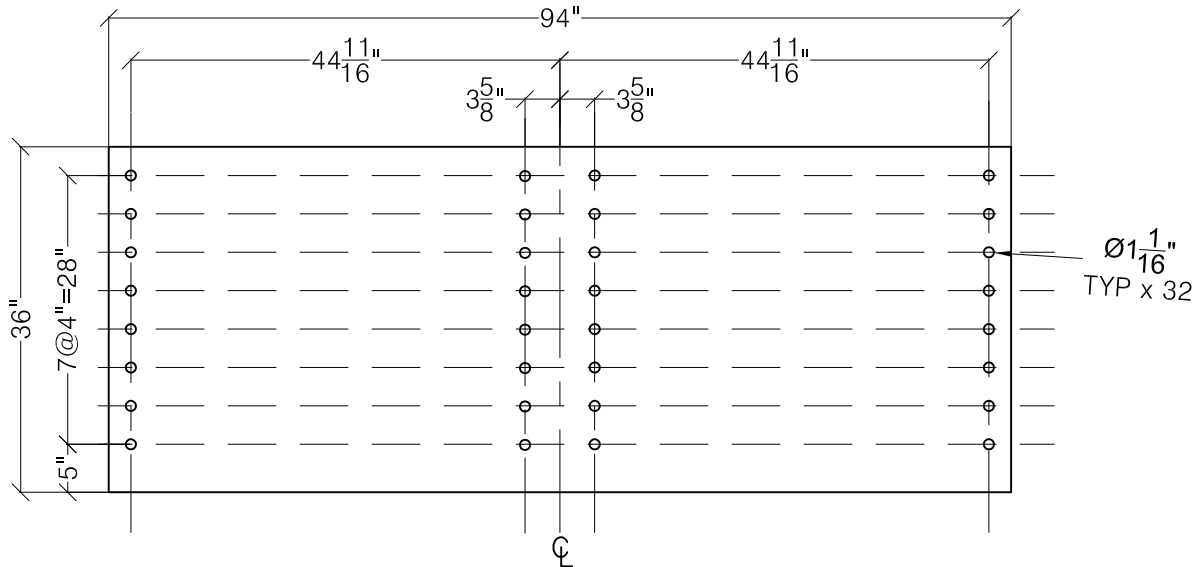


Appendix E Experimental Load Frame Shop Drawings



1:20 1 SB Flange
S-01 PL1.5x11x94 (N=4)

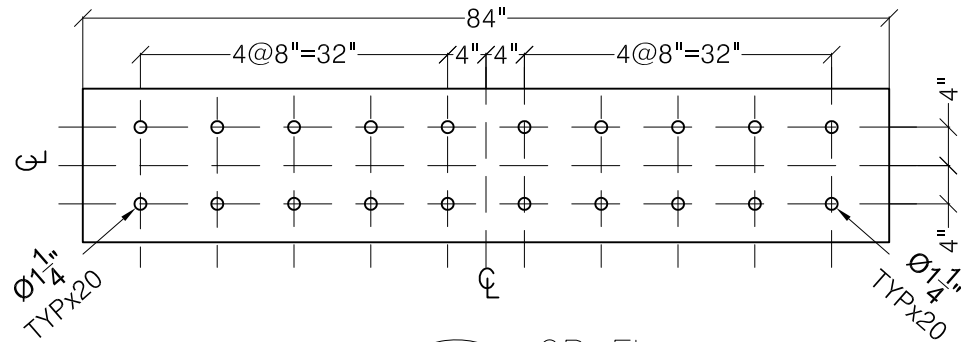
Materials				
Item	Quantity	Size (in)	Length (in)	Weight (lb/item)
Spreader Beam Flanges	4	PL1.5x11	94	440.5
Spreader Beam Web	2	PL1x36	94	961
Cross Beam Flanges	2	PL1.5x16	84	572.5
Cross Beam Web	1	PL1.25x36	94	1,222
Stiffener 1	6	PL $\frac{3}{4}$ x4	36	30.7
Stiffener 2	18	PL $\frac{3}{4}$ x6	36	46
Angle	12	L5x5x $\frac{3}{4}$	34	67



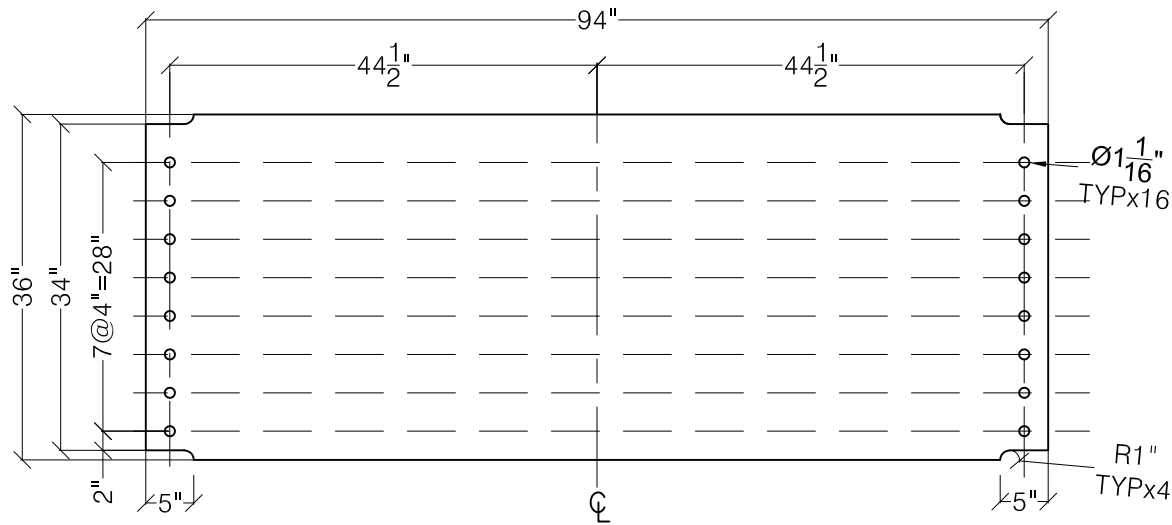
1:20 2 SB Web
S-01 PL1x36x94 (N=2)

Notes

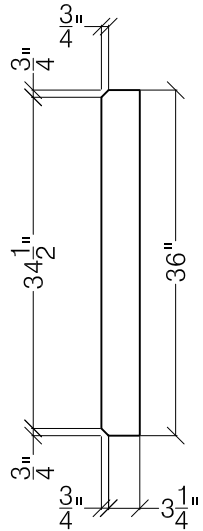
1. All steel plates are A572-Gr. 50
2. All Dimensions are from CL
3. All holes are standard, drilled
4. Holes in the flange are $\varnothing 1\frac{1}{4}$ "
5. Holes in the web are $\varnothing 1\frac{1}{16}$ "
6. Spacing of holes is C-C
7. Stiffener spacing is C-C of plates
8. Stiffeners shall be welded on both sides the top, bottom, and sides
9. Flanges shall be welded to the center of the web on both sides
10. Haunch is 5" long with a 1" radius. See sheet 2.
11. Tolerance is $\frac{1}{32}$ "



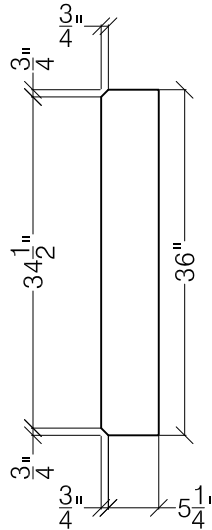
3 CB Flange
1:20 S-02 PL1.5x16x84 (N=2)



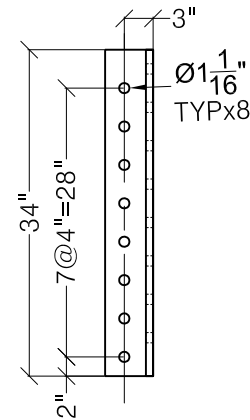
4 CB Web w/ Cope
1:20 S-02 PL1.25x36x94 (N=1)



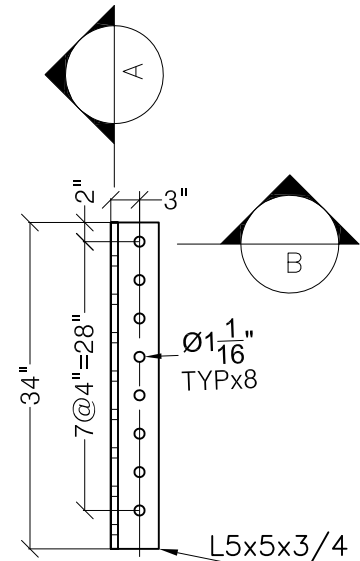
1:20 5 SB Stiffener
S-03 PL $\frac{3}{4}$ x4x36 (N=6)



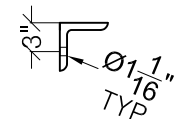
1:20 6 CB Stiffener
S-03 PL $\frac{3}{4}$ x6x36 (N=18)



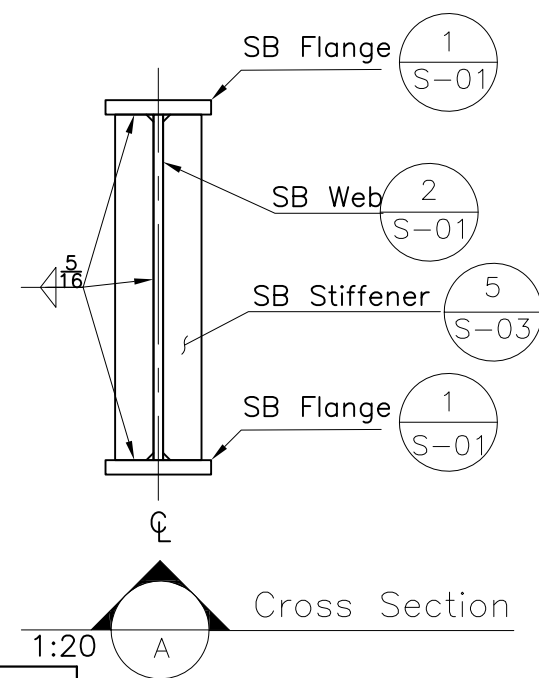
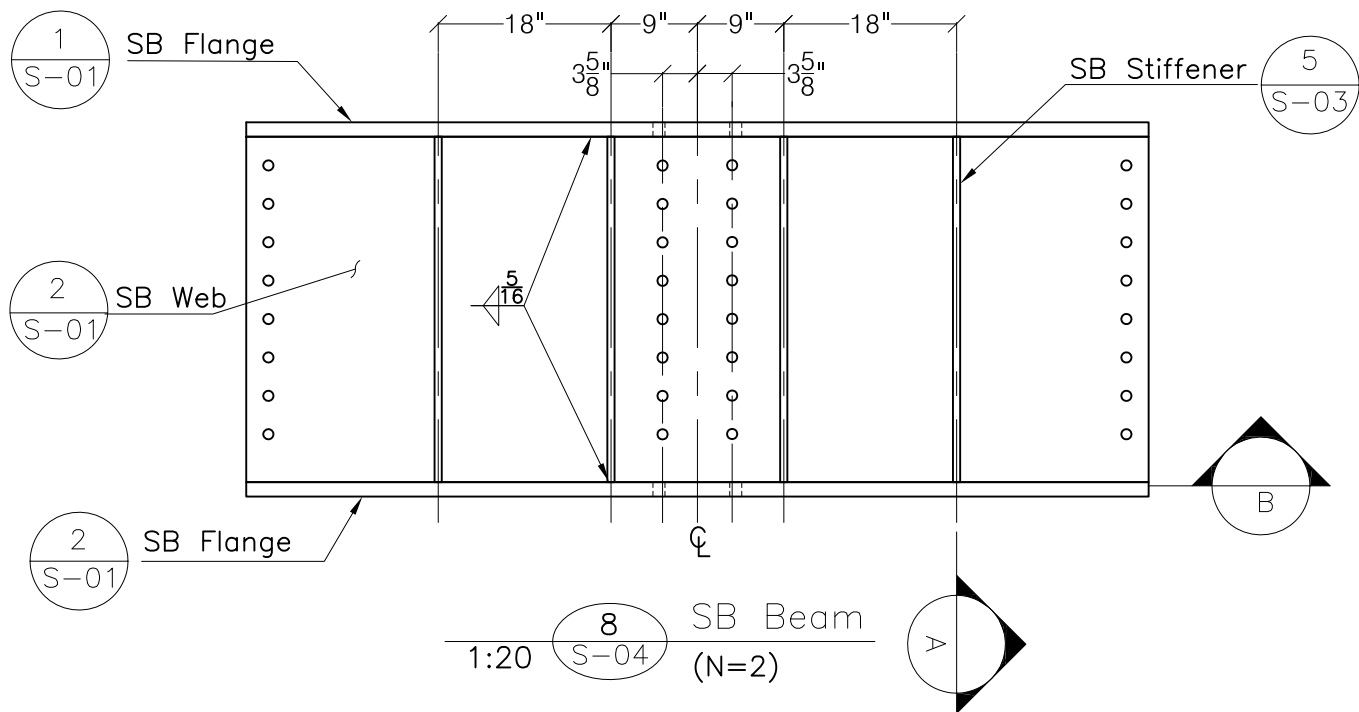
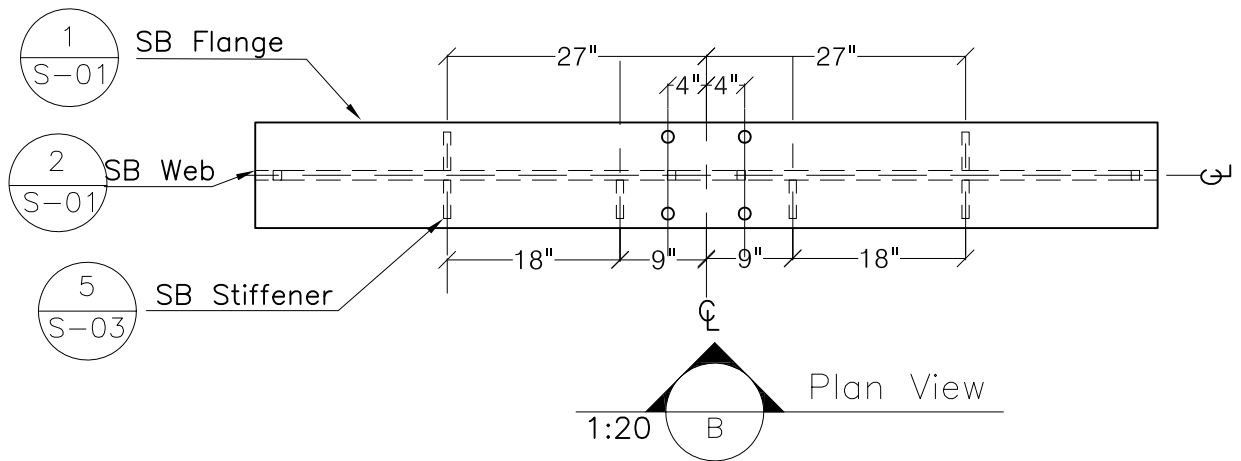
1:20 A

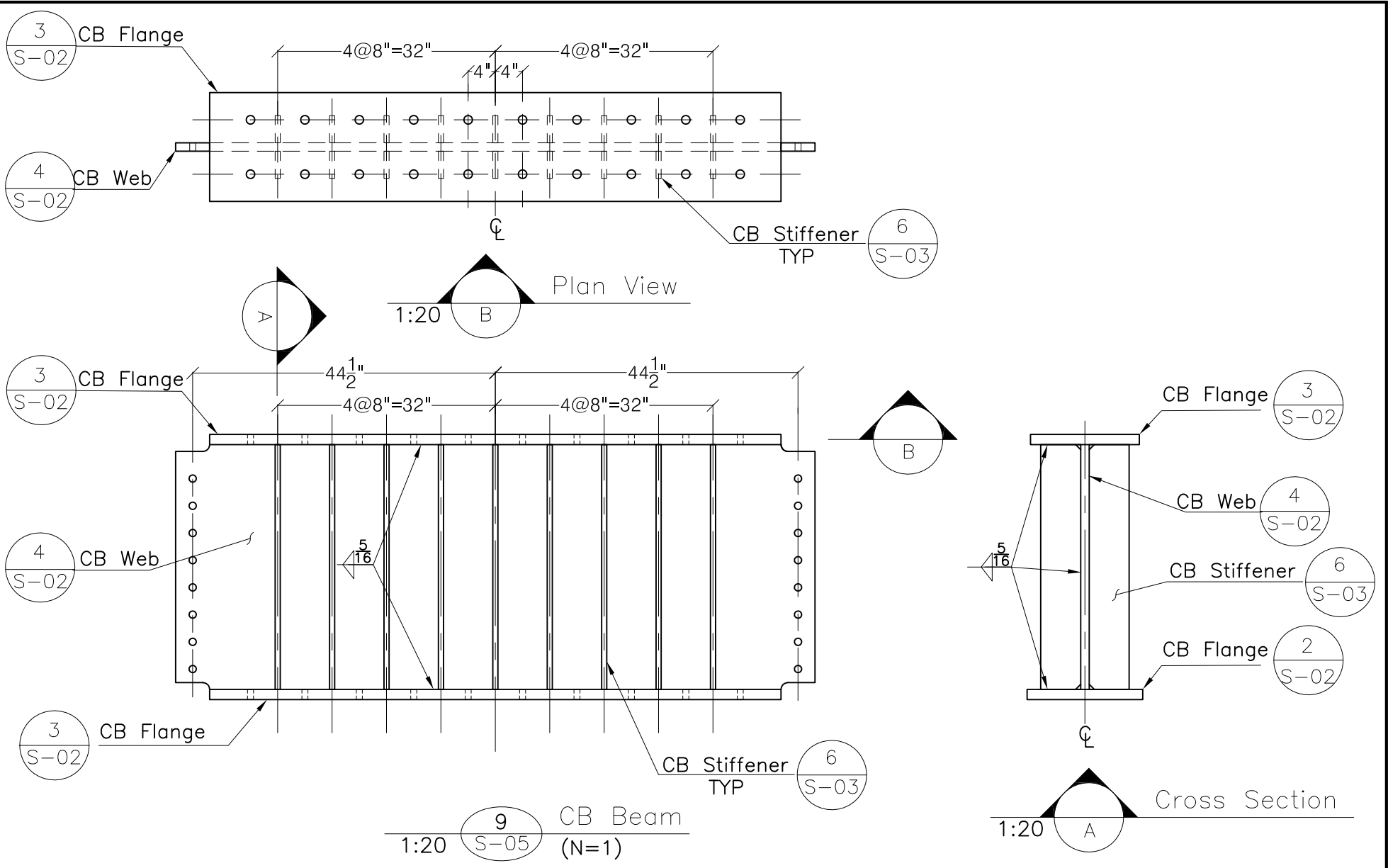


1:20 7 Angle
S-03 L5x5x $\frac{3}{4}$ (N=12)



1:20 B





Appendix F UHPC Repair Sample Calculations

Design Methods for Shear Stud Capacity for UHPC Repair

1. Strength Design

Calculations for Studs Based on HL-93 Loading and Strength 1

	Shear (kips)	Number of 1/2" Studs
Live Load Only	116	9
Strength 1	301	22

HL-93*1.75¹
2

¹Assume that Studs only carry Live Load

²Assume studs are designed to carry Strength 1

3. Capacity Design

Calculation for Studs Based on As-Built Strength

Beams With Bearing Stiffeners

Shape	Geometric Properties				Design Demand			Final Stud Design			
	Web Thickness (in)	Web Depth (in)	Total Depth of Beam (in)	Flange Thickness (in)	Design Based on Bearing Capacity (kips)	Design Based on Shear Capacity (kips)	Design based on Controlling Capacity (kips)	Strength Based on Bearing of Stud on Web (kips)	1/2" Stud Capacity (kips)	Controlling Stud Capacity (kips)	Number of 1/2" Studs
36WF135	0.600	34.02	35.60	0.790	500	426	426	41.76	15.80	13.43	32
36WF160	0.653	33.96	36.00	1.020	532	463	463	45.45	15.80	13.43	34
36WF182	0.726	33.96	36.32	0.725	579	515	515	50.53	15.80	13.43	38
36WF245	0.815	33.36	36.06	0.802	640	568	568	56.72	15.80	13.43	42
36WF230	0.765	33.36	35.88	0.765	605	533	533	53.24	15.80	13.43	40
36WF194	0.770	33.96	36.48	0.770	608	546	546	53.59	15.80	13.43	41
36WF170	0.680	33.96	36.16	0.680	549	482	482	47.33	15.80	13.43	36
36WF150	0.625	33.96	35.84	0.625	516	443	443	43.50	15.80	13.43	33
33WF141	0.625	31.39	33.31	0.960	516	410	410	43.50	15.80	13.43	31

Beams Without Bearing Stiffeners

Shape	Geometric Properties				Design Demand			Final Stud Design			
	Web Thickness (in)	Web Depth (in)	Total Depth of Beam (in)	Flange Thickness (in)	Design Based on Bearing Capacity (kips)	Design Based on Shear Capacity (kips)	Design based on Controlling Capacity (kips)	Strength Based on Bearing of Stud on Web (kips)	1/2" Stud Capacity (kips)	Controlling Stud Capacity (kips)	Number of 1/2" Studs
36WF135	0.600	34.02	35.60	0.790	225	426	225	41.76	15.80	13.43	17
33WF130	0.580	31.34	33.31	0.855	209	380	209	40.37	15.80	13.43	16

* Sample calculations for design demands are presented in the following pages

2. Fatigue Design

Calculations for Studs Based on Fatigue Calculations

	Fatigue Resistance (kips)	Number of 1/2" Studs
Wheel Load	31.50	23
Fatigue Truck	41.16	30

Controlling Number of Studs

Sample Calculation for Bearing Strength and Shear Capacity of As-Built 36WF135

Geometric Properties

Web Thickness,	t_w	0.6 in
Web Depth, D	D	34.02 in
Total Depth of Beam, d	d	35.6 in
Flange Thickness, t_f	t_f	0.79 in
Bearing Stiffener Thickness, t_{bs}	t_{bs}	0.75 in
Width of Bearing Stiffener, b_{bs}	b_{bs}	5 in
Length of Web from Edge of Stiffener to Free End	l_{free}	5.44 in
Nine x Flange Thickness	$9t_w$	5.4 in
Yield Strength of Stiffeners and Web	F_y	36 ksi
Modulus of Elasticity	E	29000 ksi

Girders With Bearing Stiffener

Axial Resistance of Bearing Stiffener

(6.10.11.2.4a,b, 6.9.4.1.1-1)

Area of effective column section if $9t_w$ is used	13.98 in ²	$2(bb_{bs}t_{bs}+9t_w t_w)$
Area of effective column section if distance to free end is less than $9t_w$	14.00 in ²	$2bb_{bs}t_{bs}+t_w l_{free}+9t_w t_w$
Moment of Inertia of Effective Column Section, I	74.44 in ⁴	$\frac{t_{bs}(2t_{bs} + t_w)^3}{12}$
Radius of Gyration, r_s	2.31 in	$\sqrt{I/A_s}$
Slenderness, λ	0.015	$\left(\frac{KL}{r_s \pi}\right)^2 \frac{F_y}{E}$
$1/\lambda$	65.03	
Bearing Force to be recovered P_n	500 kip	$.658^\lambda A_s F_y$
ΦP_n	450 kip	$.9P_n$

Shear Capacity of Girder

(6.10.9.2-2, 6.10.9.3.2-4)

h/t_w	56.7	
Shear Strength If $h/t_w < 1.10(k_v E/F_y).5$	426 kip	$.58F_y A_w$
Nominal Shear Strength	426 kip	

Girders Without Bearing Stiffeners

Web Local Yielding

(D6.5.2, D6.5.3)

Distance from Outer Face of Flange Resisting Bearing Reaction to the Web Toe of the Fillet, k	1.6875 in	
Length of Bearing, N	6 in	
Nominal Resistance to Concentrated Loading, R_n	221 kip	$(2.5k + N)F_{y(web)} t_w$
ΦR_n	221 kip	

Web Crippling

N/d	0.169	
If $N/d \leq 0.2$		
Nominal Resistance to Concentrated Loading, R_n	225 kip	$0.4t_w^2 \left[1 + 3\left(\frac{N}{d}\right)\left(\frac{t_w}{t_f}\right)^{1.5}\right] \sqrt{\frac{EF_{y(web)} t_f}{t_w}}$
ΦR_n	180 kip	

Sample Calculations of Fatigue Loads for Wheel Loads and the Fatigue Truck

Allowable Shear Force	Z_r
1/2" Stud Fatigue Capacity	1.375 kips

$$5.5 \cdot d^2$$

(6.10.10.2-1)

With Wheel Load

Dynamic Load Allowance, <i>IM</i>	1.75
Truck Wheel Load	18 kips
Shear Force at the Girder End	31.5 kips
Number of 1/2" Shear Studs	22.9

With Fatigue Truck

Multiple Presence Factor, <i>m</i>	1.2
Shear Force from Influence Line, <i>V</i>	59.7 kips
Dynamic Load Allowance, <i>IM</i>	1.15
Single Lane Distribution Factor, <i>DF</i>	0.72
Shear Force at the Girder End	41.2 kips
Number of 1/2" Shear Studs	29.9

(3.6.1.4.1)

(3.6.1.1.2)

(Table 4.6.2.2.3a-1)

$$\frac{V DF IM}{m}$$

Strength Based on Bearing of Stud on Web

$2.4F_y(stiffner)d_b$

(6.13.2.9)

Stud Load Carrying Capacity

$.75A_{stud}F_u$

Calculations or Shear Demand at Girder Ends Due to Dead Loads

Span Length	80 ft
Unit Weight of Steel	490 pcf
Unit Weight of Concrete	160 pcf
Unit Weight of Wearing Surface	140 pcf

Dead Load Due to Steel

Weight of 36WFX245 Girder	245 lb/ft
Volume of 14"x1"x63' Cover Plate	6.125 ft ³
Total Weight of Girder	22601 lb
+10% for diahragms	2260 lb
Total Weight of Steel	24861 lb

DL Due to Parapet

Cross Sectional Area of Parapet	9.725 ft ²
Total Weight of Parapets	248960 lb
Total Number of Girders in Span	10
Weight of Parapet/Girder	24896 lb

Dead Load Due to Deck	Interior Beam	Exterior Beam	
Tributary Width of Deck	9	7.25	ft
Depth of Deck	8	8	in
Total Weight of Deck	76800	61867	lb

Dead Load Due to Wearing Surface	Interior Beam	Exterior Beam	
Tributary Width of Wearing Surface	9	7.25	ft
Depth of Wearing Surface	3	3	in
Total Weight of Wearing Surface	25200	20300	lb

	Interior Beam	Exterior Beam	
Total Dead Load of Wearing Surface (DW)	25200	20300	lb
Total Dead Load (DC)	126557	111624	lb

Shear Demand	Interior Beam	Exterior Beam	
Shear at Girder End Due to Dead Load	63.28	55.81	kips
Shear at Girder End Due to Wearing Surface	12.6	10.15	kips

Factored Shear Demand at Girder End for Strength 1 Load Combination

(Table 3.4.1-1)

Loading Component	Strength 1 Load Combination Factor	Interior Beam Shear Demand				Exterior Beam Shear Demand				kips
		Unfactored		Factored		Unfactored		Factored		
		1 Lane Loaded	2+ Lanes Loaded	1 Lane Loaded	2+ Lanes Loaded	1 Lane Loaded	2+ Lanes Loaded	1 Lane Loaded	2+ Lanes Loaded	
HL-93 LL	1.75	94	116	165	203	70	104	122	183	kips
DC	1.25	63	63	79	79	56	56	70	70	kips
DW	1.5	13	13	19	19	10	10	15	15	kips
Total Shear Demand at Girder End				263	301			207	268	

Controlling Shear Demand

Interior Beams 301 kips
Exterior Beams 268 kips

Calculation for Shear Demand at Girder End Due to HL-93 Loading

Geometric Properties

Beam Spacing, S	9 ft
Span Length, L	80 ft
Slab Depth, t_s	8 in
Max Shear for Simple Span, One Lane, with IM	110.2 kips
n	8
Skew Angle, ϑ	36
Multipresence Factor (Lever Rule Only)	1.2
Moment of Inertia of Beam (36WF230), I	14812 in ⁴
Cross Sectional Area of Beam, A	67.73 in ²
Distance Between the Centers of Gravity of the Beam and deck, e_g	21.94 in
Tangent (ϑ)	0.737
Distance from CL of Exterior Web of Exterior Beam to Interior Edge of Curb, d_e	3 ft

Lateral Distribution Factors

Interior Beam	
One Design Lane Loaded	0.72
Two or More Design Lanes Loaded	0.884

(Table 4.6.2.2.3a-1)

$$0.36 + \frac{S}{25.0}$$

$$.2 + \frac{S}{12} - \left(\frac{S}{35}\right)^2$$

Exterior Beam	
One Design Lane Loaded	0.53
Two or More Design Lanes Loaded	0.795

(Table 4.6.2.2.3b-1)

Lever Rule

$$e = .6 + \frac{d_e}{10}$$

$$g = eg_{interior}$$

Skew Correction	1.191
-----------------	-------

(Table 4.6.2.2.3c-1)

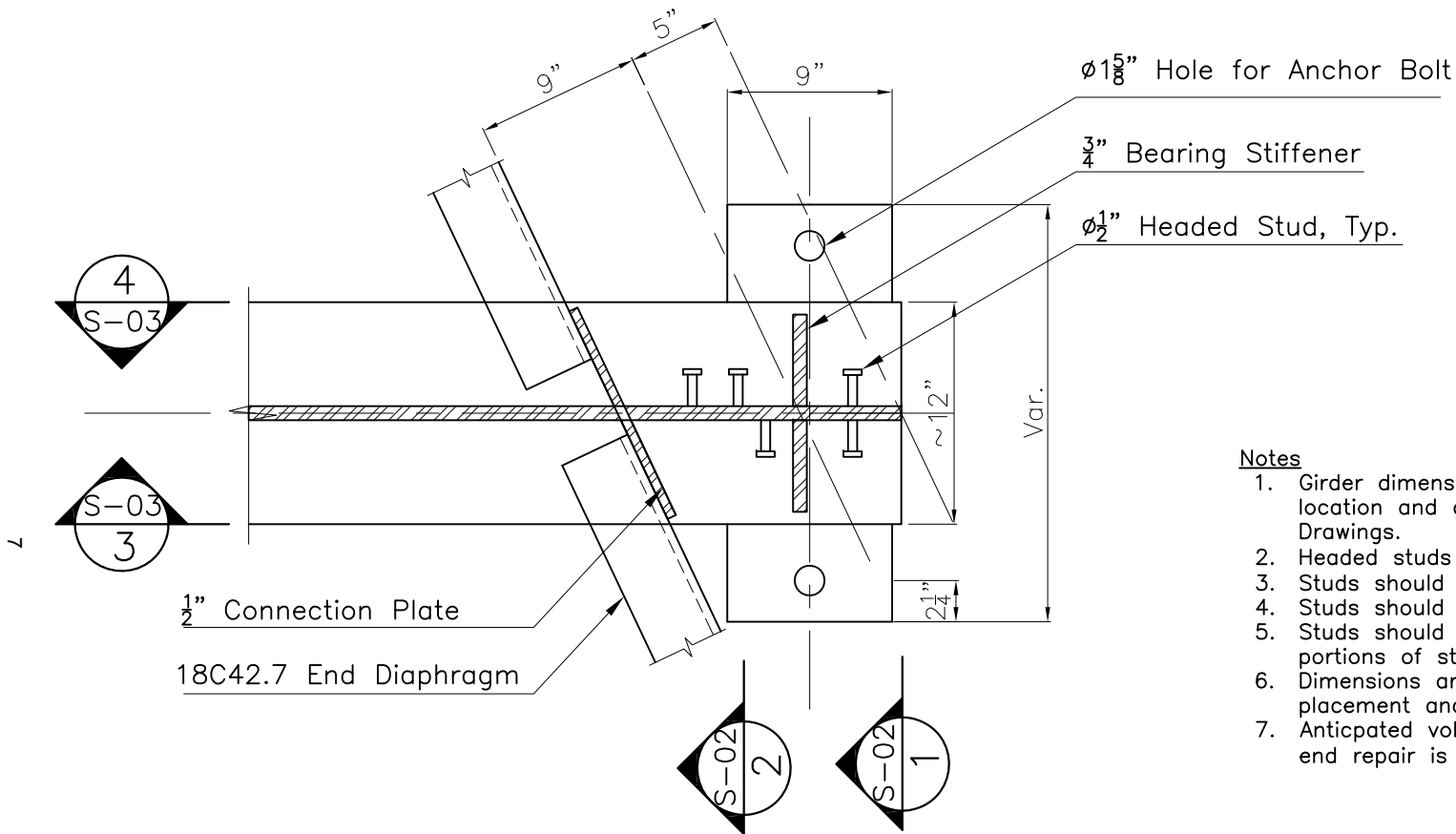
$$K_g = n(I + Ae_g^2)$$

$$1.0 + .2\left(\frac{12Lt_s^3}{K_g}\right)\tan\theta$$

Shear Demand

	Interior Beam	Exterior Beam	
Single Lane Loaded	94.5	70.0	kips
Two or More Lanes Loaded	116.0	104.4	kips

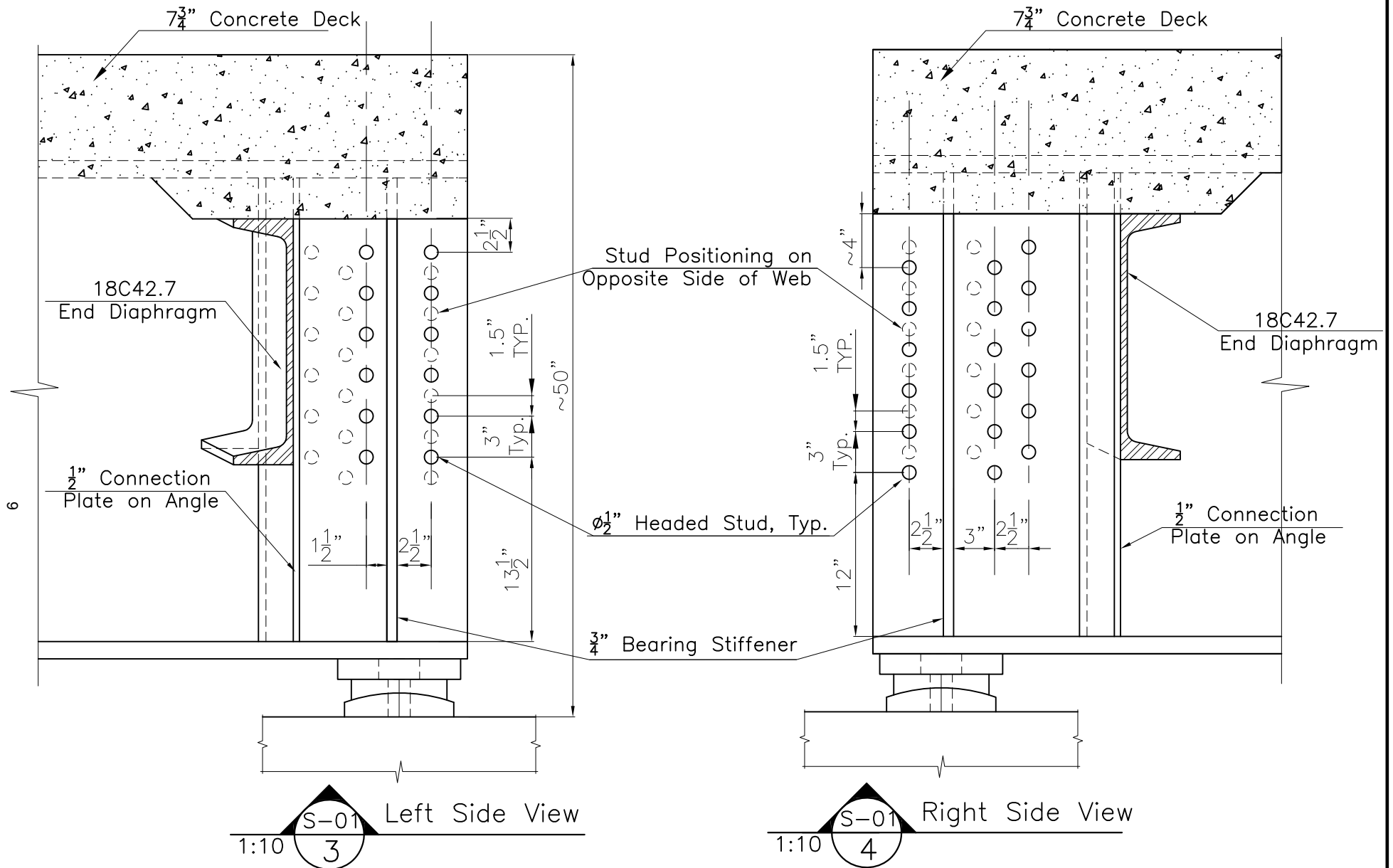
Appendix G UHPC Repair Sample Drawings



Notes

1. Girder dimensions vary depending on location and girder type. See Design Drawings.
2. Headed studs to be min. 2" in length.
3. Studs should have min. spacing of $3d_b$.
4. Studs should be welded using a stud gun.
5. Studs should be welded on uncorroded portions of steel.
6. Dimensions are for reference. Stud placement and UHPC panel may vary.
7. Anticipated volume of UHPC for one girder end repair is 0.15cy (4cf).

1:10 1 Girder Type 1
 With Bearing Stiffener



UConn
SCHOOL OF ENGINEERING

University of Connecticut



Connecticut Department
of Transportation

Project: **Bridge 3094 UHPC Repair**

Title: **Stud Layout – Girder Type 1 w/ Stiffener**

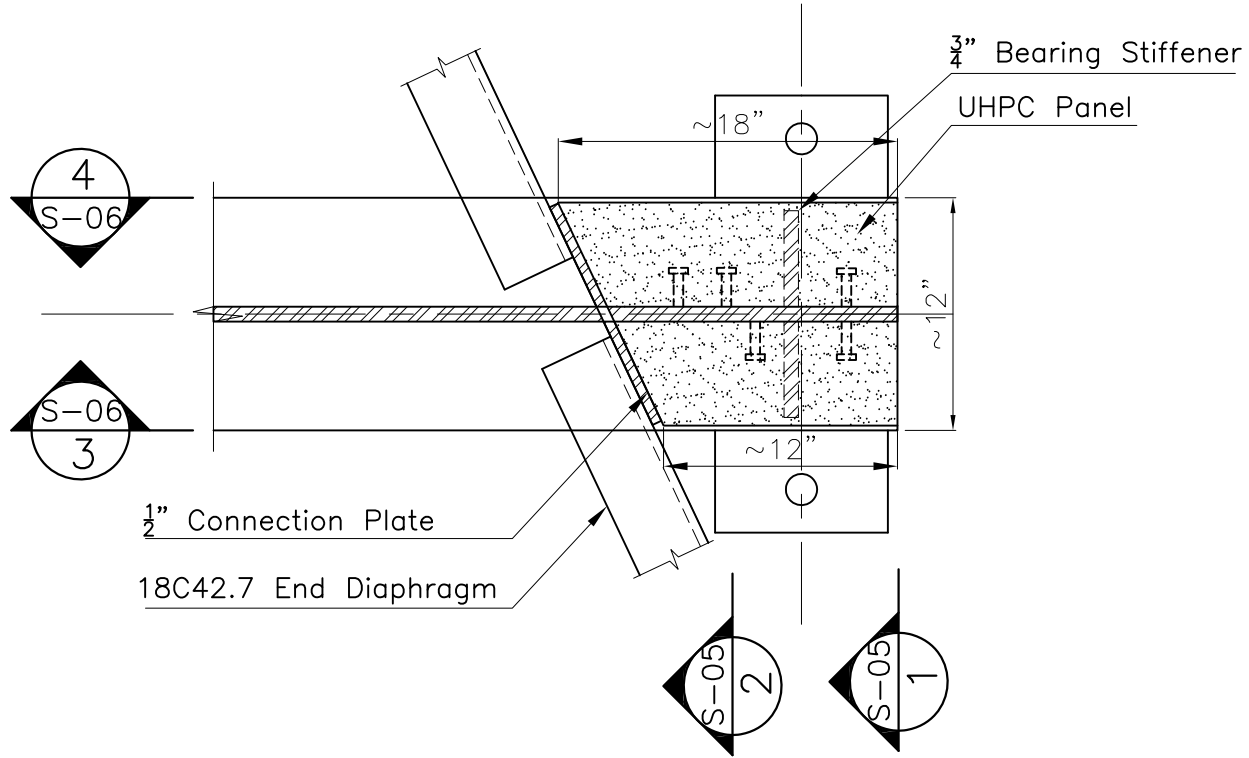
Drawn by: **Alexandra Hain**

App. by:

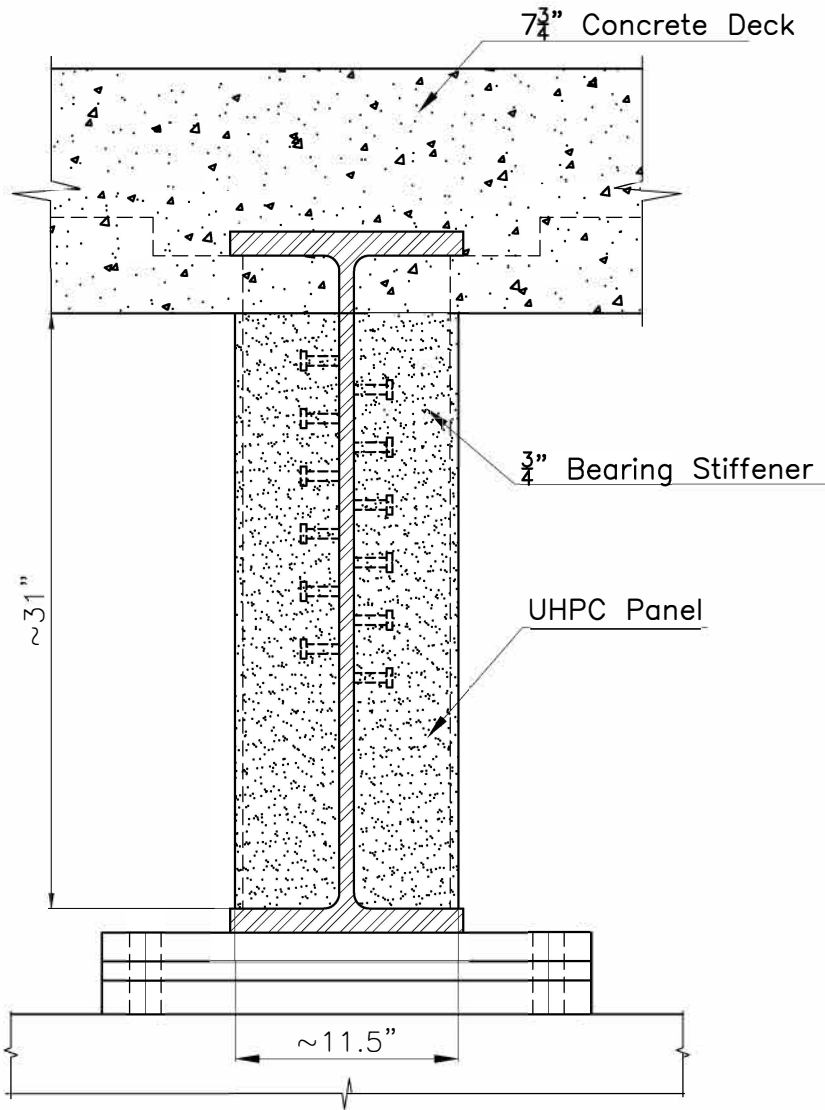
Scale: **As Shown**

Sheet No: **S-03**

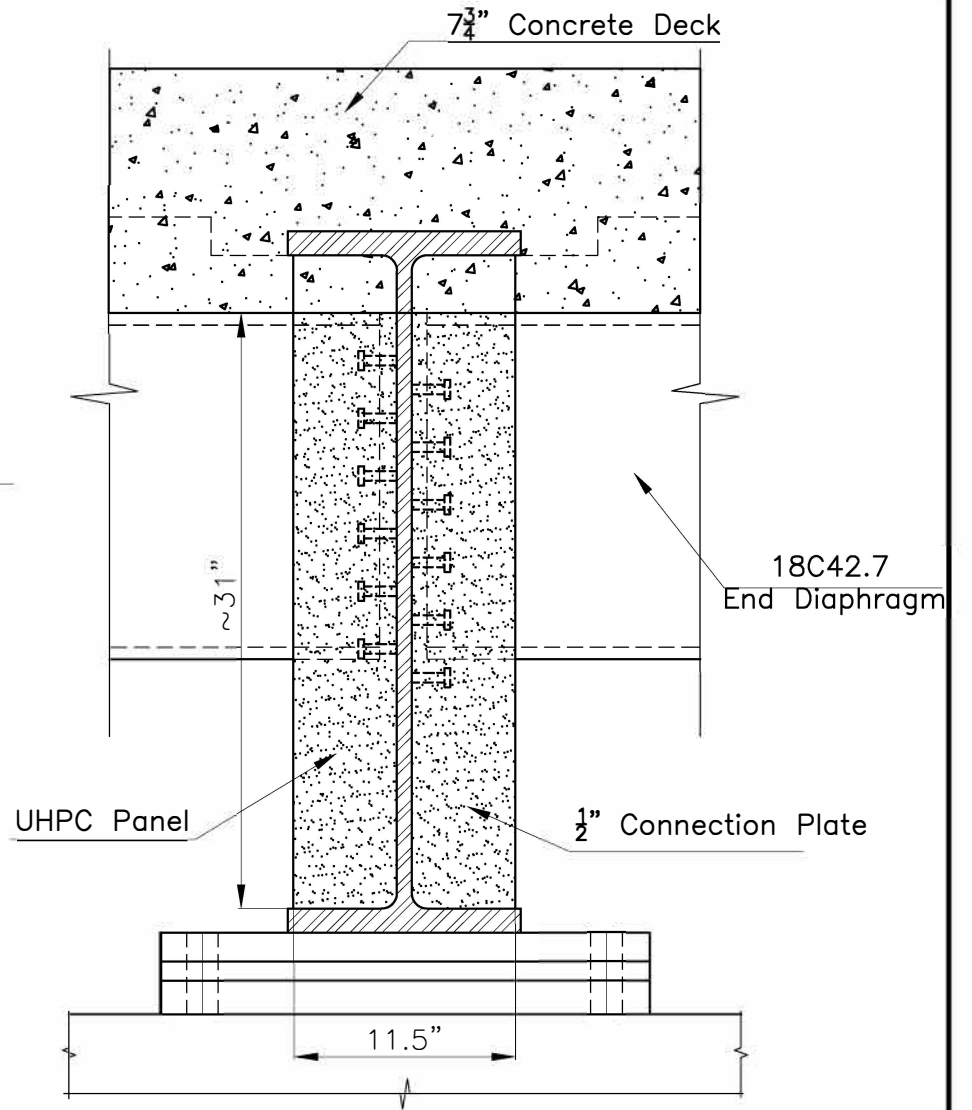
Date: **Oct. 27, 2016**



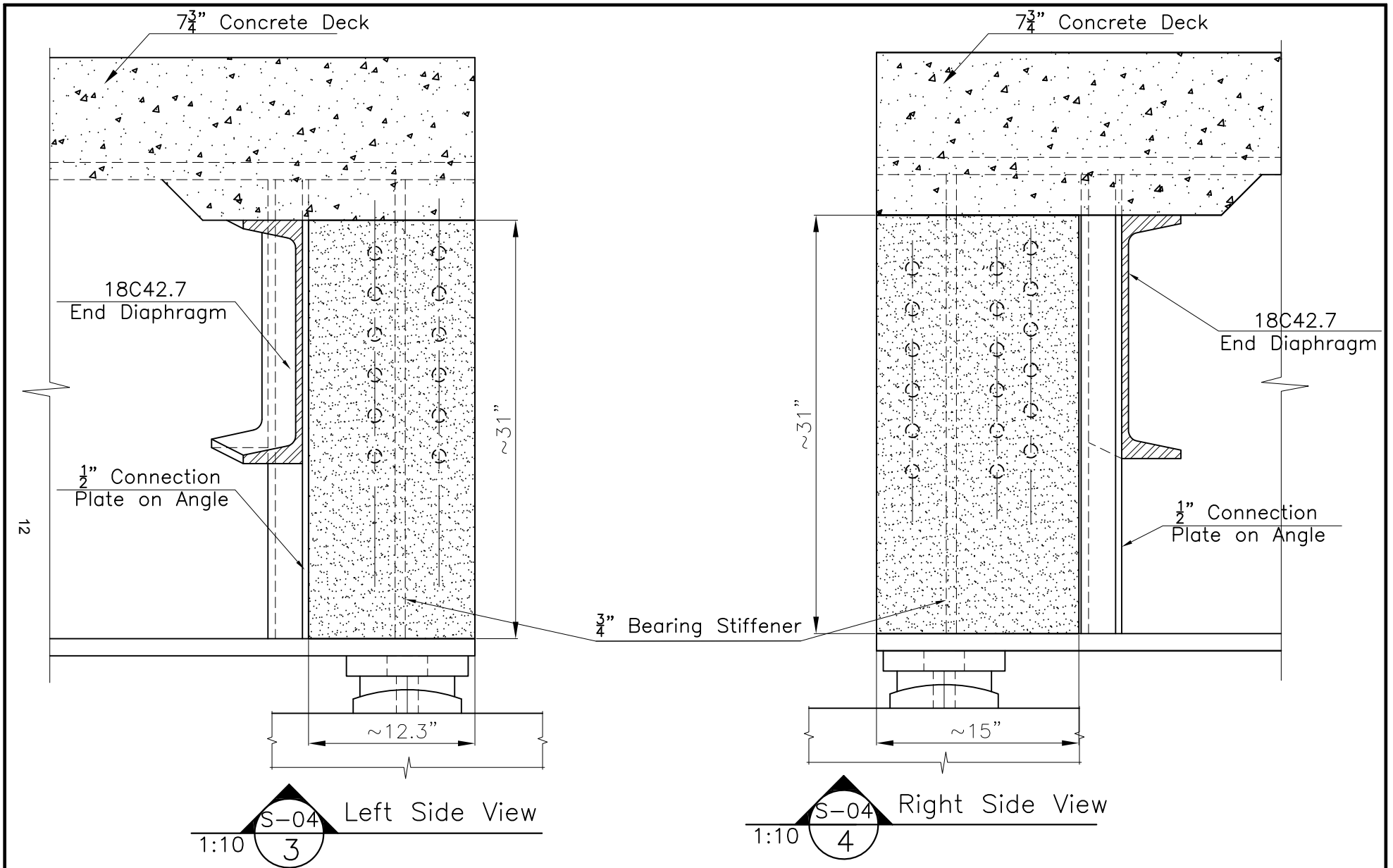
1:10 2 Girder Type 1 Repair
With Bearing Stiffener

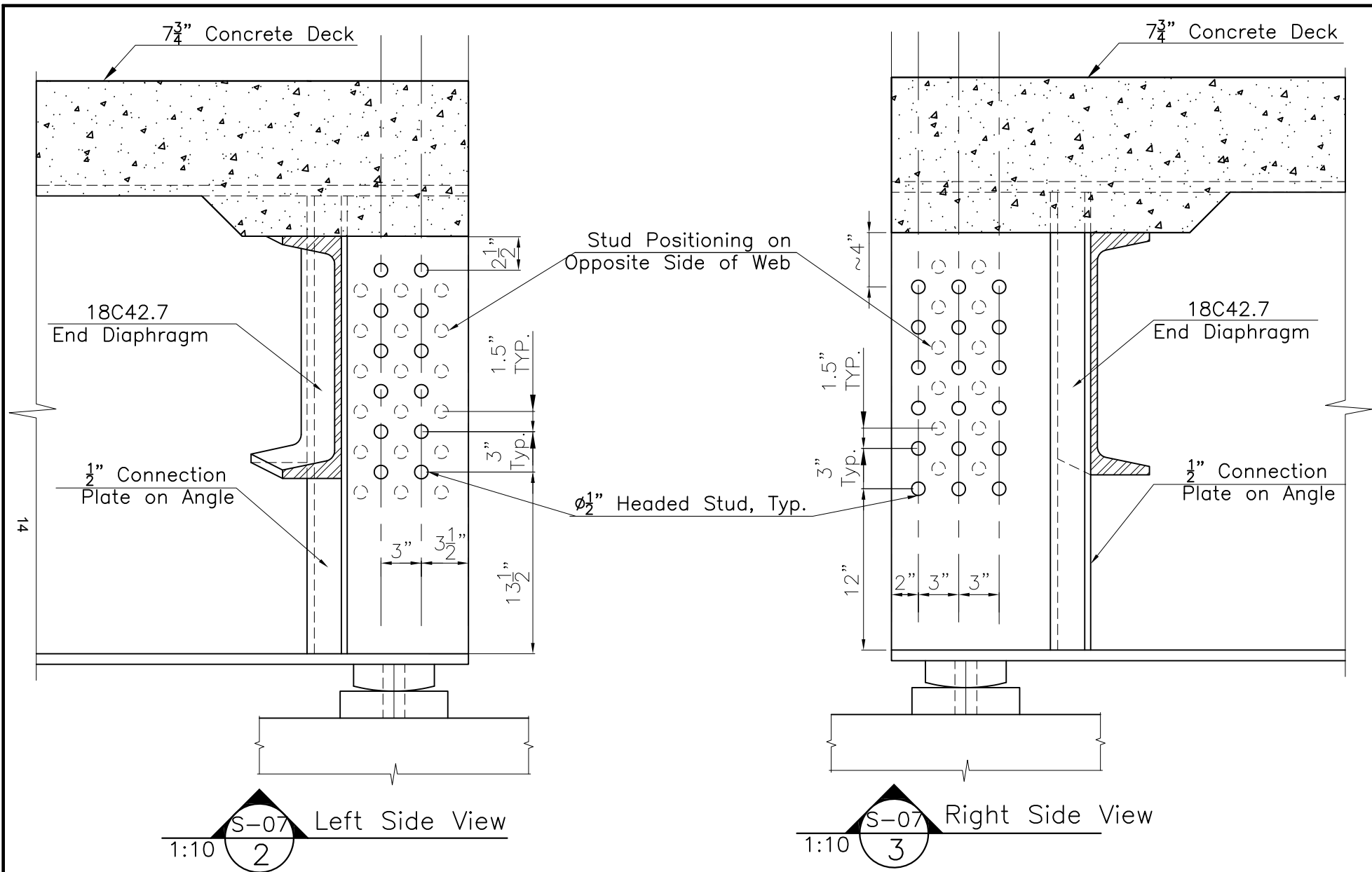


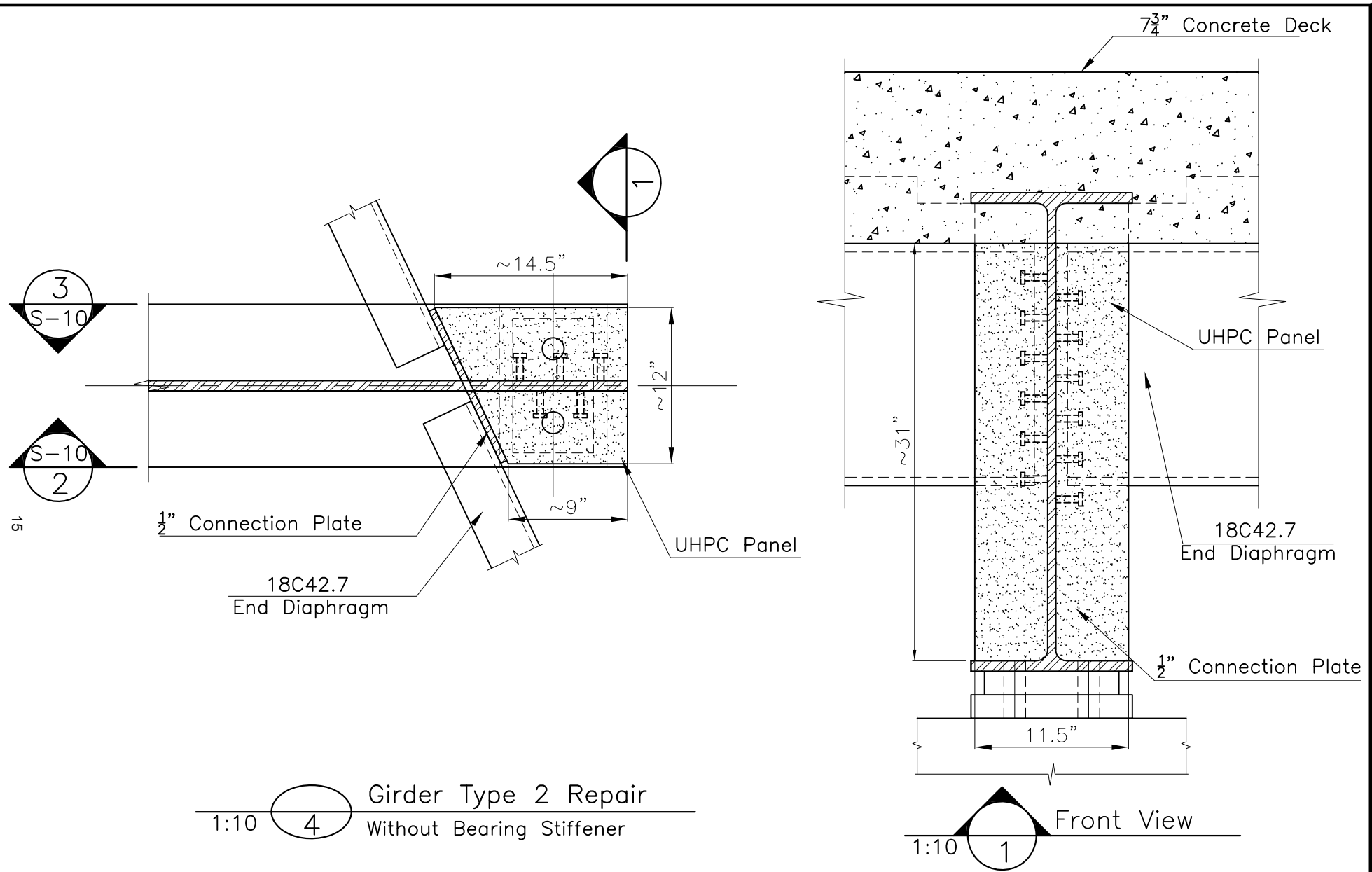
1:10 S-04 1 Front View

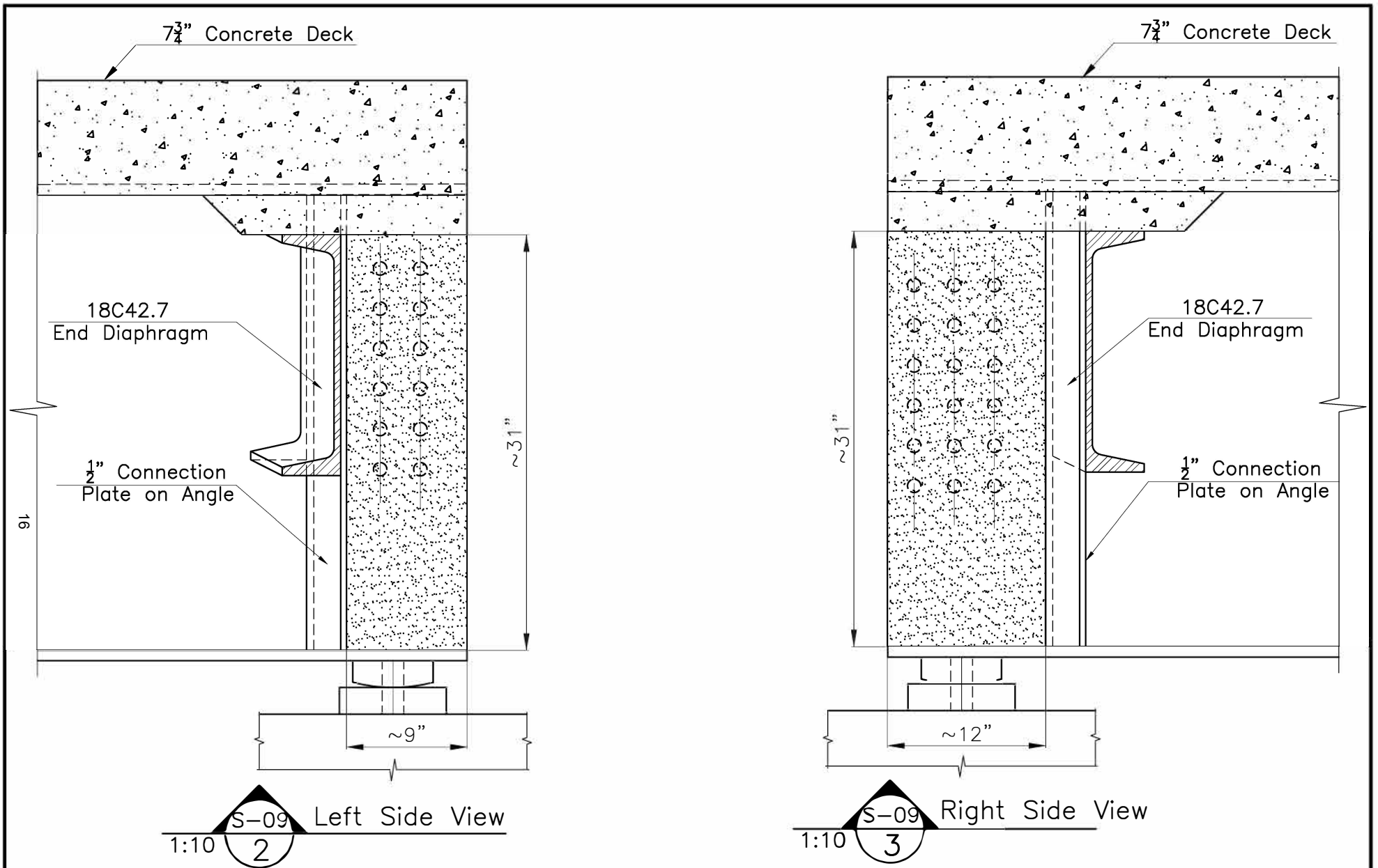




1:10 S-04 2 Cross Section









 UCONN SCHOOL OF ENGINEERING University of Connecticut	 Connecticut Department of Transportation	Project: Bridge 3094 UHPC Repair		
		Title: Stud Layout – Girder Type 1 w/o Stiffener		
		Drawn by: Alexandra Hain	App. by:	
		Scale: As Shown	Sheet No: S-10	Date: Oct. 27, 2016